QATAR UNIVERSITY

COLLEGE OF ARTS AND SCIENCES

DEVELOPMENT OF A NOVEL TAILORED ION-IMPRINTED POLYMER FOR RECOVERY OF LITHIUM AND STRONTIUM FROM REVERSE OSMOSIS CONCENTRATED BRINE

BY

SARA MOHAMMED ABDULQADER ALSHUIAEL

A Thesis Submitted to

the College of Arts and Sciences

in Partial Fulfillment of the Requirements for the Degree of

Masters of Science in Environmental Sciences

June 2022

COMMITTEE PAGE

The members of the Committee approve the Thesis of

defended on [Defense Date].

Prof. Mohammad Ahmad Al-Ghouti
Thesis/Dissertation Supervisor

Prof. Nabil Zouari
Committee Member

Prof. Mohamed,Najib Daly Yahia
Committee Member

Approved:

Ahmed Elzatahry, Dean, College of Arts and Sciences

ABSTRACT

ALSHUIAEL, SARA M., Masters: June : 2022, Environmental Sciences

Title: Development of a Novel Tailored Ion-Imprinted Polymer for Recovery of Lithium and Strontium from Reverse Osmosis Concentrated Brine

Supervisor of Thesis: Prof. Mohammad Ahmad Al-Ghouti

Seawater reverse osmosis (SWRO) desalination plants produce a large volume of brine containing a variety of concentrated metals, causing environmental concerns and obstacles. The innovation of this project is to prepare ion-imprinted polymer (IIP) with the benefit of a metal-based catalyst, which is fabricated to selectively adsorb lithium (Li^+) from aqueous solutions with an attempt to remove strontium (Sr^{2+}). The adsorption processes were carried out at different pH values, initial concentrations, and temperatures, in order to optimize the experimental conditions. The SWRO brine was physically and chemically characterized, the physiochemical characterization of the prepared IIP before and after adsorption was also performed using spectroscopic methods (SEM, TEM, FTIR, XRD, BET, EDX, and XPS). The adsorption capacity for Li^+ and Sr^{2+} from SWRO brine was evaluated, the reusability of IIP was investigated using adsorption-desorption cycles. The results showed that the IIP was efficient to remove Li^+ but not Sr^{2+}, and it follows Freundlich adsorption isotherms models. The initial concentration was a significant factor unlike temperature and pH, and the IIP was efficient to be reusable.

DEDICATION

This thesis is dedicated to my parents, the two lovely souls that provide me with unlimited love, support, and belief in me. For rising me up to believe that everything is possible and provide me with all the needs and environment to make it possible. Who gave me invaluable education opportunities and encouraged me to go through any adventure, especially this.

I hope this achievement will make you proud.

ACKNOWLEDGMENTS

First and foremost, praises and thanks to Allah, the Almighty, for His showers of blessings throughout my Master's degree journey until I completed the thesis successfully.

I would like to acknowledge the support of Qatar University for providing all the needs to achieve the requirements of this study and offering me the internal grant (QUST-1-CAS-2022-382) and a graduate assistantship position.

I would like also to express my deep and sincere gratitude to my research supervisor, Prof. Mohammad Al-Ghouti, for the continuous support of my study and research, patience, motivation, enthusiasm, and immense knowledge. His experience and guidance helped me in all the time of research and writing of this thesis. I could not have imagined having a better supervisor for my thesis.

Besides my supervisor, I would like to thank the research centers that helped me to run the analysis and characterization tests. My gratitude to the Central Lab Unit (CLU), Center for Advanced Materials (CAM), Gas Processing Center (GPC), and Department of Chemical Engineering (ChE) for their cooperation and support.

Finally yet importantly, I am extremely grateful to my parents for their love, prayers, caring and sacrifices to get my higher education and prepare me for my future.

And I will never forget to thank my caring friends who have supported me to get through the hard days, directly and indirectly, I could not have completed this thesis without your efforts to rest my mind outside of my studying.

TABLE OF CONTENTS

LIST OF TABLES

LIST OF FIGURES

1. INTRODUCTION:

Seawater desalination is an effective technology that is widely used around the world to obtain fresh potable water. The increased interest in seawater reverse osmosis (SWRO) desalination plants has raised concerns related to potential environmental problems. SWRO plants produce a large volume of water and a dense saline concentrate known as brine, which ends up in marine environments. Due to the potential for environmental concerns and obstacles from brine disposal, different methodological approaches for metal recovery have been studied.

Adsorption is a low-cost and ecologically beneficial way to extract metals such as Li^{+} and Sr^{2+} from an aqueous solution (Zhu et al., 2014). Generally, adsorbents are not specific with little selectivity for a single metal (Lu & Yan, 2004). As a result, it is critical to developing a novel adsorbent to selectively separate lithium and strontium from an aqueous solution. The current practice used in the recovery and extraction of lithium and strontium from brines is the evaporative concentration method. Although this method is cheap, the outstanding disadvantage of this method is that the method is wasteful of water, land-intensive, and time-consuming, therefore considered an impractical method of extracting lithium and strontium from brine. This brings us to the future of lithium and strontium extraction from brine; direct lithium extraction entails plucking the lithium ions from a complex geothermal soup. Nonetheless, most of the initial studies concluded that organic ion-exchange resins denoted a comparatively low selectivity when it came to lithium ions; hence, selectivity was used in the extraction process of lithium-selective sorbents (Stringfellow and Dobson, 2021).

Molecular imprinted polymers (MIPs) have drawn a lot of studies' attention in the latest years, because of their excellent features, such as constancy, cheap cost of formulation, and molecular recognition capability (Chen et al., 2016). Ion imprinting polymers (IIPs) are comparable to

molecularly imprinted polymers, however, they identify ions rather than molecules after imprinting, providing the advantages of molecularly imprinted polymers as well as a superior ion recognition capability (Otero-Romani et al., 2009). The latest studies have provided a detailed insight into the application and synthesis of organic polymers, which selectively extract lithium or strontium in favor of other metal ions. The ion-imprinting process is the basis of the method as it allows only lithium ions and not any competing ions to go through. Moreover, various approaches were explored to minimize the environmental effect of radionuclides. The adsorption method is the most dependable way for hazardous radionuclide removal and has been widely utilized (Kusumkar et al., 2021). Hence, this study aimed to explore the possibility of recovering strontium using the lithium IIP, to study if it could be used for multiple ion adsorption. The innovative objective of the project was the fabrication of imprinted polymer with the benefit of a metal-based catalyst, the elucidation of the prepared material by spectroscopic methods, and the evaluation of its adsorption capacity for Li^{+} and Sr^{2+} from brine concentrate.

RESEARCH OBJECTIVES:

- Develop a novel tailored lithium ion-imprinted polymer to extract lithium and strontium from an aqueous media.

- Investigate different experimental conditions such as the effect of pH, effect of initial ions concentrations, and effect of temperature on the adsorption processes.

- Determine the efficiency of the prepared ion-imprinted polymer in adsorbing lithium and strontium from real brine water.

- Explore the possibility of recovering lithium and strontium using the prepared ion-imprinted polymer.

2. LITERATURE REVIEW:

In many parts of the globe, increasing water shortage owing to population expansion, higher water utilization per capita, and financial development, alongside diminishing water resources because of environmental change and pollution, is worsening the water crisis (Damania et al., 2017). As per the recent assessments, 40% of the total population encounters intense water shortages, with that number expected to ascend to 60% by 2025 (Schewe et al., 2013). Moreover, for a minimum of a month every year, 66% of the total population suffers from acute water shortage (Mekonnen & Hoekstra, 2016). These insights show that typical water resources like rain, snowmelt, and stream overflow trapped in lakes, rivers, and springs are presently not adequate to fulfill human needs and desires in water-scant regions. This is a total contradiction with the sustainable development goal (SDG) 6, which expects to guarantee clean water for present and coming generations.

Water-scant nations require a revolutionary reconsidering of water resource arranging while water conservation and efficiency improvements can reduce the water supply and demand gap to some extent. These methods must be combined with an increase in supply strategy to address water shortage (Gude, 2017). Water sources management and supply improvement procedures are currently implemented in several water-insufficient locales. Regardless, enlargement is necessary, especially in regions where water shortage and water quality are worsening (van Vliet et al., 2017; Jones & van Vliet, 2018).

Seawater and high-salinity water desalination have gotten great prominence and it is even more seen as a feasible solution that mainly meets the needs of households and municipalities. Desalination is one of the most well-known methods that is used to generate water that satisfy the qualifying conditions for human being use (Darre & Toor, 2018). Desalination of seawater is a

way to expand water sources over the accessible sources by the hydrological cycle, giving a limitless, climate independent and continual source of fresh potable water (Elimelech & Phillip, 2011).

On the contrary, the desalination process produces brine in a huge amount. High-income nations create a significant proportion of worldwide brine, just as they do with desalinated water (77.9%). It should be highlighted that those nations from both highly developed global areas, where brine output is generally lower than desalinated water production, and oil-rich Gulf countries, where thermal desalination methods with poor recovery ratios are commonly used, resulting in elevated brine output (Jones et al., 2019).

Saudi Arabia, for instance, generates more than 31 million m^3 of brine every day, representing 22.2% of world production. United Arab Emirates (UAE), Kuwait, and Qatar are the following major producers of brine, representing 20.2%, 6.6%, and 5.8% of worldwide brine output, respectively. These four oil-rich countries generate 32% of the world's desalinated water and 55% of all brine.

2.1. Brine from Reverse Osmosis

Brine is very concentrated sodium chloride in water. Brine can denote salt solutions varying in concentration from approximately 3.5 percent, which is the typical concentration of seawater, to about 26 percent. Brine is produced in nature when ground saline water evaporates, but it is also produced when sodium chloride is mined (Westphal et al., 2015). It is also a co-product of several industrial processes, which includes desalination; therefore, it has to be treated before it can be properly disposed of or used furtherly (Panagopoulos et al., 2019). Brine usually contains ions like cesium, calcium, sodium, lithium, strontium, etc. that have a kind of closer

chemical and physical properties (Yang et al., 2017).

Desalination of saltwater and high brackish water has garnered the most attention among the possibilities for bolstering the water supply. It is also increasingly recognized as a realistic solution that largely serves the requirements of homes and communities. Desalination is a technique used to eliminate salts out of the water to generate water that fulfills various quality standards for human use (Darre & Toor, 2018). The desalination process is capable of supplying a climate-independent, limitless, and consistent source of potable water with superior quality beyond what is available naturally through the water process (Elimelech & Phillip, 2011).

Initial desalination facilities, mainly in oil-rich but water-limited locations, such as the Middle East, relied mostly on thermal methods. Before the 1980s, the two primary thermal methods (multi-stage flash (MSF) and multi-effect distillation (MED)) were responsible for 84 percent of all worldwide-desalinated water production (Jones et al., 2019). The development of membrane methodologies especially reverses osmosis (RO), after the 1980s steadily moved away from the favorability of thermal procedures. The generated water by desalination using thermal and reverse osmosis methods in 2000 was almost equivalent at 11.5 million m^3 per day each, representing 93 percent of the global production (Fig.1). Recently in 2019, the output of reverse osmosis desalinated water was 65.5 million cubic meters per day, representing 69 percent of the total global desalination water produced (Jones et al., 2019).

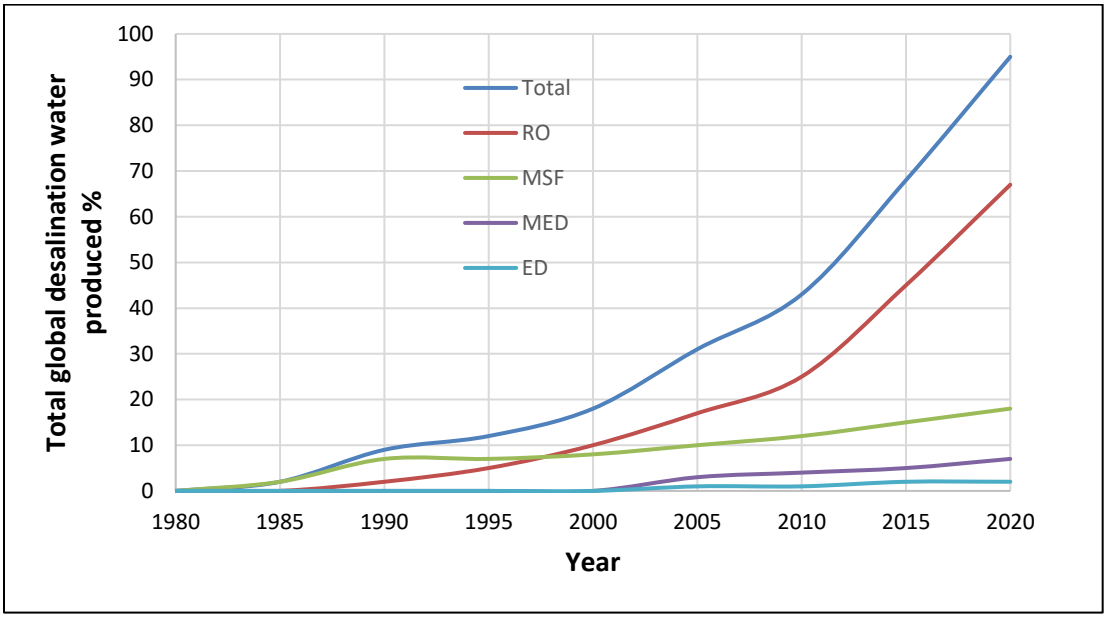

Figure 1: Desalination technology used percentage by years (adapted from Jones et al., 2019).

Safe disposal of desalination wastewater continues to be a serious technological and financial issue (Roberts et al., 2010). Worldwide brine output is now at 141.5 million m^3 per day, for a total of 51.7 billion m^3 per year. It is almost 50% more than the entire amount of desalinated water generated worldwide. North Africa and the Middle East generate about a hundred million m^3 of brine per day, representing 70.3 percent of worldwide brine output (Jones et al., 2019).

2.2. Lithium Recovery from Brine Techniques

Lithium recovery studies have started, however it is still in the early stages. It has been suggested that sorption, electrolysis, and nanofiltration be used (Lemaire et al., 2014). Table 1 shows different techniques from lithium recovery from brine. According to Tsuruta (2005), biological recovery of the lithium ions employing diverse microbes is also conceivable. Lithium may be recovered from a moderately clean aqueous solution by precipitating it with CO_3^{2-}. Li^+

ions may not be entirely precipitated, since they have a high solubility product constant of Li_2CO_3 (K_{sp} = 1.7×10^3 at 25 °C). Adsorption is a low-cost and ecologically beneficial way to extract Li^+ from an aqueous solution (Zhu et al., 2014). Generally, adsorbents are not specific with little selectivity for a single metal. As a result, it is critical to developing a novel adsorbent to selectively separate lithium from an aqueous solution.

The current practice used in the recovery and abstraction of lithium from brines is the evaporative concentration method. In this method, lithium chloride (LiCl) and lithium carbonate (Li_2CO_3) are produced through evaporative concentration that also requires additional refining purposely to crystallize the magnesium, potassium, and sodium chlorides (Toba, 2021). This leaves the concentrated lithium chloride solution, which can be further refined to lithium hydroxide or lithium carbonate while eliminating the traces of impurities. Although this method is cheap, the outstanding disadvantage of this method is that the method is wasteful of water, land-intensive, and time-consuming, therefore considered an impractical method of extracting lithium from brine.

This brings us to the future of Li^+ extraction from brine; direct lithium extraction entails plucking the lithium ions from a complex geothermal soup while leaving other metals and salts in the solution. Paranthaman et al. (2017) propagated the concept of electrochemical ion pumping, which involved integrating the lithium-exclusion method as a critical approach in recovering Li^+ from brine. More specifically, the use of a selective electrodialysis technology is quite advantageous, especially regarding metal ion recovery and water utilization. If the brine consisting an elevated amount of high Mg^{2+}/Li^+ ratio, selective-electrodialysis is merited for having greater adaptability with reference to ion fractionation of lithium and magnesium from brines. This stems from the understanding that extraction of lithium ions is affected by the acidification levels, whereby the most practical level is the pH of two to four. Similarly, it is realized that multi-stack

systems, coupled with the current increase yield greater extraction rates.

Organic sorbents and inorganic sorbents are the best representation of the direct lithium extraction method. About organic sorbents, the role of organic ion-exchange resins and ion-imprinted polymers cannot be understated. From the onset, the integration of strong acid cation exchange resins for selective recovery and collection of lithium from lithium-containing solutions and seawater has been subject to investigation and study since the 1970s. Nonetheless, most of the initial studies concluded that organic ion-exchange resins denoted a comparatively low selectivity when it came to lithium ions; hence, selectivity was used in the recovery techniques of lithium-selective sorbents (Stringfellow & Dobson, 2021).

Table 1: Processes used to Recover lithium from brines.

Brine sample	Technique	Reagents	Reference
End brine and the Dead Sea brine	Precipitation	Lithium aluminum oxide	(Pelly, 1978)
Brine from dead Sea	Gel permeation chromatography/ Column chromatography	PGA, a column of BioGel P-2 with Blue Dextran	(Bukowsky et al., 1991)
Synthetic brine	Chelating resins/ Ion-exchange	three ion exchange resin (MC50, TP207, Y80-N Chemie AG)	(Bukowsky et al., 1991)
Brine from natural gas wells	Inorganic ion exchanger/ Ion-exchange	H2TiO3 ion exchanger	(Kunugita et al., 1989)
Brine from salt lake	Inorganic ion exchanger/ Ion-exchange	H2TiO3 ion exchanger	(Swain, 2016)
Synthetic brine	Solvent extraction (LLE)	n-Butanol	(Gao et al., 2015)
Synthetic brine	Solvent extraction (LLE)	Ethohexadiol, Isopentanol, 2-Isopropoxypropane, diethyl ether	(Gao et al., 2016)
Brine	Solvent extraction (LLE)	TBP	(Shi et al., 2015)

Brine sample	Technique	Reagents	Reference
Brine from salt lake	Ionic solvent extraction	(Bmim)(Tf2N), EMIM TFSI and BMIMPF6	(Jiang et al., 2014)
Brine	Ionic solvent extraction	Amim-based ILs	(Liu et al., 2015)
Brine	Electro-electrodialysis	Bipolar membranes	(Sun et al., 2015)
Brine from salt lake	Membrane electrolysis	Bipolar membranes	(An et al., 2012)
Brine Dead Sea	Solvent impregnated membrane	Solvent-polymeric membranes, Octicizer	(Marinsky & Marcus, 2021)
Brine	Desalination	Nanofiltration membrane	(Mero, 1965)
Brine from salt lake	Desalination	Nanofiltration XLE membrane	(James, 1966)

2.3. The Modification Process of Ion-Imprinted Polymer

Recent studies have provided a detailed insight into the application and synthesis of organic polymers, which selectively adsorbs lithium more favorably than other metal ions. The ion-imprinting process is the basis of the method as it allows only lithium ions and not any competing ions to go through. For instance, to enhance Li's sorption kinetics, a hybrid nanocomposite sorbent must be prepared as opposed to sorbents that are nanopowders since they consume more energy and allow for large pressure drops in column operations (Stringfellow & Dobson, 2021). A nanocomposite sorbent is preferred for having porous polymer support such as polyacrylamide (PAM), polyacrylonitrile (PAN), and polyvinylchloride (PVC), which are embedded in an ion sieve, hence incorporated as binders of sub-micron or micron size ion sieves. The advantage of using a hybrid nanocomposite sorbent is the fact that it has a higher lithium uptake capacity. In this undertaking, selective ion exchange of Li-imprinted polymer comes in handy in binding the Li^+, therefore enhancing lithium-ion concentration at the polymer interface of the hybrid nanocomposite sorbent, thus improving the uptake kinetics of Li. On the other hand, other studies, including that of Ueda et al. (2015), have re-affirmed the use of cyclic siloxane for concentrating and removing lithium ions in cyclic siloxane-lithium compounds.

Molecular imprinted polymers (MIPs) have drawn a lot of studies' attention in the latest years, because of their excellent features, like constancy, cheap price of formulation, and molecular recognition capability (Chen et al., 2016). Ion imprinting polymers (IIPs) are comparable to Molecularly imprinted polymers, however, they identify ions rather than molecules after imprinting, providing the advantages of molecularly imprinted polymers as well as a superior ion recognition capability (Otero-Romani et al., 2009). For metal IIPs, many techniques have been described, including bulk polymerization (Esen, 2009), suspension polymerization (Hoai et al., 2010), and precipitation polymerization (Otero-Romani et al., 2008). The imprinted metal ion is separated from the polymer mote following the ion imprinting polymerization in all situations by washing with a mineral acid, which forms voids or more specifically "imprinted sites" analogous in form and size to the imprinted metal ion (Hashemi et al., 2015). Chromatography, sensing, and solid-phase extraction (Bahrami et al., 2014; Shamsipur et al., 2014) are just a few of the applications for ion-imprinted materials.

The ion imprinting process is an effective and easy way to formulate ion-imprinted polymers (IIPs) by adding template ions and then extracting them to produce precise complexing sites for the introduced ions. IIPs have a bright future for selectively recovering noble and heavy metals from hydrous solutions (Singh & Mishra, 2009; Saraji & Yousefi, 2009; Xu et al., 2018). Hoai et al. (2010) used the ion imprinting approach with bifunctional ligands methacrylic acid (MMA) and 4-vinyl pyridine (4-VP) to create pored adsorbent material to selectively recover copper ions. Li et al. (2011) used a thiocyanato functional group as the Cd binding site in an ion-imprinting polymer to adsorb cadmium ions.

2.4. Different Approaches for IIP Elaboration

Crosslinking is a crucial phase in the IIP amplification procedure that leads to the development of binding sites. Yet, the crosslinking phase might be carried out with the existence of a ligand-functionalized monomer, a non-polymerizable ligand, or linear chain polymers. The different approaches to elaborate IIP have all been classified by Rao et al. (2006) as chemical immobilization, trapping, crosslinking of linear chain polymers, and surface imprinting (Fig. 2).

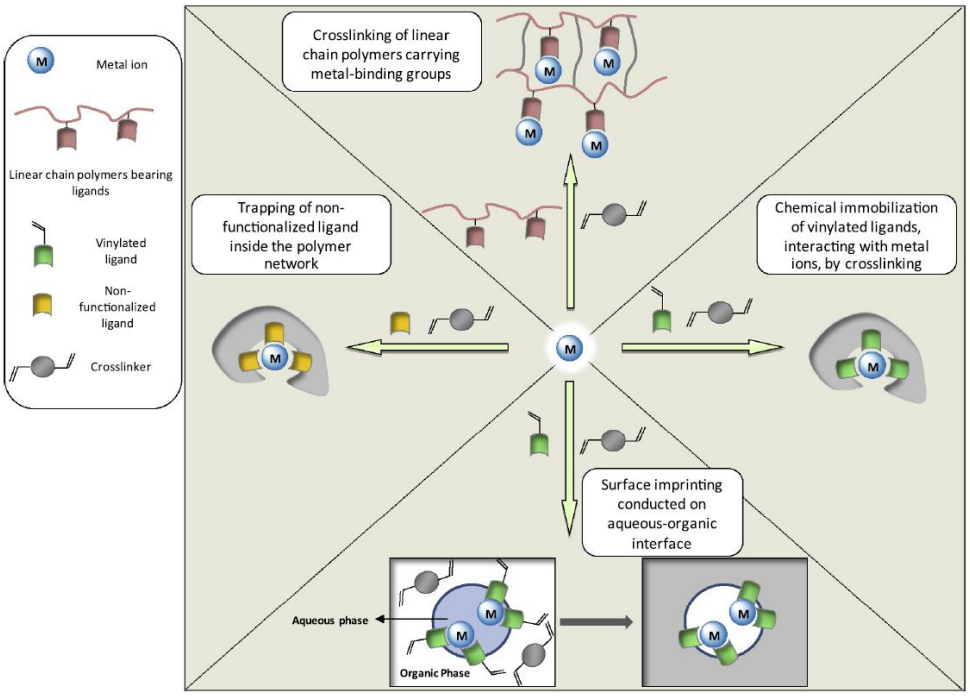

Figure 2: Approaches for IIP elaboration (Branger et al., 2013)

2.4.1. Chemical immobilization:

The IIP idea is quite comparable to the non-covalent technique of the molecular imprinted polymers production where the polymerizable functional groups are a component of the ligands that are utilized to produce ion recognition (Alexander et al., 2006). Chemical immobilization was also described as "the formation of a dual compound of metal ions and ligands possessing vinyl groups, isolation, and subsequently polymerization with matrix-forming monomers" (Rao et al., 2006), many writers have dropped the "isolation" step. Indeed, ion, chelating monomer, and

crosslinker are combined together prior to copolymerization is the most efficient strategy to incorporate the functionalized ligand into the polymer system. This method is widely used since it is simple to implement. Monomers with modest binding characteristics and no intrinsic selectivity are called simple monomers. The primary goal of IIP production is to produce highly selective materials. A selected ligand might certainly improve the IIP's recognition characteristics, according to the prediction. As a result, several researchers have focused on the functionalization of additional complicated ligands to incorporate polymerizable vinylated groups (Branger et al., 2013).

2.4.2. Trapping:

The chemical immobilization approach, as previously stated, necessitates the use of vinylated ligands, preferably those with inherent specificity. These functionalized chelators are not commercially available and are in short supply. The production of those chelators must be carried out in laboratories using procedures that are time-consuming and labor-intensive. Furthermore, because ligands might have complicated structures, introducing a vinylated function is challenging, if not impossible. Thus, ligands are employed as is, and they are trapped within the polymer templet during the polymerization process (Branger et al., 2013). The term "trapping" refers to the fact that ligands are entrapped within the polymer templet rather than chemically attached to the polymer chains. This technology has advanced to the point where it seems to be a common method for imprinting a metal complex produced from a range of ligands (Tsoi et al., 2012).

2.4.3. Crosslinking of linear chain:

The earliest method for producing IIPs is the crosslinking of linear chain polymers containing metal-binding groups. In 1976, they made their first effort to manufacture polymers for metal ion identification (Nishide et al., 1976). However, in terms of cations, this method is now mostly applied with organic linear polymers such as cellulose and chitosan. Chitosan is quickly being a preferred adsorbent for metal ion recovery due to the amino and hydroxyl compound. Imprinting technology, on the other hand, can assist improve its stability and selectivity via crosslinking. In this situation, no radical polymerization is required because the crosslinking step is provided by the thickening process with epichlorohydrin or glutaraldehyde (Chen et al., 2011).

2.4.4. Surface imprinting:

Traditional polymerization procedures are used to create IIPs arising by the chemical immobilization method or trapping approach (bulk, precipitation, suspension). Despite their excellent selectivity, these materials often have low rebinding capabilities because there is limited approachability to the binding sites inherent within a very stiff polymer system. Delayed mass transfer, which causes slow binding kinetics, is another effect of inadequate site approachability. Because the template was not completely removed, there is a significant possibility of some template ions leaking outside the IIP during its operation (Fu et al., 2012). Surface imprinting was developed to address these issues by creating binding voids on or near the imprinted polymers' surfaces. This ensures that all templates are removed, that the target species is easily accessible, and that mass-transfer resistance is low (Li et al., 2011). Rao et al. (2006) discussed surface imprinting as a result of simple or complex emulsion polymerization. At the emulsion interface, amphiphilic functional monomer formulates a compound in the presence of a template in this process. The binding cavities are mostly located near the material's surface following the

polymerization and leaching of the template. Nonetheless, the surface imprinting technique has evolved significantly in recent years. It is presently mostly accomplished by imprinting an imprinted layer on the surface of tiny particles, resulting in core-shell particles. Organic core-shell materials are a good example of that. Additional organic surface-imprinted materials were made by grafting a polyethyleneimine layer on polypropylene fibers, activating it with a (meth)acrylic monomer, and then crosslinking it with epichlorohydrin in the existence of Cu(II) ions (Li et al., 2011). However, mostly, the adapted materials are inorganic in origin and are typically made up of silica gel particles, which are mechanically and chemically stable, inexpensive, and simple to prepare and functionalize (Dakova et al., 2012).

2.5. Polymerization Techniques

Organic IIPs are mostly made via free radical polymerization, with the exception of a few rare cases of IIPs made through polycondensation. The forms of these IIPs might differ depending on the polymerization method. Bulk polymerization generates monolithic materials, while heterogeneous by suspension or emulsion, and homogeneous by dispersion or precipitation polymerization generates polymer well-defined particles. A core-shell arrangement can also be used to make well-defined spherical particles. Surface imprinting, on the other hand, mostly consists of an inorganic core in core-shell IIPs (Branger et al., 2013). The next sections will go through each of these methods in-depth and Table 2 shows the different polymerization techniques used for IIPs preparation in literature.

2.5.1. Bulk polymerization

Because a porogen solvent is usually utilized to produce imprinted polymers, the term

"bulk polymerization" is rather misleading. As a result, the right word is "solution polymerization". However, because the amounts of solvent used are modest enough to result in bulk materials, the imprinted polymers community refers to this process as bulk polymerization (Kempe & Kempe, 2008).

Bulk polymerization is a simple and convenient approach to making IIPs. It does not require any special expertise or complex equipment (Segatelli et al., 2010), and it demonstrated the benefit of the creation of novel imprinting techniques and systematic research (Daniel et al., 2005). It is widely utilized for the production of IIPs as a result of these factors. Unless the polymerization is done in a column and the components are used in their monolithic state, bulk materials must normally go through shriveling, grounding, and sieving to get the required size particles (Özkara et al., 2010). This procedure is considered difficult, and requires time and labor efforts; only about half of the prepared polymer can be retrieved. In those circumstances, scaling up is difficult. Many chromatographic and separation applications are incompatible with the uneven size and form of the particles. Furthermore, certain binding sites are susceptible to be damage by the crushing step, resulting in a significant reduction in the IIPs' loading capacity (Dam & Kim, 2009). Because of that, many attempts to manufacture IIPs straightforward in a bead structure using suspension or emulsion, and dispersion or precipitation polymerization because of these key limiting factors.

2.5.2. Suspension and emulsion polymerization

Suspension and emulsion polymerization is a heterogeneous polymerization method as it necessitates the coexistence of two non-miscible stages, one continuous and the other scattered. The monomers, initiator, porogen, and template ion are all present in the dispersion stage as the

IIP is made through suspension polymerization. This stage is usually an organic phase contacting an aqueous phase, stabilized using hydroxyethyl cellulose, gelatin, or polyvinyl alcohol, and contains sodium chloride salt at some point. In the dispersed phase's droplets, polymerization takes place, which functions as miniature reactors, resulting in polymer beads. The polymer particles' form and size may be controlled using this approach, and the porogen solvent can be used to alter the porosity (Branger et al., 2013).

Meouche et al. (2012) used inverse suspension polymerization to make Ni(II) IIPs to avoid the template ion leaving from the dispersed organic phase that is in contact with the aqueous phase. The dispersion phase was a mineral oil in the original procedure because it does not require any stabilizing agents. As the polar dispersion phase, DMSO was used to introduce the initiator, crosslinker, template ion, and functionalized ligand. Using this method, very porous IIP beads were created. On the other hand, in heterogeneous emulsion polymerization, monomers droplets are emulsified with surfactants in a continuous phase containing the initiator. Nonetheless, emulsion polymerization remains infrequent, most likely due to the difficulty of particle separation and the possibility of surfactant contamination (Branger et al., 2013).

2.5.3. Dispersion and precipitation polymerization

Because the medium is constituted of a single phase at the early stage, homogeneous polymerization is used to describe dispersion and precipitation polymerization. In the porogen, all of the used monomers, templates, and initiators are soluble, and polymerization begins in a homogenous solution. The polymerization media or the monomer swell the dispersion polymerization particles generated initially, unlike the precipitation polymerization particles that precipitate rather than swell in the medium (Branger et al., 2013). Because particle dispersions are

created without a stabilizer, they can coagulate and are insufficiently stable during formation, so, dispersion polymerization requires the use of a stabilizer.

In reality, precipitation and bulk polymerization are very similar, given that the only variation is the porogen quantity used. A little amount of solvent is used in bulk polymerization, unlike precipitation polymerization, which uses a large amount of porogen. This might be the explanation for the process's popularity since it is the second most commonly utilized following the bulk polymerization for IIP production. Shamsipur and Besharati-Seidani (2011), on the other hand, highlighted the following benefits over the latter. A strongly cross-linked polymer network cannot be formed around the imprint metal ion, resulting in its easy removal from the IIP, and this approach creates particles in the nano, submicron, and micron size, that they can all be used as all the produced polymers are in a particle form.

Table 2: Polymerization techniques used to prepare IIPs

IIP polymer	Materials	Polymerization techniques	Reference
Ni-IIP and Co-IIP	- Acrylamide - Methacrylic acid - EGDMA - Ni or Co metal ion - AIBN	Precipitation polymerization	(Işıkver & Baylav, 2018)
Ni-IIP and Co-IIP	- Acrylamide - Itaconic acid - Trimethylpropane trimethacrylate (TMPTMA) - Ni metal ion - AIBN	Precipitation polymerization	(Işıkver & Baylav, 2018)
Nano Ni-IIP	- 2- vinyl pyridine - EGDMA - 2,2′-azobisisobutyronitrile - Ni metal ion - AIBN	Bulk polymerization	(Behbahani et al., 2012)

IIP polymer	Materials	Polymerization techniques	Reference
Cr-IIP-FPANFM	- 1-vinylimidazole - 3-(trimethoxysilyl) propyl methacrylate (TMSPMA) - EGDMA - Cr metal ion - AIBN	Free radical polymerization on functionalized polyacrylonitrile nanofibrous mat (FPANFM)	(Hassanzadeh et al., 2018)
Ni-IIP	- 2-(Allylmercapto) nicotinic acid - EGDMA -Nickel(II) nitrate hexahydrate - AIBN	Precipitation polymerization	(Long et al., 2016)
Cd-IIP-NPs	- 2-aminobenzimidazole - 4-vinyl pyridine - EGDMA - $Cd(NO_3)_2$ - AIBN	Precipitation polymerization	(Dahaghin et al., 2018)
Br-IIP	- Potassium bromide - Chitosan - Glutaraldehyde - $Al(NO_3)_3$	Crosslinking of linear chain polymers	(Wang et al. 2019)
HPO_4-IIP	- Hydrogen phosphate - Cetyltrimethylammonium bromide (emulsifier) - Methacrylic acid - Divinyl benzene	Emulsion polymerization	(Alizadeh & Atayi, 2018)
Pb-II-IPN	- Methacrylic acid - EGDMA - Chitosan - Tetraethyl orthosilicate	Simultaneous polymerization	(Hande et al., 2016)
Magnetic Cr-IIP	- 4-vinyl pyridine - 2-hydroxyethyl methacrylate - EGDMA - AIBN - Cr metal ion	Sol-gel method	(Liang et al., 2017)

IIP polymer	Materials	Polymerization techniques	Reference
Li-IIMM	- Poly (vinylidene fluoride) - 2-(allyloxy)methyl-12-crown-4 - EGDMA - AIBN - LiCl	Surface-imprinted polymerization/Phase inversion technique	(Sun et al., 2017)
Li-IIP	- Vermiculite - Dibenzo-14-crown-4 - N,N-dimethylformamide - α-MAA - EGDMA - AIBN - Lithium nitrate	Dispersion polymerization	(Huang & Wang, 2019)
Li-Fe_3O_4@SiO_2@IIP	- 2-(allyloxy) methyl-12-crown-4 - MH-Fe_3O_4@SiO_2 - EGDMA - AIBN - Lithium chloride monohydrate	Surface imprinting polymerization	(Luo et al., 2015)
Li-IIP	- Benzo 12-crown-4 - MAA - EGDMA - AIBN -$LiClO_4$	Precipitation copolymerization	(Hashemi et al., 2016)

2.6. IIP Applications

2.6.1. Solid-phase extraction

Solid-phase extraction (SPE) is more favorable over liquid-liquid extraction (LLE) for a variety of reasons, including the lack of emulsion, greater enrichment factors, reduced reagent use, and a wide range of sorbents. Because IIPs have greater selectivity and adsorption efficiency than typical solid sorbents such as silica gel, activated carbon, or functionalized polymer, they are employed in SPE (Gladis & Prasada Rao, 2002). Ion-imprinted materials (IIPs) exhibit affinity

and selectivity similar to antibodies, but they are also simple to synthesize, durable in hostile environments, and affordable to manufacture. SPE preconcentration of trace quantities of ions and their separation from complicated matrices and interferents is the major application of ion-imprinted polymers (Cejner & Dobrowolski, 2015).

There have been several IIPs for harmful metals such as nickel, cadmium, arsenic, cobalt, lead, mercury, and selenium. Ion-imprinted polymers had superior selectivity and adsorption capacity than non-ion-imprinted materials in all circumstances. Ion-imprinted polymers have seen significant use as effective sorbents for noble metals in the recent decade. Ruthenium, platinum, palladium, and gold are among them (Cejner & Dobrowolski, 2015).

2.6.1.1. Wastewater treatment and samples pretreatment

In the recent two decades, the use of IIPs for the selective SPE of various hazardous heavy metal ions from aqueous solutions has gotten a lot of interest due to its great application potential. Several investigations have been undertaken to investigate the adsorptive capabilities of IIPs. Effects of pH, temperature, contact duration, starting metal concentration, adsorbent quantity, and the presence of competing ions are all widely researched characteristics. These factors are critical for heavy metal removal research because they can explain how heavy metals adsorb (El Ouardi et al., 2021). IIPs are commonly employed as selective SPE adsorbents to remediate water polluted with hazardous metal ions. Adsorption investigations may be done in batch or flow systems. Luo et al. (2015) generated a magnetic lithium ion-imprinted polymer for the recovery of lithium from real wastewater samples, and their results show excellent removal of lithium indicating great possibility in advanced wastewater treatment.

Sample pretreatment aids in the removal of matrix interference as well as the extraction

and enrichment of trace targets. Traditional pretreatment, on the other hand, might include time-consuming, arduous stages and substantial reagent use (Płotka-Wasylka et al., 2016). As a result, there is a pressing need to create high-selectivity pretreatments with easy, time-efficient, and labor-efficient processes. Imprinted polymers are utilized as extractants in the solid phase for specialized enrichment and separations since they have high specific binding sites and selective adsorption for template molecules and ions that can be desorbed later. The low cost, ease of use, and excellent extraction efficiency encourage widespread usage for sample pretreatment (Pataer et al., 2019).

Because of the structural predictability of the imprinted polymers, which allows them to create composites with diverse characteristics with other materials, SPE based on imprinted polymers technology, has been widely employed in several solid-phase extraction methods. Researchers have also undertaken significant trials to develop better IIPs and MIPs and have enhanced the SPE approach in terms of fewer processes, ease, cost-efficient, automation, miniaturization, time savings, and eco-friendly (Ghorbani et al., 2020; Háková et al., 2020).

To date, a growing number of researchers have developed several types of IIP and MIPs to use as adsorbents in extraction technology to improve extraction recovery. The technology of merging imprinting polymers with SPE is critical for identifying and detecting agricultural veterinary medication residues in actual samples (Zhang et al., 2016).

2.6.2. Sensors

Sensors might be used in a variety of fields, including food analysis, environmental analysis, clinical diagnostics, pollution monitoring, drug detection, and chemical warfare agent detection. The recognition element is the most important component of a sensor since it is the element in response to recognizing the targeted analytes in complicated samples and binding them.

Selective chemical sensors with strong thermal, mechanical, and chemical characteristics may be made utilizing ion-imprinted polymers at a reasonable cost. In ion-imprinted sensors, signal transduction is accomplished using one of two methods: spectroscopic or electrochemical characteristics. The imprinting and transduction selectivity combined can generate sensors that can detect targeted ions exceedingly effectively without interference (Murray & Manuel Uy, 2001). There have also been descriptions of sensors for lead(II), uranyl, copper(II), and dysprosium(III) ions (Prasad et al., 2006).

2.6.3. IIPs membrane separation

The ion-imprinted membrane outperformed the non-imprinted membrane in terms of adsorption affinity and penetration selectivity toward the template ions. Araki et al. used surface molecular imprinting to create a Zn(II) ion-selective membrane by water-in-oil emulsion polymerization. The polymerization was carried out with the existence of acetonitrile-butadiene rubber, resulting in a flexible and mechanically stable membrane (Araki et al., 2005). Kimaro et al. (2001) disclosed the polymerization of uranyl vinyl benzoate and styrene/DBV followed by the addition of 2-nitrooctylphenyl ether and polyester to produce a uranyl ion permselective membrane. Ion-imprinted membranes demonstrated greater uranyl ion selectivity than other bivalent transition metal ions.

Table 3: Applications that IIPs used for

IIP polymer	Application	Reference
Ni-IIP and Co-IIP	Removal of heavy metal from aqueous solution	(Işıkver & Baylav, 2018)
Nano Ni-IIP	Determination of nickel in fish, vegetables, river sediments, and river water.	(Behbahani et al., 2012)
Cr-IIP-FPANFM	Removal of Cr(VI) from aqueous solutions.	(Hassanzadeh et al., 2018)

IIP polymer	Application	Reference
Ni-IIP	Removal of Ni(II) from aqueous solution	(Long et al., 2016)
Cd-IIP-NPs	Cadmium(II)-selective glassy carbon electrode	(Dahaghin et al., 2018)
Br-IIP	Extraction of Br(I) ions from aqueous solution	(Wang et al. 2019)
HPO_4-IIP	Recognition element of graphene/graphite paste potentiometric electrode	(Alizadeh & Atayi, 2018)
Pb-II-IPN	Extraction of Pb(II) from printed-circuit-board (PCB) recycling unit wastewater	(Hande et al., 2016)
Magnetic Cr-IIP	Selective adsorption of Cr(VI) anions from aqueous solutions	(Liang et al., 2017)
Li-IIMM	IIP macroporous membranes for Li^+ targeting	(Sun et al., 2017)
Li-IIP	Lithium recovery	(Huang & Wang, 2019)
Li-Fe_3O_4@SiO_2@IIP	Recovery of lithium from wastewater	(Luo et al., 2015)
Li-IIP	Selective pre-concentration and recognition of lithium ions	(Hashemi et al., 2016)

2.7. Lithium Imprinted Polymer

Ion imprinted technique is merited in the Li^+ extraction and recovery for possessing distinguished recognition capabilities. More specifically, the IIPs are characterized by their lifelong, easy storage and re-usability capabilities, as well as low preparation costs. The IIPs possess high selectivity and high attraction for the targeted Li^+ in the brine in the extraction process. This extraction process encompasses the solid phase extraction method preferred to liquid-liquid extraction for many reasons: a wide choice of sorbents, low consumption of reagents, higher enrichment factors, and the absence of emulsion (Gu et al. 2018). In the solid-phase extraction method, the ion-imprinted polymers are used because they have a better adsorbent efficiency and a higher selectivity when compared to other common solid sorbents like functionalized polymer, active carbon, or silica gel (Zambrzycka-Szelewa et al., 2019). This

conclusion stems from several studies that, upon comparison with non-ion imprinted materials, establish that ion-imprinted polymers have better adsorption and higher selectivity capacity.

Therefore, to advance low-cost recovery and extraction of Li^+ from brine, it is imperative to use selective high-capacity reusable sorbents, like the nanostructured manganese oxide (HMO) embedded in a Li-imprinted polymer, which has been critical in the selective solid-phase lithium extraction process. In conjunction, the reusable sorbents in the extraction process ought to be nanostructured purposely to boost the sorption kinetics of lithium, thus enhancing the high flow and operational rates. The recovery process includes the use of inorganic ion sieve and inorganic sorbents like titanium oxide, manganese oxide, and aluminum hydroxide that have selective adsorption properties for lithium, and are relatively stable when high temperatures are involved and are also affordable. According to Ventura et al. (2016), HMO is preferred subject to high lithium selectivity, especially where there are large concentrations of other metal ions like magnesium, calcium, sodium, and potassium. In the solid-phase extraction process, sorbents that are in the form of nanoparticles are not recommended for use in the flow-through separation process since they consume high energy and allow for large pressure drops. As such, the separation process should encompass a hybrid nanocomposite sorbent.

2.8. Lithium Imprinted Polymers Preparation Concept

The lithium-imprinted polymers are prepared by polymerizing (Fig. 3) a crosslinking agent (ethylene glycol dimethacrylate), an optional co-monomer, and a lithium chelate monomer. The polymer sorbents play a critical role in the uptake process. For instance, to uptake lithium from a basic aqueous solution, the acidic H^+ polymer sorbents are used, whereas the Na^+ polymer sorbents are preferred for neutral aqueous solutions (Xiao et al., 2015). The essence of preparing lithium-

imprinted polymer is that once the polymers are desorbed, it leaves imprints with the arrangement, shape, and size of binding sites meant explicitly for binding Li. In agreement, the United States Department of Energy report highlighted the main selectivity capabilities of Li-imprinted polymers, especially concerning brines containing other competing metal ions like K^+ and Na^+ (Hashemi et al., 2016). According to the experiments, which involved a brine of 390 ppm K^+, 410 ppm Na^+, and 390 ppm Li^+ at 45 ºC, 75ºC, and 100 ºC, it is established that the Li-imprinted polymer had an extraction efficiency surpassing 95%.

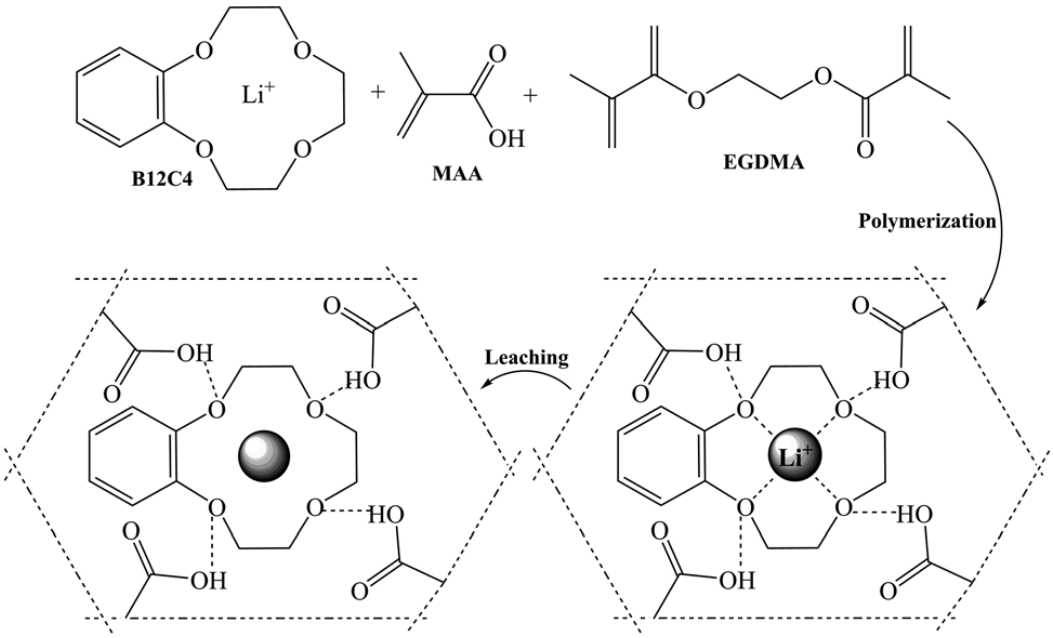

Figure 3: Synthesis of lithium ion-imprinted polymer (Hashemi et al., 2016).

On the other hand, lithium ions would not be able to interact steadily with prevalent functional monomers, which makes lithium ion-imprinted polymers formation using coordination/complexation pathways among functional monomers is problematic. As a result, Luo et al. (2015) come up with novel functional monomers to make lithium IIPs by synthesizing new

crown ethers with a double bond as a functional monomer to prepare magnetic ion-imprinted polymer with a core−shell structure (Fe3O4@SiO2@IIP) (Fig. 4). However, more studies and experiments should come in handy in recommending ways to improve both the binding affinity for the Li^+ and promote the selectivity and the capacity to generate Li-imprinted polymers and their crosslinking agents.

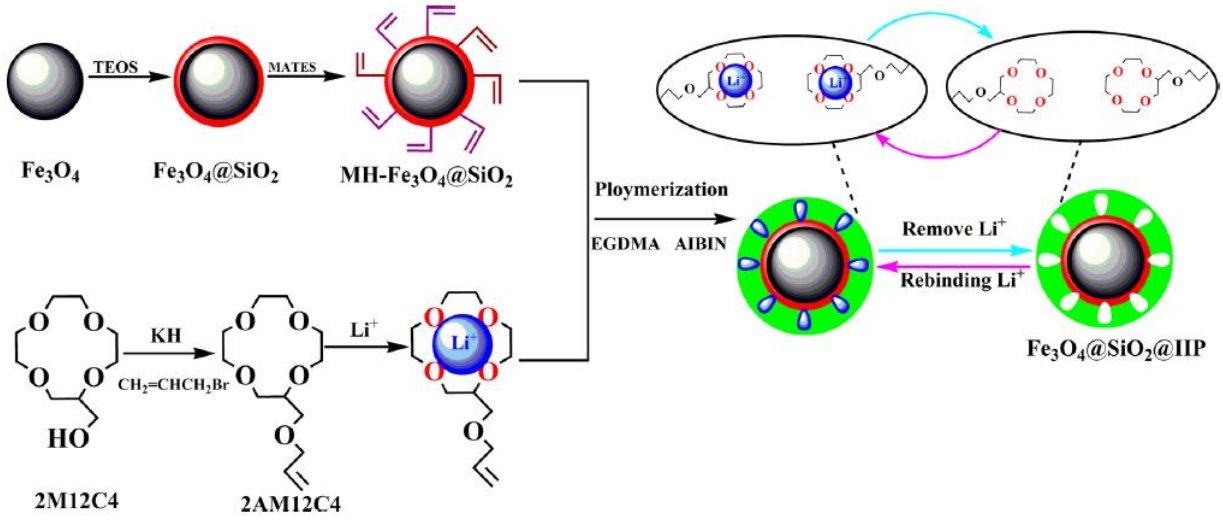

Figure 4: Synthesis of core silica-coated Fe_3O_4 and novel functional polymer to prepare magnetic ion-imprinted polymer (Fe3O4@SiO2@IIP) (Luo et al. 2015).

2.9. Crown ethers effect on the Li^+ ion-imprinted polymer

Since Pedersen (1967) discovered the selective ion-binding characteristics of crown ether compounds. A lot of studies have been performed on crown interaction with inorganic and organic cations (Izatt et al., 1991), as well as neutral molecules (Izatt et al., 1992). Crown ethers (CEs) are excellent model compounds that may be used to create more complicated chemical structures. Crown ethers are particularly appealing molecules because of their unusual features, which allow for a deep investigation of interchanges that are significant in the field of analytical chemistry

(Murray et al., 1997). The macrocyclic effect is widely recognized for increasing the steadiness and metal ions selectivity combined with cyclic ligands (such as crown ethers) as compared to their equivalent open-chain equivalents (Cabbiness & Margerum, 1969; Frensdorff, 1971).

The macrocyclic effect is widely recognized for increasing the selectivity and constancy of metal ion compounds with cyclic ligands for example the crown ethers as compared to their comparable open-chain equivalents (Cabbiness & Margerum, 1969; Frensdorff, 1971). The type of the metal ion, as well as the distance, amount, and alignment of the donor atoms of the ligand that are physically available to the combined cation, might impact the effectiveness of the interaction (Hancock & Martell, 1989; Izatt, 1995). The application of macromolecule crown ether derivatives in membrane transport (Shamsipur et al., 2010; Shamsipur et al., 2001), solid-phase (Hashemi & Shamsipur, 2015), and supercritical fluid removal of metal ions (Shamsipur et al., 2001) and the fabrication of ion-selective membrane potentiometric (Shamsipur & Mashhadizadeh, 2001) and optical sensors (Alizadeh et al., 2002) and spectrophotometric (Hasani & Shamsipur, 2005) has been earlier documented.

When crown ethers contain concavities of the right sizing and the right functional and cross-linking monomers, they have demonstrated great selectivity to attach to the target metal ions. Nonetheless, it is difficult to remove IIPs from wastewater quickly and effectively following treatment (Luo et al., 2015). 2-methylol-12-crown-4 (2M12M4C) may simply join with lithium ions due to their comparable sizes, generating a stable compound. Despite this, 2M12M4C cannot be employed as a functional monomer in polymerization without the benefit of the double bond (Luo et al., 2015).

Crown ethers, the macrocyclic host molecules second generation, have gotten a lot of interest in recent years (Liu et al., 2017; Büning et al., 2018). Metal ions that are inside of the

crown ethers have the ability to synchronize with oxygen atoms within the concavities of the crown. For stable binding and selectivity, selecting a crown ether with suitable concavities for intended ions is critical.

12-crown-4 (12C4) and its equivalents, for example, the 2-methylol-12-crown-4 (2M12C4), 2-(allyloxy)methyl-12-crown-4 (2AM12C4), and benzo-12-crown-4 (B12C4), have been extensively studied in recent years for their ability to preferentially extract Li^+ (Sun et al., 2018; Xu et al., 2018; Lu et al., 2018; Luo et al., 2015). The cavity diameter of dibenzo-14-crown-4 (DB14C4) is quite near to the ionic diameter of lithium, according to earlier investigations (Pedersen, 1967; Limjuco et al., 2017). The cavity diameter of the 12-crown-4 is 1.2, and the ionic diameter of the Li^+ is 1.46. Moreover, the toxicity studies found out that the dicyclohexano-18-crown-6 at high concentration have a toxic effect on the bacterial growth, but with the addition of alkaline metals ion, like sodium chloride and potassium chloride, none of them caused any significant lag in the growth curve of the bacteria (Carrasquel-Ursulaez et al., 2020). Thus, it is expected that the use of crown ether would not cause a toxic effect on the living organisms, as it will be capsulated into a polymer.

2.10. Adsorption Performance of Ion-Imprinted Polymers

The adsorption capabilities of ion-imprinted polymers vary, and they are affected by many reasons and factors. An analysis of various adsorption experiments expounds on the impact of pH on the adsorption rates and tests. In all the experiments, it is concluded that the pH is among the most pertinent factors impacting the adsorption rate of various metal ions on the non-imprinted polymer. Luo et al. (2015) experimented with investigating the effect of pH values of 1 to 9 on the Li^+ ion sorption on Fe_3O_4@SiO_2@NIP and Fe_3O_4@SiO_2@IIP. From the experiment, they

established that when the pH of the solution is raised from 1 to 6, the adsorption capacity of Li^+ on Fe_3O_4@SiO_2@NIP and Fe_3O_4@SiO_2@IIP also increases. Similarly, it was observed that as the pH is increased from 6 to 9, the adsorption rate decreases slightly, and this is mainly because of the deprotonation of the crown ether group. When the pH values are below 3, the Li^+ adsorption capacity is meager because of the protonation of the crown ether group. Other than the pH effect, the adsorption performance is affected by the absorption capacity. From the same experiment by Luo et al. (2015), it is further established that the adsorption capacity is directly proportional with the concentration of the Li^+ ions, in that, for a 2.5 mmol/L – 45 mmol/L concentration range, the monolayer coverage, and the saturation values were realized at the 15 mmol/L concentration.

2.11. Lithium Ion-Imprinted Polymer Selectivity Toward Strontium

Radioactive strontium was created and disseminated from nuclear weapons or nuclear reactors, polluting the environment; it has been a source of worry and investigation (Cai et al., 2020). Celestite ($SrSO_4$) and strontianite ($SrCO_3$) are two naturally occurring minerals that contain Sr (Skoryna, 1981). Because of its long half-life of around 29 years, radioactive ^{90}Sr is extremely hazardous to wellbeing health, and the environment, which plays a role in food chains, as well as its preference for depositing in plants and bones/skeleton (EPA, 2021). Although non-radioactive strontium has minimal toxicity, excessive exposure in youngsters might cause bone development issues (Dorsey et al., 2004). The major toxicological consequence of high strontium in experimental animals is abnormal skeletal development (Dorsey et al., 2004).

As a result, mineral abstraction from saltwater and brine effluents from desalination plants has piqued the interest of academics all over the world, owing to the advantages of lowering environmental impact and desalination costs while also varying the land mining activity (Al Bazedi

et al. 2013). Mineral extraction profits are mostly determined by the mineral market price and the amount of it in the brine. Na, Ca, Mg, K, Li, Sr, Br, B, and U have been identified as possibly desirable for extraction (Loganathan et al. 2017).

Various approaches were explored to minimize the environmental effect of radionuclides. The adsorption method is the most dependable way for hazardous radionuclide removal and has been widely utilized (Kusumkar et al., 2021). Ion-imprinted polymers (IIPs) are frequently utilized in adsorption and removal procedures to overcome this problem. Li et al. (2010) used bis(trimethoxysilylpropyl) amine (TSPA) to make strontium ion-imprinted hybrid gels for the removal of Sr^{2+} and Ca^{2+} ions utilizing dicyclohexano-18-crown-6, methacrylic acid (MAA), and ethylene glycol dimethyl acrylate (EGDMA) removal. Bahraini et al. (2011) made Sr^{2+} IIP by crosslinking dicyclohexano-18-crown-6 (D18C6), MAA, and EGDMA with dicyclohexano-18-crown-6 (D18C6), MAA, and EGDMA. The reagents utilized for the formulation of strontium IIP are closely similar to the reagents used for the preparation of lithium IIP. This study aims to explore the possibility of recovering strontium using the lithium IIP, to study if it could be used for multiple ion adsorption.

2.12. Electronegativity Effects on Li^{+} and Sr^{2+}

Electronegativity refers to an atom's tendency to attract electrons to itself. The Pauling scale sign is often used to indicate a dimensionless quantity in this context. Lithium has an electronegativity of 0.98. In general, both the atomic number and distance of the valence electrons from the nucleus affect the electronegativity of an atom. Higher electronegativity values imply that an element or combination is more efficient at attracting electrons. Strontium has the chemical symbol Sr and the atomic number 38 (Sathiyapriya et al., 2021). Strontium is a soft metal yellow

metallic element with a high degree of chemical reactivity. It is an alkaline earth metal. When exposed to air, the metal acquires a black oxide covering. It has an electronegativity of 0.95.

Lithium atoms are composed of three protons and three electrons, respectively. A particle can become an ion after losing one of its electrons (Fig. 5). With more positive protons than negative ones, the bit now has a positive charge in total. As a result, it is a positively charged ion. Thus, lithium quickly loses an electron from its outer shell when bombarded by a more electronegative substance. Lithium has one of the lowest electronegativity levels of any element, a value of 1.0, due to its minimal pull on electrons. To determine an atom's electronegativity, you must know its atomic number as well as the atom’s sizes—an element's ability to attract electrons increases with increasing electronegativity. Electro-positivity, which measures an element's capacity to give electrons, is the polar opposite of electronegativity. Therefore, lithium having a smaller atomic size and radius loses electrons, thereby having a lower electronegativity (Miyoshi et al., 2020). Lithium-ion electronegativity is derived using experimental observations of molecular or structural characteristics rather than being assessed directly. However, it comes down to it, and electronegativity is mainly controlled by the protons in the nucleus and the quantity and position of additional electrons in an atom's shell. Significant protons in an atom mean more "pull" on electrons with negative charges; thus, the nuclear mission is critical. There is a connection between electron location in space, and the amount of positive charge that valence electrons experience. The further away the valence electrons are from the nucleus, the less positive charge they will have (Shaaban et al., 2020). The other charged particles in the lower-energy core electron shells shield the electron density from the atomic nucleus. As a result of a diagonal connection, Lithium's electronegativity is equivalent to magnesium's. Strontium ions have an electronegativity of 0.95, almost the same as lithium ions, thereby having similar effects.

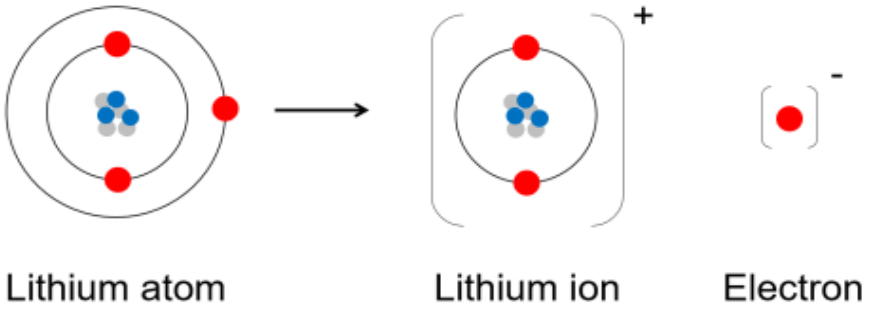

Figure 5: Lithium atom losing the valence electron to make lithium ion (Cher, 2020).

2.13. Binding Mechanism of Li^+ and Sr^{2+} by the lithium-ion Imprinted Polymer

Lithium ions preferentially attach at the interface between the crystalline and amorphous subdomains in composites comprised of both instead of the typical intercalation process seen in graphitic anodes. Binder materials keep the lithium-ion battery's electrode's active material particles together so that the electrode and contacts have a solid electrical connection. These binders are usually non-toxic and play a vital part in the battery's overall manufacturing process (Alkathy et al., 2021). The interaction between the functional groups of monomers and the template is one of the essential requirements for the efficient adsorption and selection of the metal ions Li^+ and Sr^{2+} to the imprinting material. The kind of bonding present governs interactions between monomers and templates. To imitate natural recognition mechanisms, molecular lithium-ion imprinting allows the development of highly cross-linked polymeric materials. Bio macromolecules, viruses, and even live cells may be targeted explicitly by molecularly these imprinted polymers, which have binding sites with customized selectivity. A successful imprinting procedure hinges on selecting the exemplary functional monomer, the suitable crosslinker, and the right type and specificity of template–monomer interactions (Fig. 6) (Wiśniewska et al., 2020). To improve imprint fidelity, it has been found that using a metal ion to

mediate the interaction between the monomer and template (acting as ligands) increases the selectivity of molecularly lithium imprinted polymers or gives the Polymer additional properties like stimuli-responsiveness or catalytic activity.

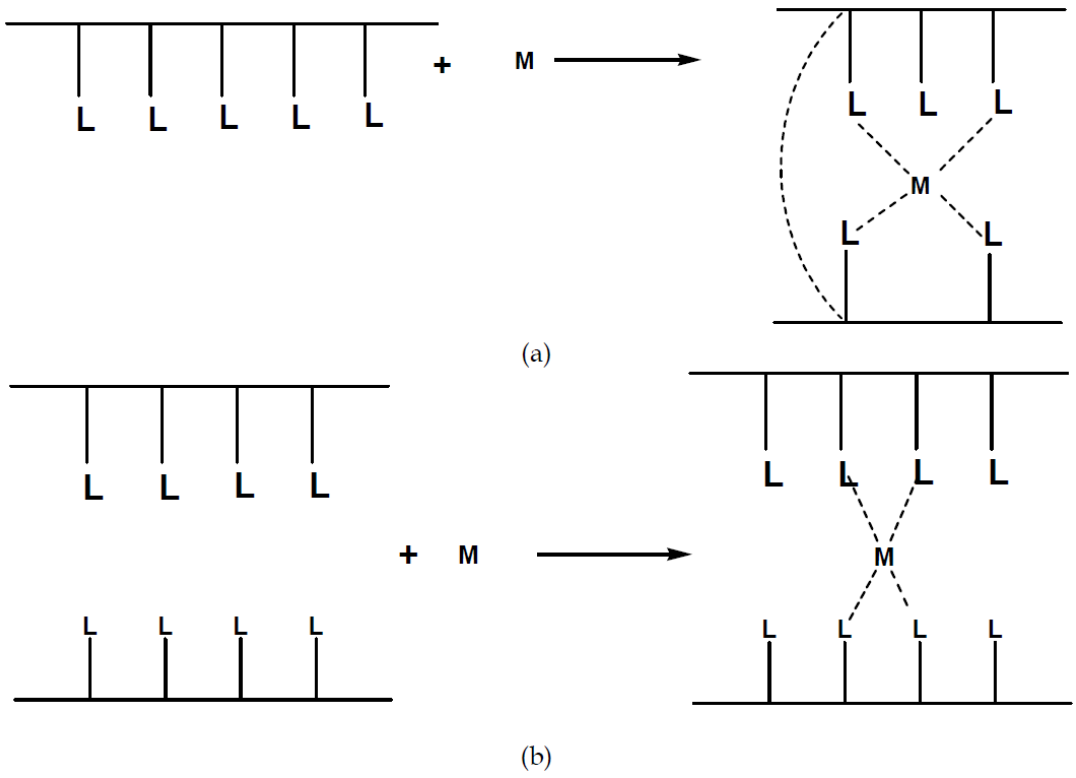

Figure 6: Polymer-metal interaction: (a) intra-molecular, and (b) inter-molecular. Where L: Coordinate atom (or) group, and M: Metal ion (El-Sonbati et al., 2012).

2.14. Thermodynamic Studies

Thermal activation of initiators necessitates the thermostability of the template. The heating technique should not be used if the molecules form a complex with template ions through hydrogen bond formation. However, low stability templates and interactions are more reliable when employing a photochemically activated initiator. Concerning aqueous solutions, the connection between equilibrium adsorption and equilibrium concentration capacity may be used

to explain an adsorption isotherm's behavior at a given temperature. Since they influence the randomness of the adsorption mechanism, lithium adsorption thermodynamic pieces of training are critical for every process of adsorption. For example, Gibb's free energy (ΔG°) is a valuable indicator of impulsive behavior (Wang et al., 2019). If ΔG° (Eq. 1) has a negative value at a particular temperature, a spontaneous reaction will occur. The heat of adsorption or enthalpy (ΔH°) and entropy (ΔS°) (Eq. 2) are essential thermodynamic measurements for enthalpy and entropy variations. Al-Ghouti and Al-Absi (2020) were used to compute the three thermodynamic properties (ΔH°, ΔG°, and ΔS°). The construction of appropriate adsorption isotherms is required for studying the adsorption route and the equilibrium connection between sorbent and sorbate. According to isotherms, the characteristics and behaviors of sorbents in various sorption systems will be suitable.

$$\Delta G^\circ = -RT\, lnk_L = \Delta H^\circ - T\Delta S^\circ \quad (1)$$

$$lnk_L = \ln\left(\frac{Q_e}{C_e}\right) = \frac{-\Delta H^\circ}{RT} + \frac{\Delta S^\circ}{R} \quad (2)$$

Since the Fermi level is so close to the d-bands of heavy alkaline earth metals, this makes them more susceptible to changes in temperature and pressure. High pressures and temperatures soften specific phonon modes, indicating that anharmonic effects may significantly influence lattice dynamics and associated characteristics. The phonon density of states must be computed for each volume to determine free energy and other thermodynamic factors using the traditional method. By combining the mean-field potential approach with the comparatively soft local pseudopotential, researchers could evaluate the free significance at various temperatures and pressures using an alternate strategy. The mean-field potential (MFP)

method and the quasi-harmonic approximation's p-dos findings for phonon frequency changes at limited temperatures are comparable (Basuki et al., 2021). The MFP method was validated to estimate the system's vibrational response at high temperatures and high pressures with the local pseudopotential. Many thermophysical characteristics of elemental strontium were investigated using this method, including the melting curve at high pressure and the temperature along with the Huguenot shock (Al-Ghouti & Al-Absi., 2020).

2.15. Adsorption Isotherms Models

Describing the phenomena of transferring a specific substance from aqueous media to a solid media at constant temperature and pH (Limousin et al., 2007). Over years, different types of adsorption isotherms can have formulated when the adsorbate is contacted with the adsorbent for sufficient time to reach the equilibrium state by adding a quantity of adsorbent into adsorbate samples at constant temperature and keeping the samples in a motion. Based on potential theory, thermodynamics, and kinetic consideration, the amount of contaminant adsorbed can describe through modeling analysis. Adsorption isotherm study is an important field in understanding the mechanism of adsorption through different models designed and done in batch adsorption systems.

2.15.1. Langmuir isotherm model

Langmuir model is a theoretical equation, which firstly refers to homogenous adsorption on the adsorbent surface and each site can only adsorb one solute molecule, secondly, only a monolayer of adsorbate is formed on the adsorbent surface, which means that no interaction happens among the adsorbate molecules on the adsorbate surface. It also decreases the intermolecular attractive forces to the increase of distance, when one molecule occupies the site.

Another assumption stated that the adsorbed molecules could transform back to the liquid phase through thermal motion.

Langmuir isotherm can be expressed in the following equation after the equilibrium state is reached (Chung et al., 2015).

$$Qe = \frac{Qm\ b\ Ce}{1+b\ Ce} \quad (3)$$

Where Q_e is the mass of adsorbed solute per the mass of the adsorbent at the equilibrium (mg/g), Q_m is the maximum capacity of the adsorption when the monolayer is complete (mg/g), C_e is the concentration of the adsorbate (mg/L), and b is Langmuir constant (L/mg).

2.15.2. Freundlich isotherm model

Freundlich model describes the most important empirical model that can be used for multilayer adsorption. It is heterogeneous adsorption of the adsorbate onto the adsorbent, and it is applied for high interactive organic compounds (Alimohammadi et al., 2017). This model of adsorption takes place on all sites of the adsorbent, the first binding will be for the stronger site, and then it exponentially decreases until the adsorption process is complete. Freundlich model does not have the restriction of the monomolecular layer, which will have no stacking of the adsorbed molecules. Freundlich isotherm can be expressed in the following equation (Dada et al., 2012).

$$Qe = Kf\ Ce^{1/n} \quad (4)$$

Where Q_e and C_e have the same meaning as in the Langmuir model equation, K_F is the Freundlich isotherm constant (mg/g) and it indicates the adsorption capacity, and n is the adsorption intensity, and as 1/n is greater in value, the adsorption will be higher.

2.15.3. Dubinin-Radushkevich model

Dubinin-Radushkevich (D-R) model is one of the empirical models that describe the adsorption on a heterogeneous surface by microporous materials, which have a carbonaceous origin. This model is based on the potential energy change between the gases, energy of the adsorbent and adsorbed phases. Moreover, it explains the overlapping of the potential fields of opposite pore walls (Nguyen & Do, 2001). As Freundlich isotherm model, Dubinin-Radushkevich failed at high pressure. Dubinin-Radushkevich model is suitable for moderate ranges of concentration, and is expressed in the following equation (Alimohammadi et al., 2017):

$$Qe = qs\, e^{-K\,\varepsilon^2} \quad (5)$$

Where Q_e has the same meaning as in the Langmuir model equation and Freundlich model equation, q_s is the theoretical isotherm saturation capacity (mg/g), K is the adsorption energy constant, and ε is Dubinin-Radushkevich isotherm constant.

2.16. Analytical Techniques for IIP Characterization

2.16.1. Scanning Electron Microscope (SEM) and Transmission Electron Microscope (TEM)

2.16.1.1. SEM and TEM Utilization

The scanning electron microscope (SEM) is a class of electron microscope used to examine the exterior of solid materials. At the same time, the transmission electron microscope is a quantifying technique with a high magnification that utilizes the transference electrons to generate an image. The primary variation between scanning electron microscope (SEM) and transmission electron microscope (TEM) is that SEM images are generated from detecting knocked of electron while TEM utilizes electrons that are Trans versing through the examined material (Shariatinia, 2014).

Scanning electron microscopy (SEM) requires a milligram amount of samples to be examined to establish the shape, texture, and size. A thin stream of electrons is transverse through the material in a sequence of collateral tracks. These electrons associate themselves with the sample and generate various signals that can be exposed and presented on the monitor of the cathode ray tube. Hence, particles as minimum as 1 nm can be observed, and the exterior surface information can be produced. SEM needs critical specimen preparation compared to optical microscopy, and it cannot differentiate between crystalline and non-crystalline samples (Sarabadani et al., 2014).

2.16.1.2. Technique Implementation

In an analytical experiment to characterize a nanocomposite lithium ion-imprinted polymer $Li[Li_{0.2}Ni_{0.2}Mn_{0.6}]O_2$, the cathode material was alga mated by utilizing a solid-state technique that was a prerequisite in acids. It was characterized by using SEM and TEM. After the experiment, it was discovered that the first effluence efficiency of $Li[Li_{0.2}Ni_{0.2}Mn_{0.6}]O_2$ after preconditioning in acid had been substantially enhanced. However, the mid voltage had significantly reduced. The main cause of acid filtrate modification was accredited to the aspect of the spinel structure

$Li_4Mn_5O_{12}$ that was filled in lithium ion-imprinted polymer (Babu et al., 2017).

2.16.2. Fourier-transform Infrared Spectrophotometer (FTIR)

2.16.2.1. FTIR Utilization

The FTIR is used to acquire the optical spectrum of immersion, secretion, and photoconductivity of gases, liquids, and solids. It is used in exposing various categories of PHB. This is a powerful technique used to recognize distinctive functional groups from the spectral bands to explore the amalgamation between the nanomaterial and the immersed biomolecules (Mahamuni, 2009).

FTIR spectrum evaluation examines the chemical composition of the available group in the specimen. It examines the association between the electromagnetic (EM) fields in the optical regions and matter. FTIR characterizes a polymer by bracing the molecular vibrations with the EM waves in the optical region. In simple terms, it characterizes an ion-imprinted polymer by gripping the infrared region radiation, thus stirring the particles to an elevated vibrational state. Since the primary objective of FTIR spectroscopy is to obtain the chemical functional class in the specimen, it ensures that the elemental frequencies of the infrared radiation are encompassed by the various functional classes (Mourdikoudis et al., 2018).

2.16.2.2. Technique Implementation

In the synthesis and characterization of metal ion-imprinted polymers, FT-IR was utilized for characterization. Each metal ion-imprinted polymer noted a C-H strong alkane with a broadening stripe in the FTIR evaluation 2956 cm^{-1}. This observation highlighted that the C-H strong alkane occurred in the ion-imprinted polymers at this particular wavenumber intensively.

In addition, the analysis by FTIR led to the observation of a strong carbonyl C=O, C=C alterable alkane, and an N-H strong amid broadening were also significantly observed (Işıkver & Baylav, 2018).

2.16.3. X-Ray Diffraction (XRD)

2.16.3.1. XRD Utilization

XRD is a rapid inquisitive method mainly utilized to recognize crystalline material. X-ray diffraction is a versatile technique that dispenses chemical information for fundamental evaluation and time analysis. In addition, the technique is quite useful for quantifying stress and texture evaluation (Ghodke, 2021).

In XRD characterization of polymers, the latter variable is approximated by utilizing the Scherer equation by applying an intensified peak of an XRD estimation to a particular specimen. The constituents of the molecules are established by contrasting the location and vigor of the peaks in relation to the various patterns in place in the international center for diffraction data (ICDD) (Mourdikoudis et al., 2018).

2.16.3.2. Technique Implementation

XRD was used to characterize the polymers in a study on the amalgamation and classification of metal ion-imprinted polymers. In the XRD evaluation, the patterns of the polymers and imprinted ions were obtained and displayed. An angular position was used to characterize the XRD patterns. It was observed that values of $2\theta = 16.5, 18.6, 29.2, 32.8, 35.5, 37.5$ were found to be diffraction peaks in XRD patterns of $NiCI_2.6H_2O$ salts. These peaks were also evident in the unleached polymers, but it was not very significant due to the amorphous nature of the polymers

(Işıkver & Baylav, 2018).

2.16.4. Thermogravimetric analysis (TGA)

2.16.4.1. TGA Utilization

This is an inquisitive method in which the mass of a specimen is quantified over time while observing the temperature changes. TGA detects the weight change that transpires when the compound is exposed to heat at a constant rate. After pretreatment, it is used to evaluate biochemical constituents such as lignin, cellulose, hemicellulose of beech wood, alkaline, lignin, and switch grass (Brittain, 2020).

In this method, a nanomaterial specimen is heated and its constituents with various degradation temperatures leading to vaporization and degrading of the component, thus resulting in a mass change. The new temperature and the decrease in mass are taken into account by the TGA equipment. In addition, the beginning specimen mass recorded and the category and amount of the Nanoparticles organic ligands are also established (Mourdikoudis et al., 2018).

2.16.4.2. Technique Implementation

TGA was utilized to characterize metal ion-imprinted polymers in the synthesis and characterization. The TGA thermograms were able to detect thermal degradation characteristics in the polymers. The observation showed that the control polymer (without metal ion) and the percolated IIP polymers had a one-step thermal disintegration process. On the other hand, the unleached IIP polymers had a two-step thermal disintegration process. These findings signified that leaching is an effective process in removing IIP polymers metal ions. Moreover, the unleached polymer has elevated temperature levels compared to leached polymers. This is attributed to the metal ion concentration (Işıkver & Baylav, 2018).

2.16.5. Energy Dispersive X-Ray Analysis (EDX)

2.16.5.1. EDX Utilization

EDX is a curious technique used to inquire about the constituents of solid materials (Titus et al., 2019). The information created by the EDX evaluation encompasses the spectra that display peaks that help in establishing the true constituents of the specimen being evaluated (Girão et al., 2017).

X-rays have elevated energetic photons, which can be attributed to the electronic transference that occurs in the atoms of a selected specimen due to an applied incident electron beam. To characterize the polymer, the incident electron comes into contact with the sample's atoms and strikes out an electron from the K-Shell of the sample, thus resulting in a vacancy in the shell. If an electron from a different shell occupies the hole, then x rays are emitted. The effused electron spectrum released by the sample dispenses both theoretical and mathematical information, thus enabling the exposure of the elements located in the sample (Girão et al., 2017).

2.16.5.2. Technique Implementation

Energy dispersive spectroscopy was used in examining the structure and electrochemical performance of the composite $Li_4Ti_5O_{12}/Cu_2O$. After applying elevated heat levels, the composite was initially formed by ball grinding $Li_4Ti_5O_{12}$ and Cu_2O. The results showed that the $Li_4Ti_5O_{12}/Cu_2O$ composite displayed elevated rates of capability and increased volume power compared to $Li_4Ti_5O_{12}$. The effluent volume of the composite was found to be at a 2 °C rate, which sharply raised to 122.4-mAh g^{-1} after 300 cycles. The composite also had a volume retention of 91.3%, which was quite elevated compared to $Li_4Ti_5O_{12}$ (89.6 mAh g^{-1}) (Babu et al., 2017).

2.16.6. Zeta Potential

2.16.6.1. Zeta Potential Utilization

The physical attributes of nanoparticles and suspension highly depend on the essence and degree of the particle liquid surface. The characteristic of aqueous dissemination between the particles and liquid is certainly delicate to the ionic and electrical formation of the interface. The zeta potential is a variable that quantifies the electrochemical equipoise at the particle liquid surface. It computes the immensity of the electrostatic repulsion or attraction between the particles (Mourdikoudis et al., 2018).

Zeta potential utilizes two techniques: electrophoretic light scattering and electroacoustic determination. It is a crucial measure of the sturdiness of colloidal dispersions. To characterize polymers, elevated positive and negative charged molecules are inclined to repel each other. These results in sturdy colloidal solutions, which display a minimal tendency to agglomerate. These elevated charged molecules are associated with pH values distant from the "isoelectric point" of a solution. This refers to the pH of the solution being zero at the zeta potential (Mourdikoudis et al., 2018).

3. METHODOLOGY:

3.1. Lithium Ion-Imprinted Polymer Preparation (Li-IIP)

The precipitation polymerization technique was done using the method developed by Hashemi et al. (2016) methodology with some modification to prepare lithium IIP (Fig. 7). In a 50 mL glass bottle, 20 mL of acetonitrile was added with 74.5 mg of Dicyclohexano-18-crown-6 and 21.28 mg of $LiClO_4$ dissolved in it for 20 minutes at room temperature and sonicated with an ultra-sonicator (Grant XUB series, digital ultrasonic bath). Then 792.9 mg ethylene glycol dimethacrylate (EGDMA) (Crosslinker), 128.17 mg tertbutyl acrylate (monomer), and 25 mg of potassium persulfate were mixed with the previous solution and sonicated at again 25^{o}C. It was then purged with N_2 for 10 minutes, sealed, and thermally polymerized in an oil bath at 65°C for 24 hours. Following 24 hours, the polymer was filtered to discard the solvents. Then, the powder IIP was washed with methanol to remove the un-reacted materials and leached with 1 mol/L HNO_3 until the washed solution was free from lithium ions. Lastly, the lithium IIP was washed with distilled water until it reaches neutral pH. The final IIP should be fully dried.

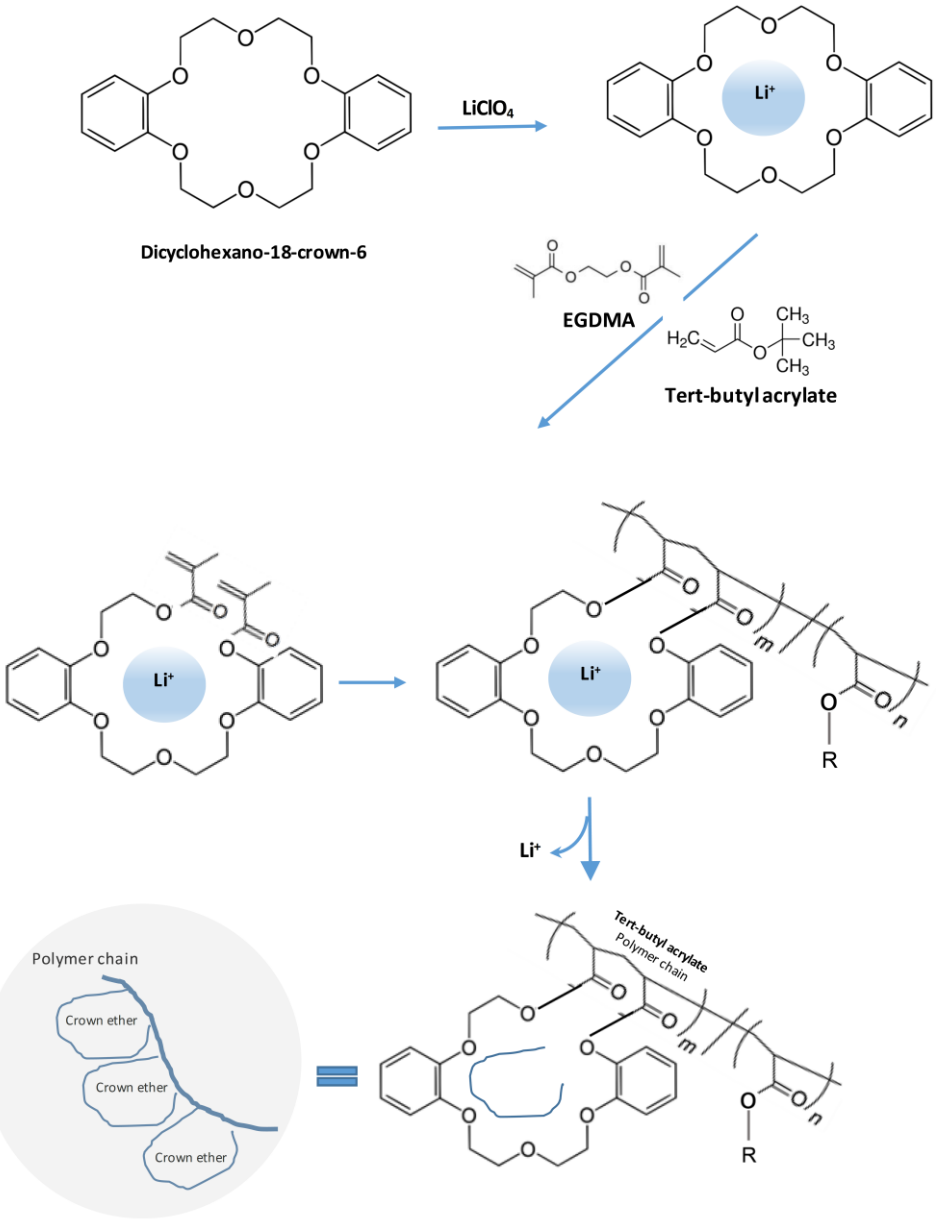

Figure 7: Scheme of lithium ion-imprinted polymer synthesis.

3.2. Physical and Chemical Characterization of the Ion imprinted polymer

The prepared ion-imprinted polymer was characterized before and after adsorption using a scanning electron microscope (SEM) (Nova^{TM} Nano SEM 450 – FEI), transmission electron

microscopy (TEM) (TEM TECNAI G2, TF20 – FEI), Fourier-transform infrared spectrophotometer (FTIR) (PerkinElmer, spectrum range: 400 cm^{-1} to 4000 cm^{-1}), and X-ray diffraction (XRD) (Empyrean XRD platform and PIXcel^{1D} detector). Specific surface area and pore size distribution were determined by Brunauer-Emmett-Teller (BET) (Quantachrome Corporation, Nova 3000). Energy Dispersive X-Ray Analysis (EDX) was also done to identify the elemental composition of the imprinted polymer, and X-ray photoelectron spectroscopy (XPS) (Ultra DLD XPS Kratos) was used to quantify the surface composition of the polymer.

3.3. Optimizing the experimental conditions

To optimize the adsorption batch experimental conditions, stock solutions of lithium (100 ppm) and strontium (100 ppm) ions were prepared. Then, the optimized experimental conditions were applied to the real brine sample.

3.3.1. Effect of pH

To investigate the effect of pH on the adsorption processes, batch adsorption experiments were carried out at different pH values (2, 4, 6, 8, and 10). 10 mg of IIP was added to 30 ml from each different pH values solution with continuous shaking for 24 hours, the solution was filtrated after adsorption, and both the treated solution and the IIP were preserved separately for further testing.

3.3.2. Effect of concentration

To investigate the effect of initial ions concentration on the adsorption processes, the stock solutions of Li^{+} and Sr^{2+} were prepared to different concentrations, namely (0 (control), 5, 15, 30, 45, 60, 75, 90, 100 ppm or mg/L). 10 mg of IIP was added to 30 ml from each diluted solution

with continuous shaking for 24 hours, the solution was filtrated after adsorption, and both the treated solution and the IIP were preserved separately for further testing.

3.3.3. Effect of Temperature

To test the effect of solution temperature on the adsorption experiment, the adsorption experiment was done at different temperatures (25°C, 35°C, and 45°C). 10 mg of IIP was added to 30 mL solution with continuous shaking in an incubator shaker (Shel-lab SSI10R-2, Orbital-Shakin) for 24 hours under different temperatures, the solution was filtrated after adsorption, and both the treated solution and the IIP was preserved separately for further testing.

3.3.4. Verifying the optimized experimental conditions

The concentrations of Li^+ and Sr^{2+} were tested using inductively coupled plasma (ICP) (ICP-OES Optima 7300 DV – PerkinElmer) to find out the amount of lithium and strontium adsorbed under different conditions and to decide the optimum conditions for the following experiments.

3.4. Isotherm Models

The experimental data is used to fit the different isotherm models using the following equations:

Langmuir model: $Qe = \frac{Qm\ b\ Ce}{1+b\ Ce}$ (6)

Where Q_e is the amount of metal adsorbed per gram of adsorption (mg/g), C_e is the equilibrium concentration of adsorbate (mg/l), Q_m is maximum adsorption capacity (mg/g)

(constant), and b is Langmuir constant.

Freundlich model: $Qe = Kf\ Ce^{1/n}$ (7)

Where Q_e is the amount of metal adsorbed per gram of adsorbate at equilibrium (mg/g), C_e is the equilibrium concentration of adsorbate (mg/L), K_F is Freundlich isotherm constant (mg/g), and n is adsorption intensity.

Dubinin-Radushkevich model: $Qe = qs\ e^{-K\ \varepsilon^2}$ (8)

Where Q_e is the amount of adsorbate in the adsorbent at equilibrium (mg/g), q_s is theoretical isotherm saturation capacity (mg/g), K is adsorption energy constant, and ε is Dubinin-Radushkevich isotherm constant, which can be calculated by RT ln $[1+\frac{1}{C_e}]$, where R is the gas constant (8.314 J/mol K), T is the absolute temperature (K) and C_e is the adsorbate equilibrium concentration (mg/l).

Temkin model: $Qe = \frac{RT}{Bt}\ln(At\ Ce)$ (9)

Where Q_e amount of adsorbate in the adsorbent at equilibrium (mg/g), C_e - equilibrium concentration of the adsorbate (mg/l), A_T - Temkin isotherm equilibrium binding constant (L/g), and B_T - Temkin isotherm constant, where R is the gas constant (8.314 J/mol K), and T is the absolute temperature (K).

To fit the isotherm equation, some parameters should be calculated by linearizing the isotherm models. To linearize the isotherm models, Table 4 is used to draw the graphs of each model. Then from the linear plotting equation, the models' parameters are calculated as shown in

table 5.

Table 4: Isotherm models linearization graph axis.

The Isotherm Model	X-axis Vs Y-axis
Langmuir isotherm model:	1/ce (x-axis) Vs. 1/qe (y-axis)
Freundlich isotherm model:	ln(ce) (x-axis) Vs. ln(qe) (y-axis)
D-R isotherm model:	e^2 (x-axis) Vs. ln(qe) (y-axis)
Temkin isotherm model:	ln(ce) (x-axis) Vs. qe (y-axis)

Table 5: Calculating the model parameters from the liner plotting equation.

Model	Langmuir	Freundlich	D-R	Temkin
Parameters	Q_m = 1/intercept	n = 1/slop	q_s = e^intercept	A_t = e^ intercept / slop
	b = 1/slop*Q_m	K_f = e^intercept	K = slop	B_t = (RT/B) where B=slop

3.5. Batch Desorption Experiment / Adsorption-Desorption Experiment

The IIP previously dried and kept from the previous isotherm experiments were used in this experiment to test the Li^+ recovery ability from IIP. The used IIP samples were washed with 10 mL of 0.5 mol/L HNO_3 with continuous shaking for 24 hours at room temperature. Using ICP, the eluted ions concentrations were measured.

To calculate the recovered % of ions from the IIP, first, the amount of ion adsorbed on the IIP was calculated by subtracting the final concentration from the initial concentration($Co - Ce$). Then the recovery % was determined as follows:

$$R\% = \frac{Eluted\ ions\ concentration}{Co-Ce} \times 100 \quad (10)$$

A second adsorption-desorption cycle is run in the same used IIP after drying from the desorption experiment, performing the same adsorption steps as in section 3.3.2 and a second batch

desorption experiment. The difference between the adsorption capacities is used to evaluate the IIP regeneration performance.

3.6. Batch Adsorption Experiment – real brine sample

The following batch method was used to investigate the adsorption of Li^+ ions and the selectivity toward Sr^{2+} ions by the prepared Li^+ ion-imprinted polymers. 10 mg of IIP was added to 30 mL brine in the batch experiment. 0.5 mol/L HNO_3 was used to keep the pH around the optimized pH.

To calculate the adsorption removal percentage of IIP to adsorb lithium and strontium ions, the initial concentration (Co), and equilibrium concentrations (Ce) will be compared as follows:

$$AR\% = \frac{(Co-Ce)}{Ci} \times 100 \quad (11)$$

The IIP particles' adsorption capacity (mg/g) in relation to the imprint metal ion will be determined as follows:

$$Qe = (Co - Ce)\left(\frac{V}{m}\right) \quad (12)$$

Where V is the volume of the brine (L), and m is the mass of the IIP used (g).

3.7. Statistical Analysis

The statistical analysis was generated using MINITAB statistical analysis software. Two-way ANOVA was calculated using the temperature and initial concentration as two independent factors, to determine the significance of each factor from the P (probability) -value. Tukey grouping method with a 95% confidence level was also used to determine the significant difference between each value within the factor. Furthermore, factorial plots were drawn for Qe main factors and interaction plots to understand if the factors are dependent or independent.

4. RESULTS AND DISCUSSION:

4.1. Ion-Imprinted Polymer physicochemical Characterization

The prepared ion-imprinted polymer was characterized using a scanning electron microscope (SEM), transmission electron microscopy (TEM), Fourier-transform infrared spectrophotometer (FTIR), and X-ray diffraction (XRD) to study the morphology of the adsorbents and their functional groups. Specific surface area and pore radius was determined by Brunauer-Emmett-Teller (BET). Energy Dispersive X-ray Analysis (EDX) was also done to identify the elemental composition of the imprinted polymer and X-ray photoelectron spectroscopy (XPS) was used to quantify the surface composition of the polymer.

4.1.1. Scanning Electron Microscope (SEM) and Transmission Electron Microscopy (TEM)

The characteristics of IIPs, like other metal-ion sorbents, are closely connected to their morphology: their form and porous structure. Figure 8 shows the SEM images of the prepared polymer before adsorption and after adsorption of lithium and strontium showing their morphology at 5μm in 20.00 KX magnification.

The SEM scans of the polymer revealed an irregular spherical shape of the polymer with a very regular porous and consistent surface structure of the IIP, with a rough and mound surface. On the surfaces of the polymers, there exist local pores, which are evenly dispersed. It is noticed that the leached IIP has a rough and porous surface, which indicates empty binding sites for the target ions with an increase in the surface area to improve the adsorption and facilitate the capture of targeted ions. The removal of the template ion increases the roughness of the surface of the imprinted polymer (Branger et al., 2013). Long et al. (2016) refer that the polymer particles have

a spherical shape because of the mechanism of precipitation polymerization. In addition, Xu and Guo (2012) explain that the porous texture aids in increasing the adsorption superficial area and exposes the surface binding sites.

The BET results show that the multi-point specific surface area (SSA) is 40.80 m^2/g and Barrett–Joyner–Halenda (BJH) adsorption average pore radius is 4.83 nm. Compered to Al-Ajji and Al-Ghouti (2021) hazelnut shell adsorbent with 3.7 m^2/g SSA and 50.6 nm pore radius size, it can be noticed that the IIP had more than 10 times larder SSA with pore radius sizes that are smaller by more than 10 times. This indicates that the IIP is highly porous with small pores that increase the surface area and roughness of the surface. On the other hand, copper IIP has 93.2 m^2/g SSA and a 9.5 nm pore radius size (Xu & Guo, 2012), which is double the Li IIP values. This could be due to the fact that Li^+ is much smaller than Cu^{2+}, which in consequence will have an effect on the IIP structural sizes while preparing it using the ion templets. This fact was also shown in the cobalt IIP and nickel IIP, where the IIPs had 74.94 m^2/g and 89.04 m^2/g SSA and 9.3 nm and 12.4 nm pore radius size respectively (Zhao et al., 2022; Zhao et al., 2021). This could be as a result of the fact that both Co^{2+} and Ni^{+2} are also bigger than Li^+, where they have almost the same size as Cu^{2+}.

The SEM images show a significant difference in morphology observed between the leached IIP and unleached IIP. The lithium adsorption on IIPs causes a visual change in the surface structure (Fig. 8B), while strontium adsorption SEM images and the leached IIPs are similar to each other in the context of the polymer surface roughness. The adsorption of lithium as a target ion used in the polymerization can be the cause of the morphological variations between them.

Unleached Li-IIPs reveal more than the target ion, which is bonded evenly in SEM images. Due to the bounded lithium ions, a rough and aggregated structure was seen on the surface of

unleached IIPs (Işıkver & Baylav, 2018).

Because leached IIPs are results of cross-linking and imprinting processes, which increase the adsorption surface area and provide open areas on the surface permitting binding, there are numerous micropores on the surface of leached IIPs, allowing the target ion to bind readily (Işıkver & Baylav, 2018).

To investigate the microstructure of the IIP, a further step was taken by using the TEM. Figure 9 shows the TEM image of the pure IIP before adsorption, and after adsorption of Li^+ and Sr^{2+}. As in the SEM image, the TEM image of IIP after strontium adsorption and the pure IIP TEM image are similar to each other, and nothing major is observed. While the after Li^+ adsorption IIP TEM images can clearly show the adsorption of the lithium ions in a multilayer behavior with the interaction between the ions. This indicates that Freundlich isotherm adsorption behavior is expected.

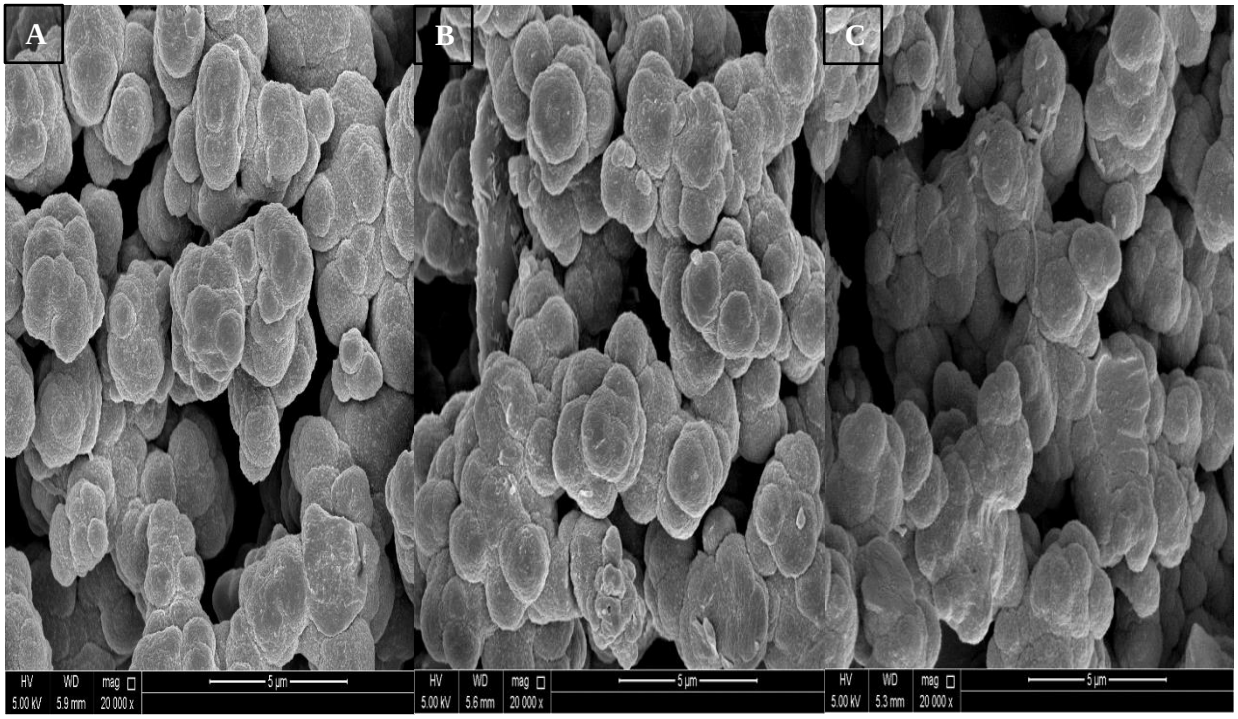

Figure 8: SEM image of IIP (A) Before adsorption, (B) After Li^+ adsorption, and (C) After Sr^{2+}

adsorption.

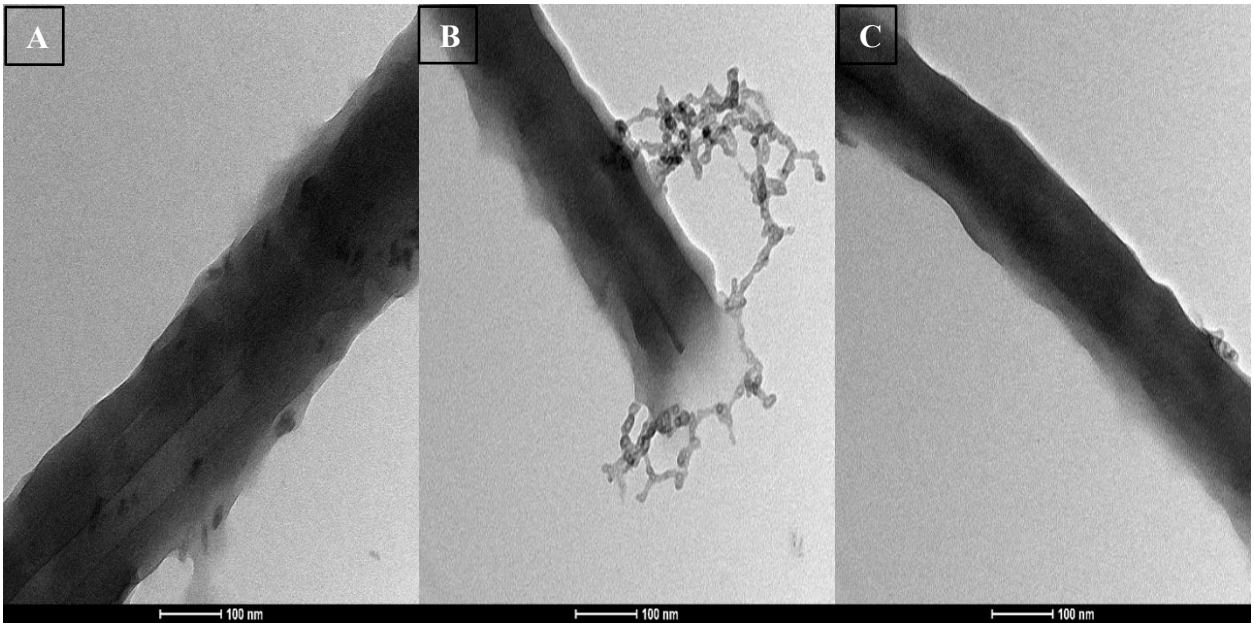

Figure 9: TEM image of IIP (A) Before adsorption, (B) After Li^+ adsorption, and (C) After Sr^{2+} adsorption.

4.1.2. Fourier-Transform Infrared Spectroscopy (FTIR)

The prepared ion-imprinted polymer was characterized using FTIR to study the adsorbent functional groups. Figure 10 shows the FTIR spectra were the adsorption due C–O stretch (alkyl-substituted ether) (1140 cm^{-1}), C–O bend (aromatic ethers) (1250 cm^{-1}), -CH_3 (methyl) (1390 cm^{-1}), N-H stretch (Amide) (1459 cm^{-1}), C=O stretch (Carbonyl) (1720 cm^{-1}), C–H (aliphatic) strong alkane stretch (2993 cm^{-1}), and normal ‘‘polymeric’’ OH stretch (broad) (3400 cm^{-1}) were observed.

The prepared Li^+ ion-imprinted polymers spectra results were compared with the Li^+ ion-imprinted polymers prepared by Hashemi et al. (2016) FT-IR spectra. The spectrum shows closely similar functional groups, where they contain C=O stretch, C–O stretch, C–O bend, C–H stretch, -CH_3 bend, and N-H stretch.

According to Işıkver and Baylav (2018), the strong C–O stretching band at 1150 cm^{-1} appears because of the monomers in the polymeric structure bearing –COOH groups. It was also recognized that the C–H strong alkane stretching band at approximately 2950 cm^{-1} wavenumber was identified in all-metal ion-imprinted polymers, which was observed in the prepared IIP at wavenumber 2993 cm^{-1} This accentuates the presence of the C–H group in the group polymers at this wavenumber. Moreover, strong carbonyl C=O stretching and N–H strong amide stretching bands were also found in all the polymers (Işıkver & Baylav, 2018).

Hashemi et al. (2016) study compared the unleached and the leached ion-imprinted polymer FT-IR spectra. The comparison shows that the leaching process does not affect the functional groups of the IIP, suggesting that the IIP is reproducible. In addition, in Işıkver and Baylav (2018) experiments, they compare the leached IIP and the control polymer spectra, it was found that they show a similar spectrum, which indicates that the leaching process is considered to cause no damage to the polymer network while removing the ions. This explains the fact that the spectrum of the IIP before adsorption (leached) and after adsorption of Li and Sr (unleached) were similar (Fig. 10).

A close interpretation of the spectra (Fig. 11) revealed that there are not many differences between the spectral features and the functional groups of the IIP before adsorption and after adsorption, except some changes in the transmittance percent of some bands as well as some slight shifts in the exact position of the bands, which was noticed mostly in the after Li^+ adsorption IIP. This change proposes that the structure of the IIP shows the effects on the exact position of the bands and shifts in the bands when the internal structure is changed while capturing the Li^+ ions.

The FTIR are generally sub-divided to four main region including: fingerprint region (500 cm^{-1} to 1500 cm^{-1}), double bond region (1500 cm^{-1} to 2000 cm^{-1}), triple bond region (2000 cm^{-1} to

2500 cm^{-1}) and single bond stretch region (2500 cm^{-1} to 4000 cm^{-1}). Figure 11 shows a zoomed view of the major peaks in each region. It was noticed generally that the FTIR after Li^+ adsorption is obviously different from the IIP before adsorption and IIP after adsorption of Sr^{2+}. This indicates that the IIP after Sr^{2+} adsorption is actually rarely adsorbing an ion, which means that the binding sites are still empty as much as it was before adsorption. This supports the theory that the IIP was designed with a templet of lithium ions to be selective for lithium recovery. In the fingerprint region (Fig. 11A) and the double bond region (Fig. 11B), it was observed that the after Li^+ adsorption peaks were shifted. The C-O stretch peak at 1140 cm^{-1}, which appears because of the monomers in the polymeric structure bearing –COOH groups were shifted from 1140 cm^{-1} before adsorption to 1145 cm^{-1}, and it was wider and less transmitted. This could be due to the interaction of the lithium ions with the monomer when it was captured in the binding sites. The carbonyl C=O stretch at 1720 cm^{-1} was also wider, less transmitted, and shifted from 1720 cm^{-1} before adsorption to 1723 cm^{-1} after Li^+ adsorption. In the case of the C–H (Aliphatic), strong alkane stretch (2993 cm^{-1}), and Normal ‘‘polymeric’’ OH stretch (3400 cm^{-1}) were observed. After Li^+ adsorption peaks are still less transmitted and wider, but it was also noted that the peaks of the IIP before adsorption is smothered than the peaks after adsorption of both Li^+ and Sr^{2+}, and the after Sr^{2+} adsorption peaks are a bit wider than the peaks before adsorption. This is due to the fact that there is adsorption even if it is a small quantity, which indicates that this small quantity affects the single bonds in opposite to the other bonds.

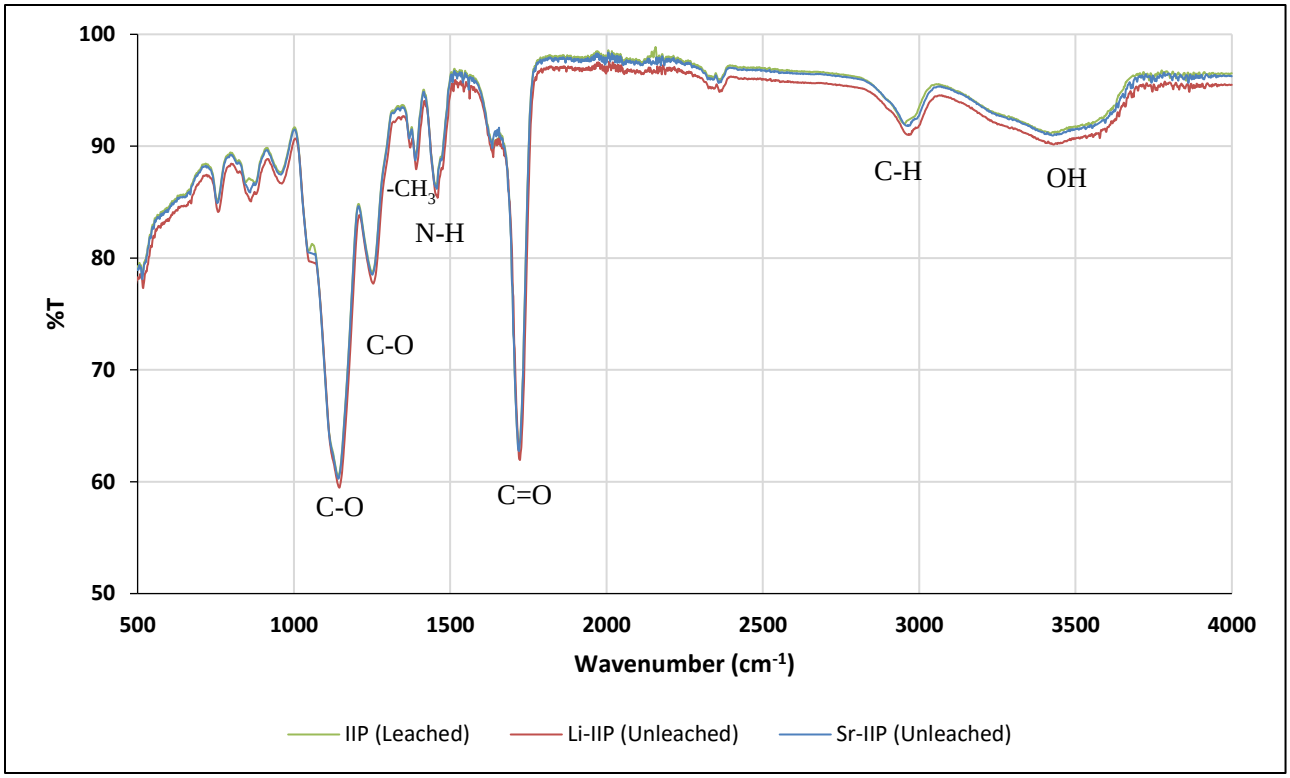

Figure 10: Fourier-transform infrared (FTIR) Spectrum of IIP.

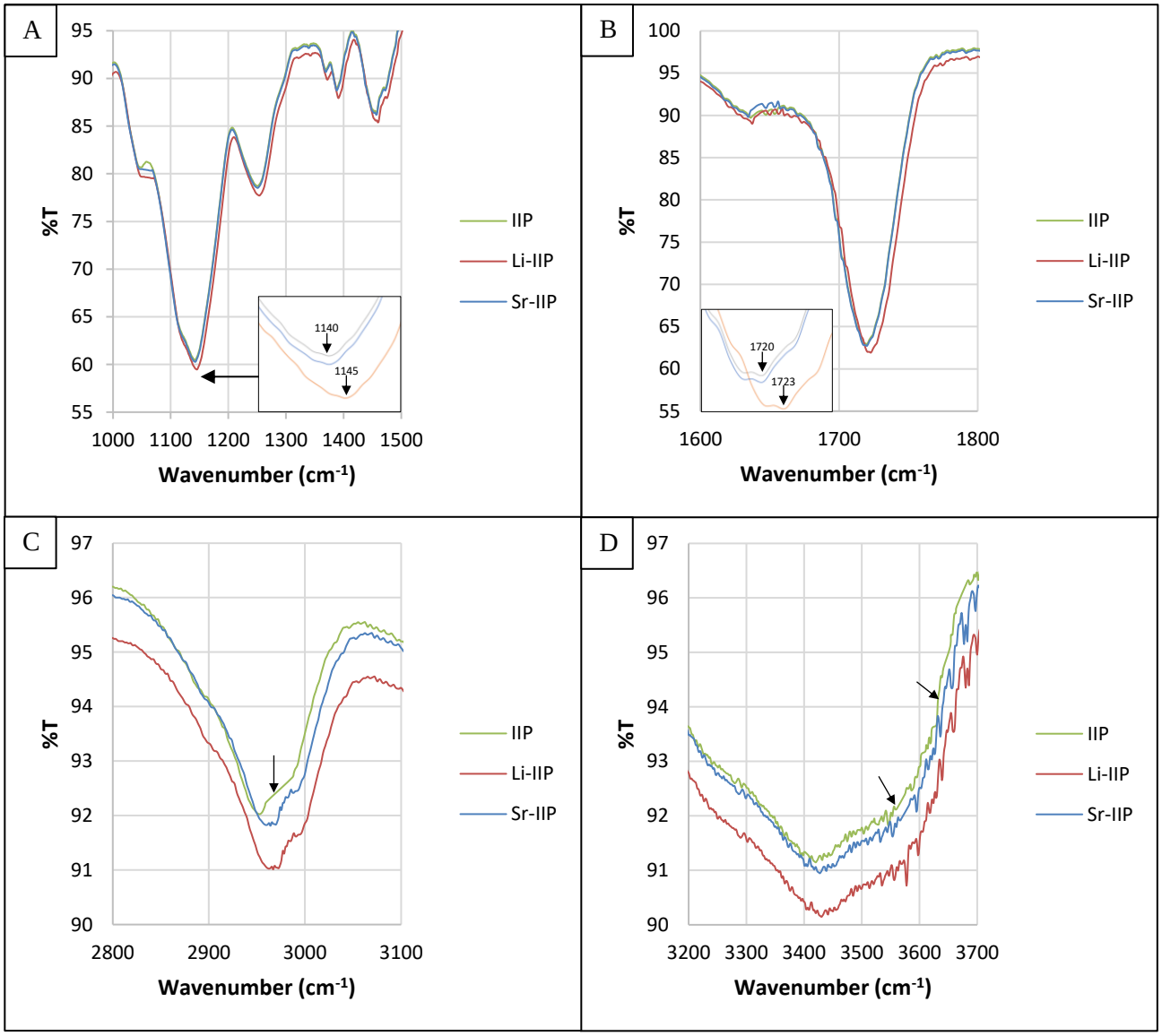

Figure 11: FTIR spectra sub-regions major peaks (A) fingerprint region 1000 cm^{-1} to 1500 cm^{-1} (B) double bond region 1500 cm^{-1} to 1800 cm^{-1}band (C) C-H (Aliphatic) strong alkane stretch 2800 cm^{-1} to 3100 cm^{-1} and (D) Normal "Polymeric" OH stretch 3200 cm^{-1} to 3700 cm^{-1}.

4.1.3. X-Ray Diffraction (XRD), Energy Dispersive X-Ray (EDX), and X-ray photoelectron spectroscopy (XPS).

To evaluate the existence or absence of lithium and strontium ions in the ion-imprinted polymer matrix before and after adsorption, different kind of X-ray spectroscopy analysis (X-ray

diffraction (XRD), energy dispersive X-ray (EDX), and X-ray photoelectron spectroscopy (XPS)) was investigated.

In the first X-ray spectroscopy analysis, the XRD diffractogram of the IIP (Fig. 12) shows similar patterns before and after adsorption, except for a few peaks at 2θ = 32.67, 36.15, 51.55, and 64.82 degrees. These intense diffracted peaks in the after Li^+ adsorption pattern are corresponding to lithium, which indicates the adsorption of the lithium ions on the IIP. Trivedi et al. (2015) studied the properties of the lithium powder. The XRD diffractogram of lithium samples shows peaks at 2θ = 32.67, 36.15, 52.16, 64.56, 64.84, and 65.02 degrees, this confirms that the intense peaks are a result of the presence of lithium in the sample. In addition, as these peaks are not shown in the leached IIP, this insure that the lithium ions used as a template in the preparation steps of the IIP were completely washed off leaving available imprinted sites for lithium. Moreover, there is a small intense peak at 2θ = 31.08 degrees in the after Sr adsorption diffractogram, this can be corresponding to the small amount of strontium adsorbed by the IIP. Boanini et al. (2019) analyzed the XRD pattern of strontium in a study comparing strontium and zinc substitution in β-tricalcium phosphate. They found that the strontium showed a very intense peak at 2θ around 31 degrees. This agreed that the diffracted peak at 31.08 is corresponding to strontium.

The characterization of metal ion-imprinted polymers using XRD was done by Işıkver and Baylav (2018) for the nickel IIP and cobalt IIP experiments and in Behbahani et al. (2012) for the nickel nanostructured IIP. In all of those metal ion-imprinted polymers, the XRD pattern of the leached and unleached IIP was similar except in a few peaks corresponding to the metal used in the IIP preparation. Moreover, it can be noticed that the ion-imprinted polymers generally show closely similar XRD diffractogram that is highly zigzag due to the polymer amorphous nature

(Işıkver & Baylav, 2018).

Moreover, when the material is more amorphous it shows higher diffraction intensity (Yang et al., 2018), this can explain the fact that it can be noticed that the IIP before adsorption has a higher intensity, followed by the IIP after Sr^{2+} adsorption, then the IIP after Li^{+} adsorption. This is mainly because the IIP before adsorption has a more imprinted binding site and is rougher as shown before in the SEM surface image. The IIP after Li^{+} adsorption is smother, as the Li^{+} occupy most of the imprinted binding sites, and the IIP after Sr^{2+} adsorption is just in between both of them, as the IIP was designed to selectively adsorb lithium ions, but this did not eliminate the fact that some other ion can be adsorbed rarely.

In the second spectroscopy analysis, the EDX spectrum of the IIP before adsorption (Fig. 13A) shows that the IIP is composed mainly of carbon, oxygen, and a trace amount of chloride. The element composition weight percentage in Table 6 shows that 73.27% of the IIP is composed of carbon, 25.30% is composed of oxygen and the other 1.43% is chloride. It is noticed that the ion-imprinted polymer is totally free of lithium, which indicates that the lithium was leached perfectly, while a small amount of chloride was indicated, which is most probably due to the lithium chloride used to prepare the IIP.

The EDX spectrum after lithium adsorption (Fig. 13B) shows a good peak corresponding to lithium in the composition of the IIP, indicating successful lithium adsorption. On the other hand, the EDX spectrum after strontium adsorption (Fig. 13C) shows a very small peak corresponding to strontium, which means that the IIP was not able to adsorb strontium in the same efficiency of adsorbing lithium. In addition, it was observed that there is a peak corresponding to calcium in the after adsorption spectra, this could be due to a random error in the used distilled water purification system, which lead to the availability of calcium ions as a competitor to be

adsorbed.

Branger et al. (2013) mentioned the use of EDX spectroscopy to analyze polymers used to adsorb Cu(II) ions before and after extraction. It was stated that the EDX is capable to show the ions in the surface and the core of the polymer, and their results show the clear decrease in the Cu(II) ions composition after leaching it from the polymer particles. Also, in an experiment to selectively remove Cr(VI) using IIP grafted on the electrospun nanofibrous mat of functionalized polyacrylonitrile (FPANFM) (Hassanzadeh et al., 2018), the EDX spectroscopy analysis was used. It was characterized the composition of the IIP before and after the removal of the Cr(VI) ions, but it was further employed to verify the existence of the FPANFM structure in the IIP to confirm the successful preparation of IIP-functionalized-PANFM. Liu et al. (2015) also used the EDX to confirm the successful imprint of the nickel in the ion-imprinted polymer while preparing it based on graphene oxide/SiO_2

In the third spectroscopy analysis, the XPS spectrum of the IIP before adsorption (Fig. 14A) shows that the IIP is composed mainly of carbon and oxygen. The XPS surface quantification of the IIP is shown in table 7. The mass concentration shows that 69.96% of the IIP is composed of carbon, 29.28% is composed of oxygen and the other 0.76% is lithium. It is noticed that even though, there is no peak corresponding to lithium in the XPS spectrum, it was detected in the surface quantification. This could be a leftover that was not totally leached while preparing the IIP. It was a very trace percentage, which is acceptable.

After lithium adsorption, the XPS spectrum (Fig. 14B) shows a peak corresponding to lithium in the surface composition of the IIP, assuring that the lithium was efficiently adsorbed. On the other hand, the XPS spectrum after strontium adsorption (Fig. 14C) is not showing any peak corresponding to strontium, which means that the IIP was not able to adsorb strontium in a

detectable amount, as the XPS cannot detect anything less than 1% mass concentration.

Long et al. (2016), in their IIP preparation for the removal of nickel, used XPS to observe the adsorption mechanism by detecting the changes in the IIP composition before and after the adsorption of nickel. XPS was also done before leaching and after leaching in an IIP experiment that was prepared to selectively remove bromine ions (Wang et al. 2019). Their results showed that bromine was found in a trace amount after leaching it from the IIP, revealing that roughly all of the imprinting sites on the surface of polymers were successfully imprinted, and polymer leaching was successful. The negligible quantity of bromine that persisted in the polymer after leaching was attributable to the fact that a tiny fraction of the imprinted sites were thoroughly buried during the imprinting process, and leaching of these remaining bromine ions was challenging under the leaching conditions.

Overall, all of the three X-ray spectroscopic analyses gave the same conclusion that the IIP before adsorption was perfectly leached from almost all of the Li ions templates while preparing it and it shows superior selective adsorption of lithium while the strontium adsorption was weak. The IIP composition results from the EDX and the XPS were very close to each other, highlighting that it is mainly composed of carbon and oxygen.

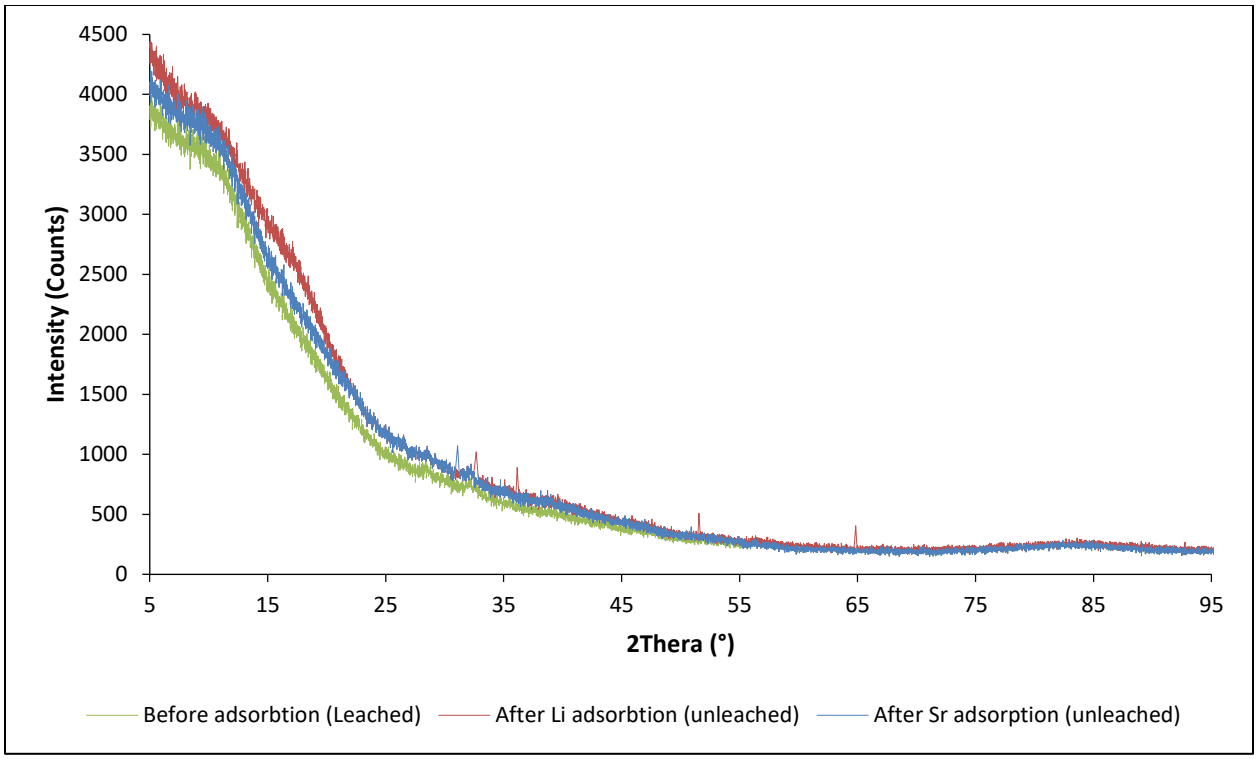

Figure 12: XRD diffractogram of IIP before adsorption and after adsorption.

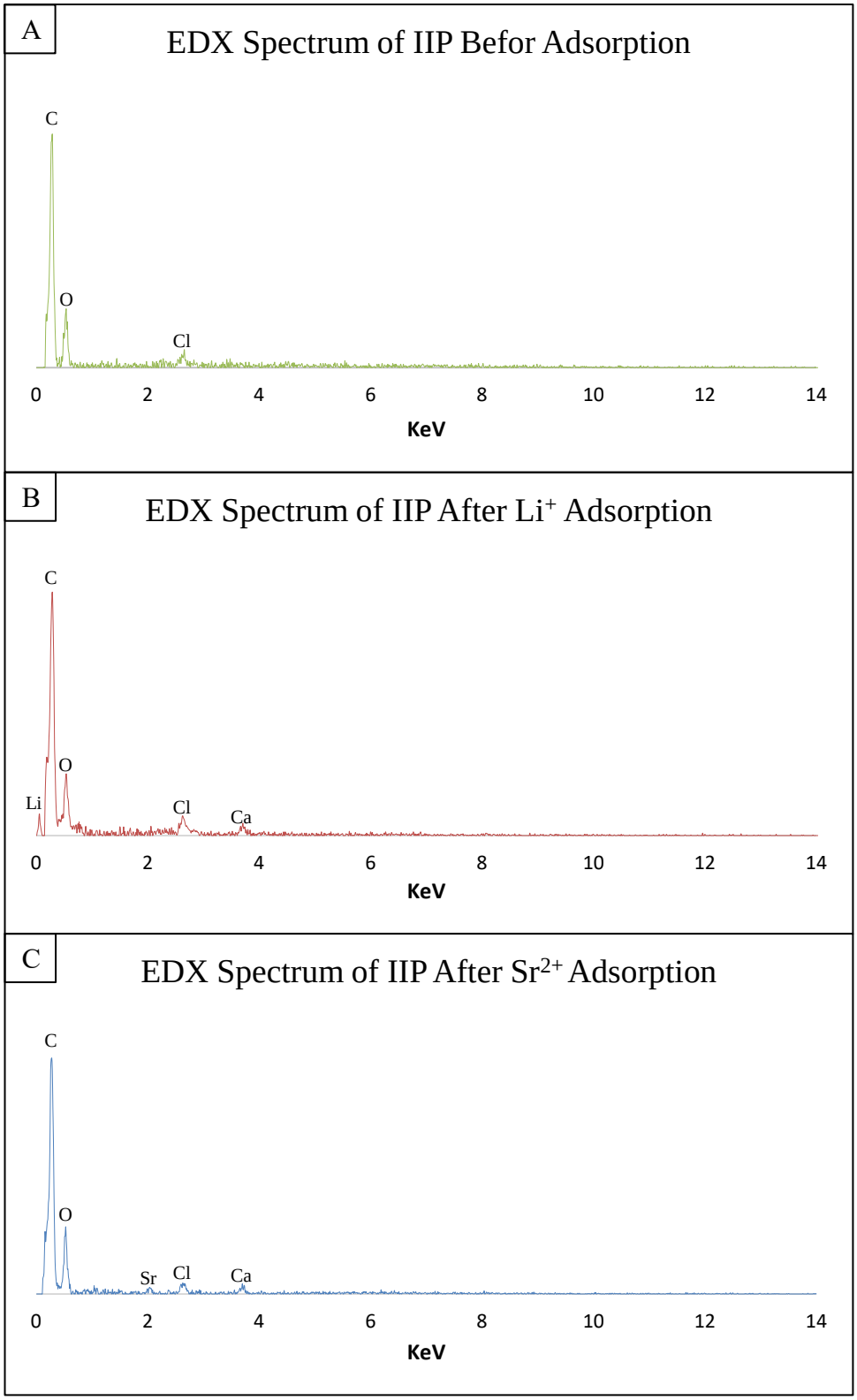

Figure 13: EDX spectra of IIP (A) Before adsorption, (B) After Li^{+} adsorption and (C) After Sr^{+2} adsorption.

Table 6: EXD element composition of the IIP.

Element	Wt %	At %
C	73.27	79.00
O	25.30	20.48
Cl	1.43	0.52
Total	100.00	100.00

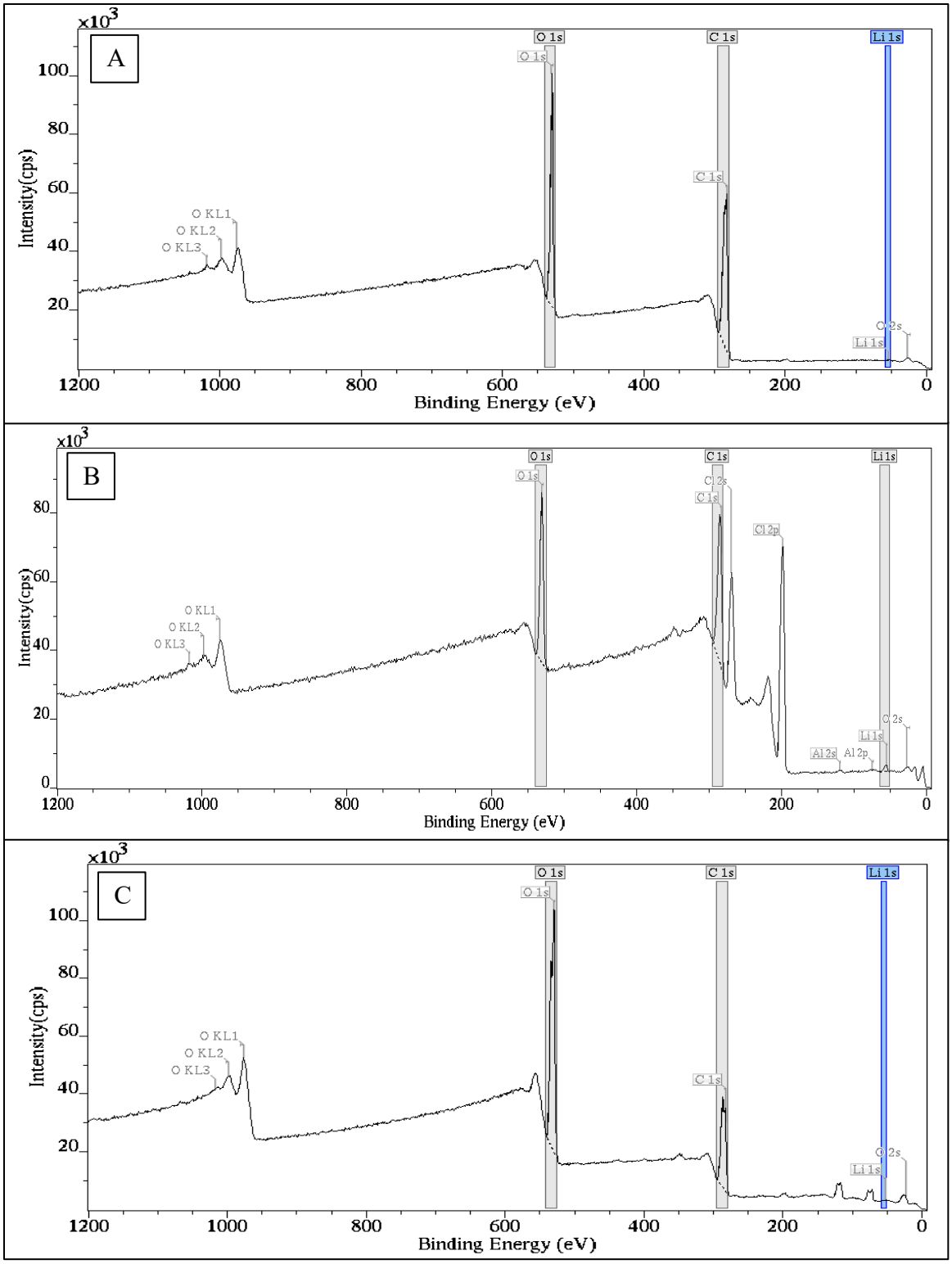

Figure 14: XPS spectra of IIP (A) Before adsorption, (B) After Li^{+} adsorption and (C) After Sr^{+2} adsorption.

Table 7: XPS surface quantification of the IIP.

Element	Mass Conc. %	Atomic Conc. %
C	69.96	75.02
O	29.28	23.58
Li	0.76	1.40
Total	100.00	100.00

4.2. Sea Water Reverse Osmosis Brine Characterization

Seawater reverses osmosis concentrated brine from desalination plant was physically and chemically characterized, where pH, salinity, total dissolved solids (TDS), conductivity, and elemental composition were tested. Table 8 shows the physical and chemical characteristics of the seawater reverse osmosis (SWRO) brine in comparison with other SWRO brine characteristics from the literature. The pH of the brine used in the current study is closer to 8, which indicates that it is alkaline. This is similar to the other brine results, where all of the pH values are between 8 to 12 indicating that all the brine water is alkaline ranging from weak to strong alkalinity. The salinity of the brine water was 61.7 ppt. It was noticed by Khan et al. (2021) that the salinity of the brine was more than 160% higher than the seawater standard salinity. The conductivity of the SWRO brine was 91.56 mS/cm. Conductive ions are generally made up of dissolved salts and inorganic elements such as chloride, alkalis, sulfides, etc. (Zhong et al., 2022). As a result, a high water conductivity is a result of a high ion concentration. Thus, as the principle charge carriers in brine are Na and Cl, it is obvious to find that the conductivity of the brine is high, as the elemental analysis of the brine (Fig. 15) shows that Na and Cl are available in high quantities in the brine water.

The elemental analysis of the seawater reverse osmosis brine is shown in Figure 15. The analyzed trace metals include copper (Cu), zinc (Zn), iron (Fe), sodium (Na), potassium (K),

magnesium (Mg), calcium (Ca), barium (Ba), strontium (Sr), lithium (Li), lead (Pb), and vanadium (V). The analysis revealed a significant concentration of minerals in the brine sample like Na (30575 mg/L), Mg (2757 mg/L), K (1700 mg/L), and Ca (1690 mg/L). It also revealed a low concentration of trace metals in the analyzed brine sample, like Ba (0.16 mg/L), Zn (0.845 mg/L), Fe (1.31 mg/L), Cu (1.165 mg/L), Pb (1.505 mg/L), and V (3.88 mg/L), except Li and Sr which shows a higher concentration of 43.32 mg/L and 16.93 mg/L respectively. The chemistry of brine, the desalination process utilized, as well as the chemicals used, and the geological context of the region all impact the concentration composition of trace metals in brine (Loganathan et al., 2017).

As noticed that strontium and lithium are present in a higher concentration. This can be due to the presence of carbonates in the brine, chemical and physical weathering, as well as the leaching of rocks and soils. These can all contribute to strontium higher concentrations (Onwuka et al., 2019), and the comparatively high proportion of lithium in brine, assures the fact that seas are key lithium reservoirs across the world (Son et al., 2021).

Table 8: Physical and chemical characteristics of SWRO brine.

pH	Salinity (ppt)	TDS (g/L)	Conductivity (mS/cm)	Reference
7.89	61.7	67.64	91.56	current study
8.2	39.2	NR	NR	(Frank et al., 2017)
10	NR	69.17-72.36	88-132	(Bindels et al., 2020)
8	NR	30.73	77	(Nguyen et al., 2017)
8.17	NR	71.827	11.204	(Son et al., 2021)
8-8-12	NR	58.85	NR	(Naidu et al., 2018)

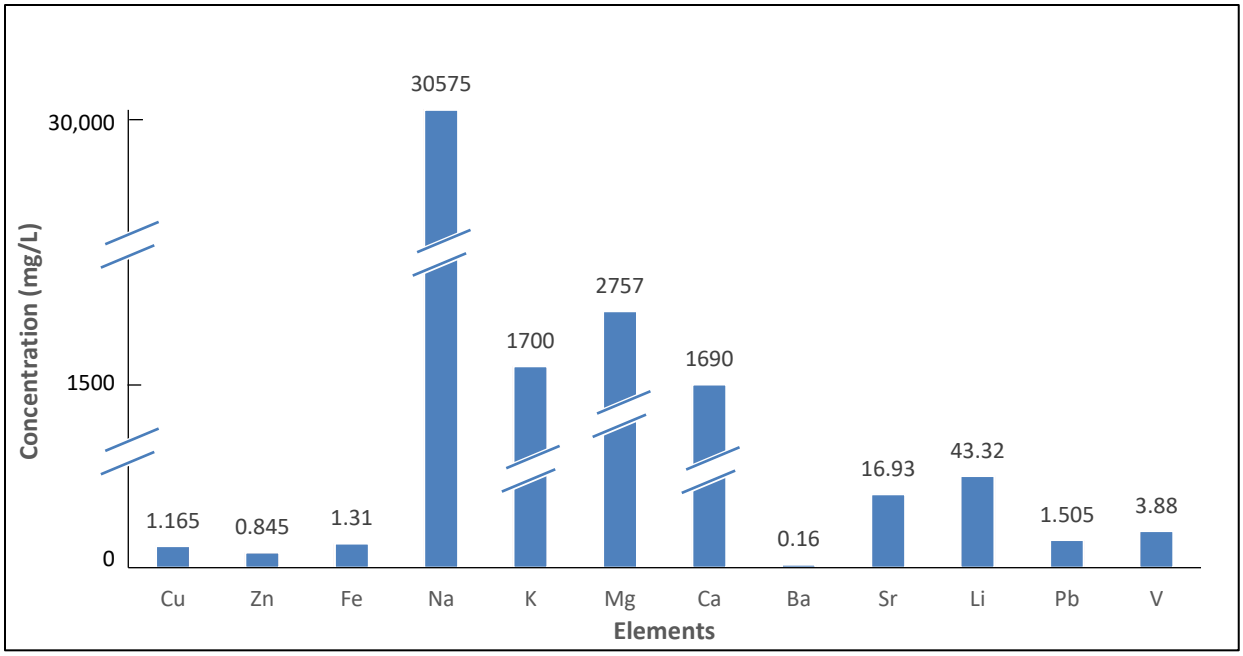

Figure 15: Elemental compositions of the SWRO brine according to ICP-OES analysis.

4.3. Effect of pH

pH is among the most pertinent factors impacting the adsorption rate of various metal ions on the polymers, thus, different pH between pH 2 and pH 10 were used to study the behavior of the ion-imprinted polymer when the pH is changed. The experiment results show that the adsorption removal percentage of lithium (Fig. 16A) was ranged between 98.6% and 99% with a difference of 0.4% between the highest and lowest adsorption removal percentage. On the other hand, the adsorption removal percentage of strontium (Fig. 16B) was more irregular, ranging between 2% to 99% with no regular trend. So, pH 10 was selected to be the optimum pH for the experiments, as it was the highest efficient pH to adsorb Sr^{2+}, and in the case of Li^{+} adsorption, there was no big difference between pH 10 and the highest adsorption removal percentage (0.4%), taking into account that the K_{sp} of the lithium and strontium at 25 °C is $8.15x10^{-4}$ and 3.2×10^{-4}, insuring that they will not precipitate at the high pH as they have a high solubility (Ciliberto et al.,

2008).

Işıkver and Baylav (2018) in their IIP experiment investigated the effect of pH on five different pHs from 3 to 7. Their results show that the higher the pH, the higher the adsorption. They justify this phenomenon as that the polymers having –COOH groups get ionized when pH rises, resulting in increased interactions with metal ions. Moreover, the tendency for metal ion–HQ complex formation increases as pH rises. Behbahani et al. (2012) in their nano IIP also tested different pH values. They also found that the adsorption raised with the pH raising from 2 to 8. They also noticed that the quantitative retention of the sorbent was reduced by reducing the pH value of the solution due to electrostatic repulsion of the protonated active sites of the sorbent with the positively charged metal species.

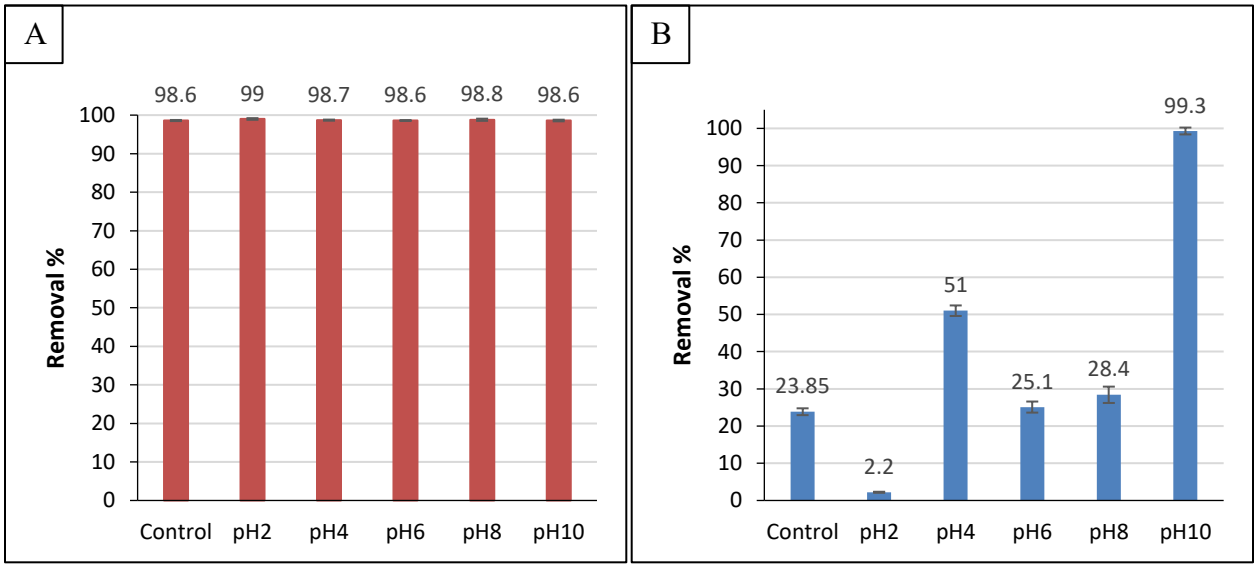

Figure 16: Effect of pH on the IIP adsorption removal % toward (A) Lithium and (B) Strontium.

4.4. Effect of Temperature and Initial Concentration

The second factor affecting the metal ion adsorption is the temperature and the metals ion's initial concentration. Thus, three experiments were run in parallel, each at a different temperature

at 25ºC, 35ºC, and 45ºC. In each experiment, eight different initial concentration (5, 15, 30, 45, 60, 75, 90, and 100 ppm) was used for both lithium and strontium, and all the solutions were adjusted to pH 10. The results in Figure 17A show that as the initial concentration of Li^+ increase, the adsorption capacity of the IIP increase, this shows a positive correlation between the Li^+ concentration and the adsorption capacity. Huang and Wang (2019) recovered lithium using IIP loaded on pretreated vermiculite. They found that the adsorption curve is directly proportional to the Li^+ initial concentration, regardless of the changes in the adsorption time or the monomer dosage ratio. This was also observed by Luo et al. (2015) in their experiment, it was established that the adsorption capacity is directly proportional with the concentration of the Li^+ ions, for a 2.5 mmol/L – 45 mmol/L concentration range.

Unlike the Li^+ adsorption, the Sr^{2+} adsorption (Fig. 17B) did not show a linear correlation between the initial concentration and the adsorption capacity of IIP, this was expected as the ion-imprinted polymer was tailored to have selectivity toward Li^+ only and not for Sr^{2+}. This means that the Sr^{2+} uptake is not consistent and it could be adsorbed at different temperatures and concentrations. Işıkver and Baylav (2018) described this as a memory effect of the adsorbate ion with the adsorbent in the imprinting process of the polymer; this is due to the fact of strong intermolecular interaction of the imprinted polymer and the used templet.

Figure 18 shows the influence of temperature on the adsorption capacity of IIP on Li^+ and Sr^{2+}. The adsorption of Li^+ on IIP favored endothermic conditions. In general, the increase in temperature also increased adsorption capacity. For example, at 45 ºC the equilibrium concentration is 3 mg/L of Li^+, as compared to 3.2 mg/L of Li^+ at 25 ºC and 3.67 mg/L of Li^+ at 35 ºC, which means that less concentration of Li^+ is left unadsorbed at 45 ºC. According to Al-Ajji and Al-Ghouti (2021), an increase in adsorption capacity can be due to the increase in the diffusion

rate of the adsorbate molecules due to the decrease in solution viscosity. Additionally, an increase in temperature also influences the biosorption activity by increasing the kinetic energy of the solute as well as the surface activity. Furthermore, it is also possible that high temperatures increase the flexibility of the crown of the imprinted polymer, allowing more ions to reach the binding site. On the other hand, strontium adsorption is irregular, this can be as a result of the expansion behavior of the crown, which allows the strontium ion to get in the binding site when it expands, but it will not be stably bound for a long time, as it cannot fit properly, which then will be desorbed again.

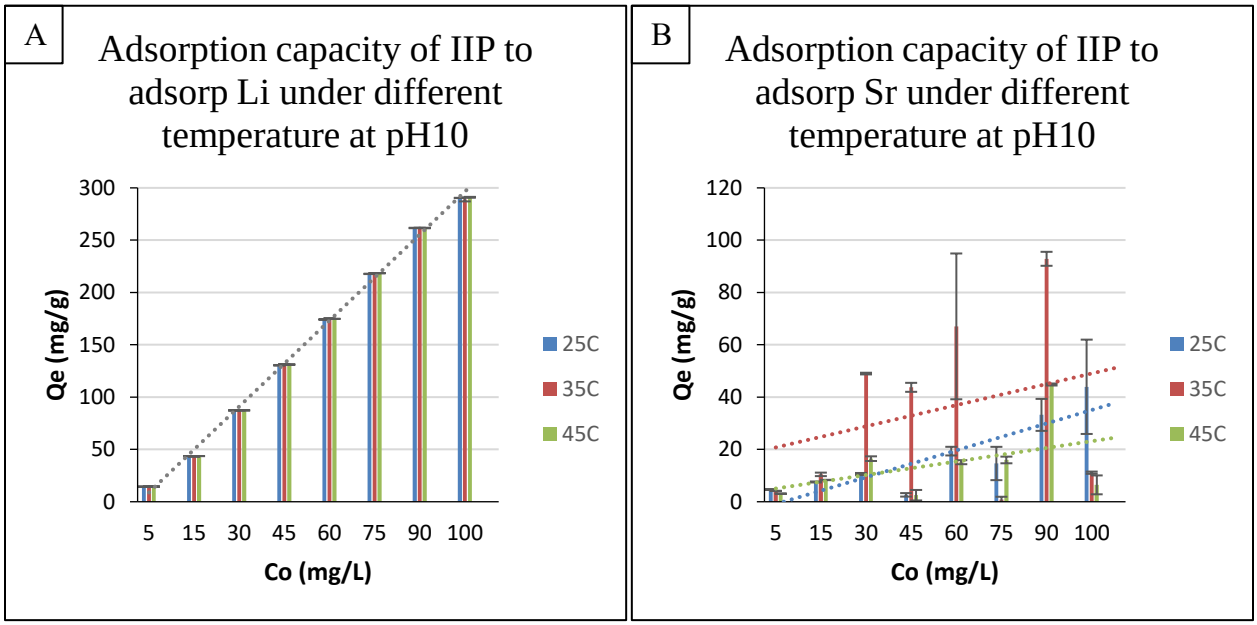

Figure 17: Effect of initial concentration on the adsorption capacity of the IIP toward (A) Lithium initial concentration and (B) Strontium initial concentration.

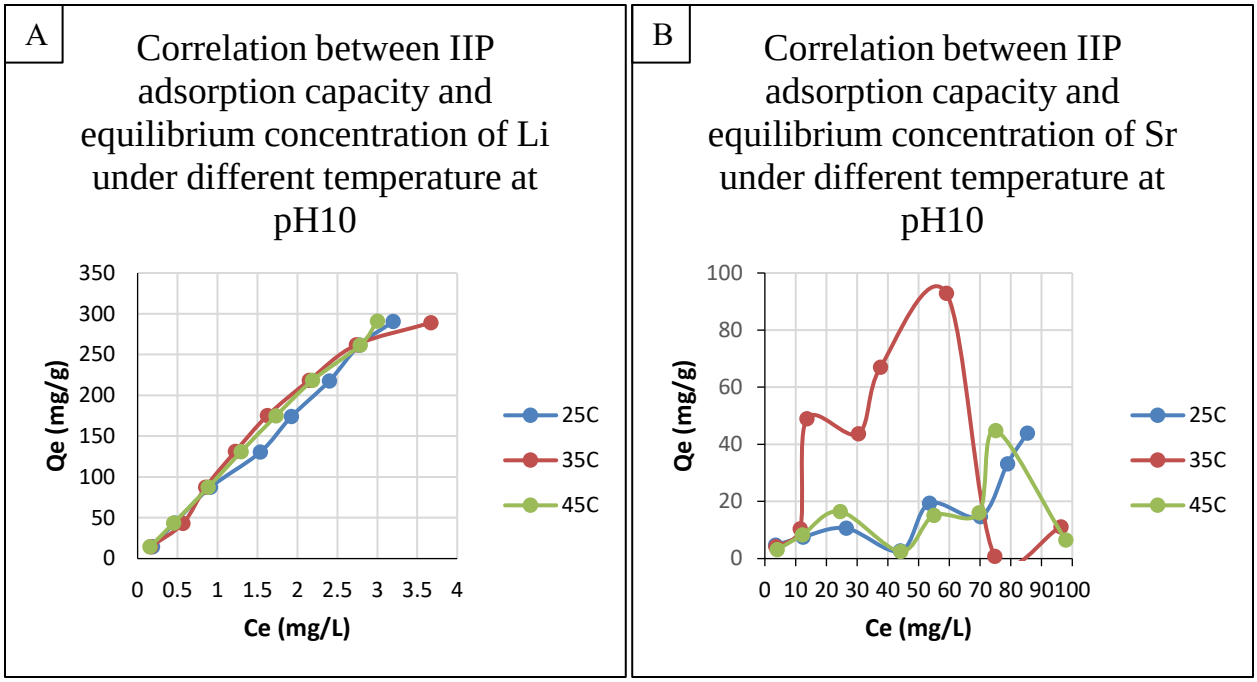

Figure 18: The correlation between the IIP adsorption capacity and equilibrium concentration of (A) Lithium and (B) Strontium.

4.5. Isotherm Models and Adsorption Mechanism

The IIP adsorption data was used to observe which isotherm model is the best-fitted for each temperature. As mentioned in section 3.8, the isotherm models were first linearized as shown in Figure 19, and then the parameters for each temperature were calculated in table 9 using the values of the linear plotting equation of the graphs (Fig. 19).

Langmuir isotherm refers to homogenous adsorption on the adsorbent surface and only a monolayer of adsorbate is formed on the adsorbent surface, which means that no interaction happens among the adsorbate molecules on the adsorbate surface. The correlation coefficient (R^2) of Langmuir isotherm at the different three temperatures was 0.99, which is so close to 1, indicating that the experiment could be explained as a Langmuir isotherm. Moreover, the maximum adsorption capacity (Q_m) was rising as the temperature rise from 714 mg/g at 25°C to 2500 mg/g

at 45°C. Likewise, the Freundlich isotherm R^2 values at the different three temperatures were also 0.99, adding the possibility that the experiment could be explained as a Freundlich isotherm. In contrary to Langmuir, Freundlich suggests that heterogeneous adsorption takes place and forms a multilayer adsorbate on the adsorbent surface, due to interactions among the adsorbate. Moreover, Freundlich adsorption capacity (K_f) was also rising as the temperature rise from 89.14 $(mg/g)/(g/L)^{1/n}$ at 25°C to 97.55 $(mg/g)/(g/L)^{1/n}$ at 45°C. Dubinin-Radushkevich and Temkin was not a favorable model to describe the adsorption behavior of the IIP, as the R^2 values were much lower than Longmire and Freundlich, ranging between 85 and 89. Branger et al. (2013) mentioned the possibility that IIP adsorption could follow Langmuir and Freundlich models, where it is capable to have the IIP heterogeneous characteristics along with the saturation behavior at high concentration. This model was employed in Fasihi et al. (2011) uranyl IIP adsorption isotherm and Daniel et al. (2005) palladium (II) IIP. However, nowadays, this model is less popular than Langmuir and Freundlich's model independently.

Figure 20 shows the experimental data and the different models plot fitting at each temperature. It can be observed that the Freundlich model fits the experimental data perfectly in all of the different temperatures used, unlike Langmuir and Temkin models. This indicates that the binding sites are following heterogeneous adsorption of the adsorbate onto the adsorbent, and suggesting that the IIP adsorption behavior is multilayer adsorption, where Freundlich model does not have the restriction of the monomolecular layer. This was expected from the TEM image (Fig. 9B) in section 4.1.1, where it was shown that the lithium ions were aggregated on the IIP in multilayers. It must be brought that the Dubinin-Radushkevich model was not feasible to be fitted in the graphs, which excludes its applicability to be the followed model.

The lithium IIP that was prepared by Huang and Wang (2019) was following the Langmuir

model more than Freundlich and Temkin, indicating that it had a homogeneous binding site and behave as a monolayer adsorbent. However, their polymer was loaded on pretreated vermiculite, which could be the reason behind the differences in the adsorption behavior. On the other hand, an IIP selective for Br(I) was following Freundlich model adsorption behavior much better than Langmuir and Temkin isotherm model behavior (Wang et al., 2019), While Hassanzadeh et al. (2018) Cr(VI) IIP was following Temkin model, which suggests that reversible heterogeneous ion adsorption are happening on the IIP surfaces.

Figure 21 shows the different possible adsorption mechanisms for IIP. If a chemisorption mechanism toke place, this will result in monolayer adsorption, which describes the Langmuir model behavior. This mechanism needs a chemical bond between the adsorbate and the adsorbent surface, and it is a naturally irreversible mechanism. However, if a physisorption mechanism took, this will result in multilayer adsorption, which describes the Freundlich model behavior. This mechanism involves weak Van der Waal forces, and it is a naturally reversible mechanism. The third adsorption mechanism is aggregates adsorption, where in this mechanism there is a particle-particle interaction between the adsorbate themselves and particle-surface interaction between the adsorbent and the adsorbate.

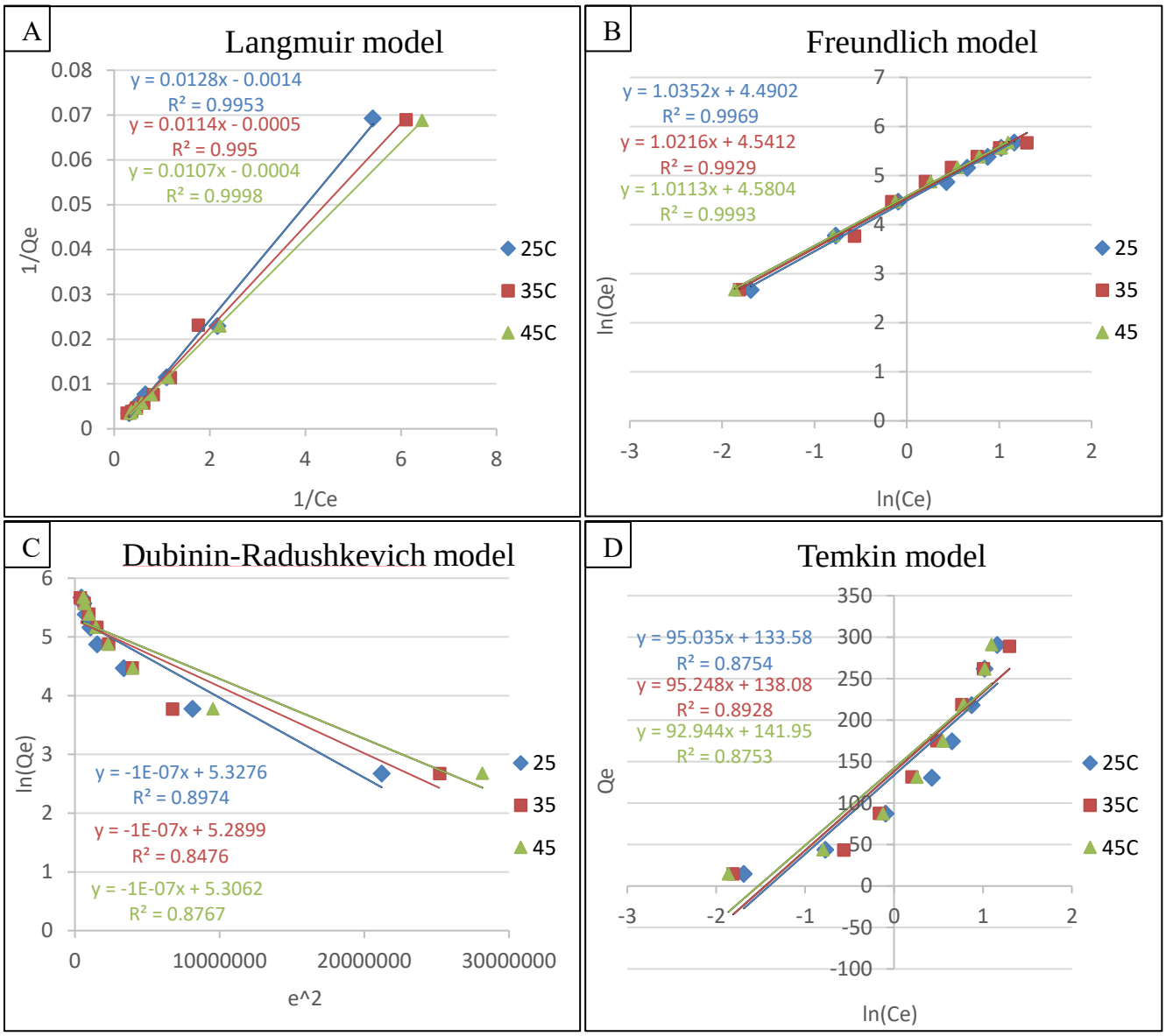

Figure 19: Linearizing graph for the isotherm models under different temperatures (A) Langmuir (B) Freundlich (C) D-R and (D) Temkin model.

Table 9: Adsorption isotherm constants of IIPs under different temperatures.

Model	Langmuir	Freundlich	D-R	Temkin
25 °C	R^2 = 0.99	R^2 = 0.99	R^2 = 0.89	R^2 = 0.88
	Q_m = 714.3	n = 0.97	q_s = 206.44	A_t =4.08
	b = 0.109	K_f = 89.14	K = -0.0009	B_t = 26.08
35 °C	R^2 = 0.99	R^2 = 0.99	R^2 = 0.85	R^2 = 0.89
	Q_m = 2000	n = 0.98	q_s = 198.34	A_t = 4.26
	b = 0.044	K_f = 93.80	K = -0.0009	B_t = 26.90
45 °C	R^2 = 0.99	R^2 = 0.99	R^2 = 0.88	R^2 = 0.88
	Q_m = 2500	n = 0.99	q_s = 202.35	A_t = 4.61
	b = 0.037	K_f = 97.55	K = -0.0009	B_t = 28.46

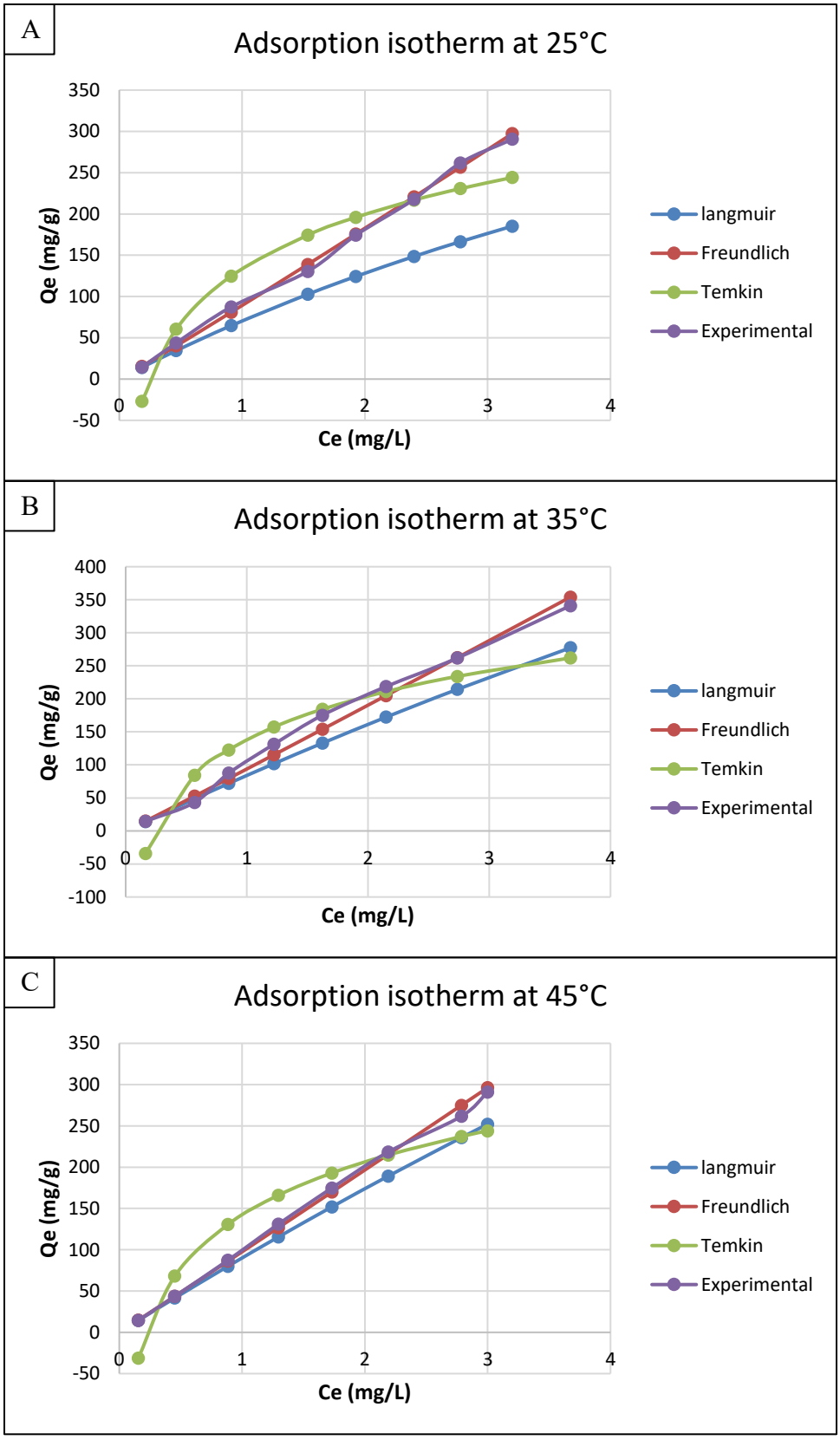

Figure 20: IIP adsorption isotherm at (A) 25°C (B) 35°C (C) 45°C.

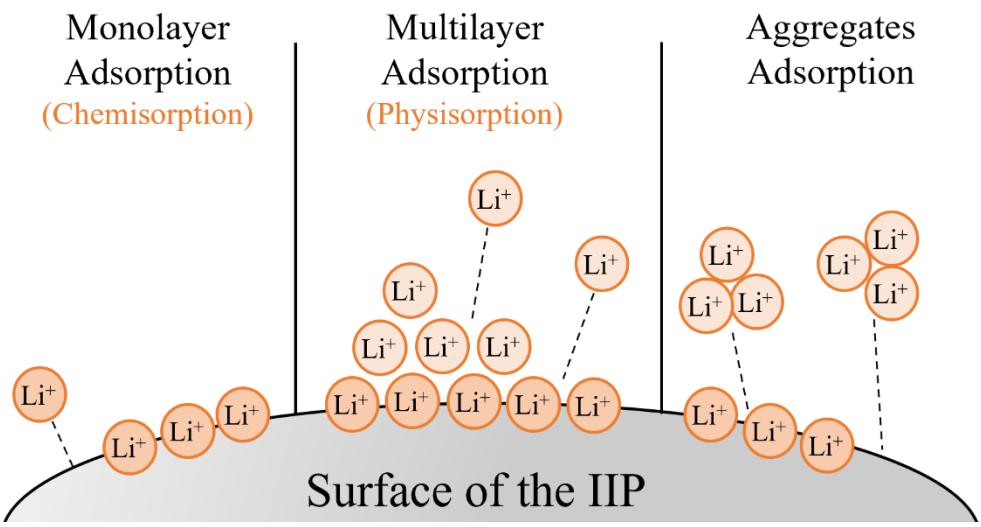

Figure 21: Adsorption mechanisms of IIP.

4.6. Desorption recovery and Desorption-Adsorption study

The ions adsorbed on the used IIP from the previous isotherm experiments were desorbed by leaching using 0.5 mol/L HNO_3 to evaluate the possibility to recover ions from the IIP. Figure 22 shows the recovered ions % that was adsorbed on the IIP. The Li^+ desorption results (Fig. 22A) show that 94.03% - 94.71% of the ions were recovered, while the Sr^{2+} desorption results (Fig. 22B) show that 96.35% - 96.56% of the ions was recovered. It can be observed that strontium recovery is higher than lithium recovery. This could be due to many reasons, one of them is the low adsorbed concentration of strontium initially, which makes the desorption process more efficient to leach all of the ions. Another reason is that the IIP is designed to selectively adsorb Li^+, this could make the binding of the ions to the IIP stronger, which needs a higher force to leach them. Alternatively, it may be that some IIP was already lost to the filters while filtering the adsorption solution before or while drying the filters, which mean that some ions were directly, lost with the IIP. Overall, the recovered percentage is considered high for both Li^+ and Sr^{2+}. In an experiment that was done by Al-Ajji and Al-Ghouti (2021), hazelnut shell adsorbent and nano-adsorbents were repeatedly used

and desorbed 3 times, and the average recovery percentage was about 88% and 71% respectively. This result suggested that the adsorbents are reusable efficiently.

To assess the reusability and the IIP stability, the polymer was reused again to adsorb Li^+ in a second cycle after the desorption process, as the regeneration of the IIP is a significant characteristic to consider adsorbent as economic and ecofriendly.

Figure 23 shows the IIP regeneration performance using different initial Li^+ concentrations (5, 15, 30, 45, 60, 75, 90, and 100 mg/L) at 25°C and pH10. The results show the adsorption capacity of two adsorption-desorption cycles, it can be observed that the difference between cycle 1 adsorption capacity and cycle 2 adsorption capacity decreased between 1.37% - 1.54%. It is also noticed that as the Li^+ initial concentration increased, the difference between the adsorption capacities increased. This could be as a result of fewer binding sites available when the concentration of ions is higher. Overall, the results suggest that the IIP can be reused successfully with high adsorption efficiency, which indicates that even after multiple-use; the IIP upholds a memory effect and strong structure (Işıkver & Baylav, 2018).

An ion-imprinted microporous membrane to adsorb lithium was prepared by Sun et al. (2017), and it was used for 6 times adsorption-desorption experiments to evaluate the regeneration performance. A decrease of 9.09% of the adsorption capacity was observed, and this percentage concluded that the ion-imprinted membrane was stable and had high regeneration performance. Huang and Wang (2019) IIP for lithium recovery was also run for 10 adsorption-desorption cycles, and the adsorption capacity difference between the first and the tenth cycle was decreased by 13.1%, indicating that the IIP can be used even more than 10 times with high efficiency to adsorb Li^+.

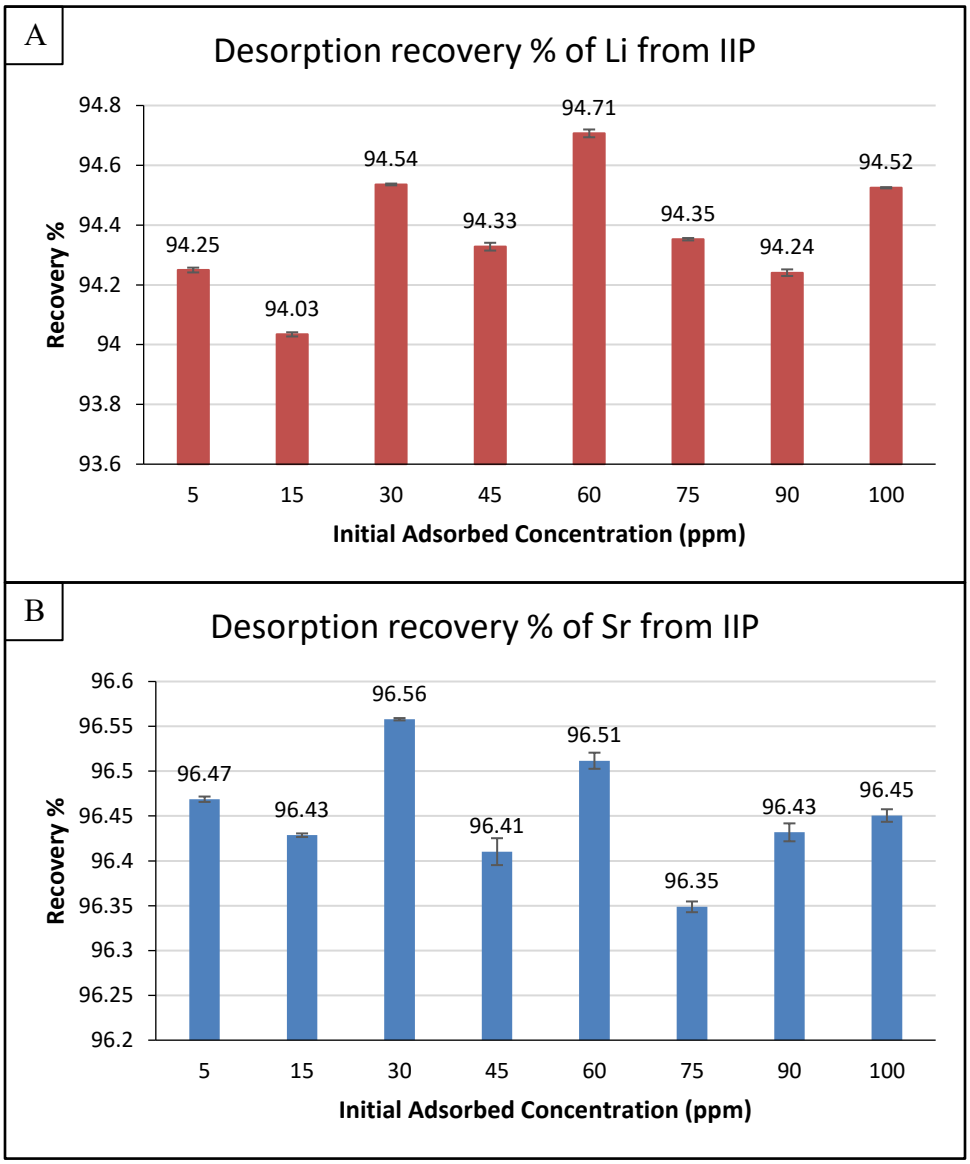

Figure 22: IIP ions desorption recovery efficiency of (A) Lithium, and (B) Strontium.

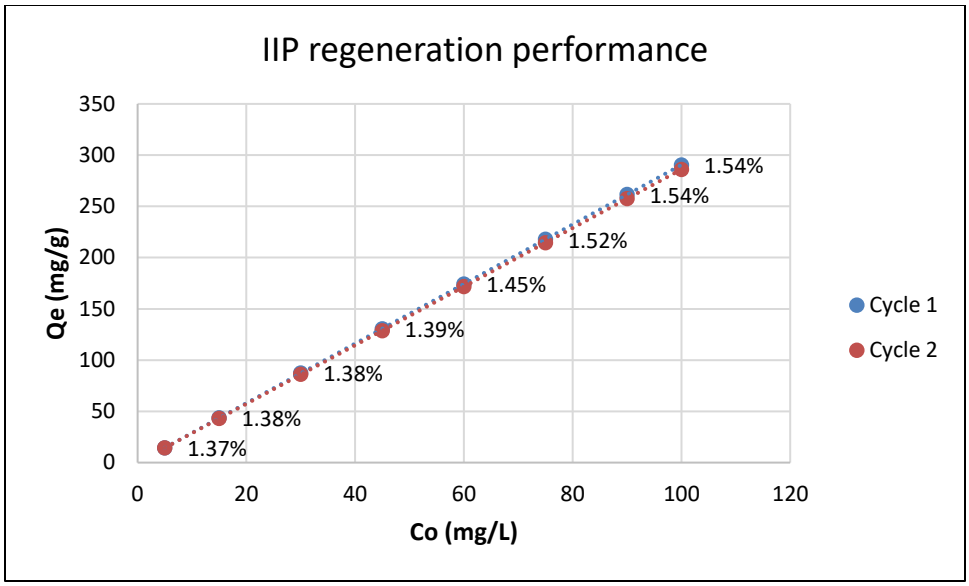

Figure 23: IIP regeneration performance of 2 adsorption-desorption cycles at 25°C and pH10.

4.7. Real Brine Batch Adsorption

After characterizing the IIP and evaluating its performance using the synthetic ionic solution, the IIP was used on real SWRO brine at 25°C and pH10. The efficiency of IIP to adsorb lithium and strontium from brine is shown in Figure 24, where the adsorption removal% of Li^+ was between 84.21% and 84.68%, while the adsorption removal% of Sr^{2+} was between 3.83% and 10%. It can be noticed that the removal% of Li^+ in brine was less by around 15% compared with the removal% of Li^+ from the synthetic solution (Fig. 16A), as well, the Sr^{2+} removal% from brine is less compared with that from the synthetic solution. This indicates that the ionic complexity of the solution affects the IIP performance. This could be due to the increased competition on the binding sites, and the extremely high salinity of the brine. Moreover, it should be taken to account that the ions in the brine are electrostatically bonding to each other with intermolecular forces, which increase the difficulty for single Li^+ to be adsorbed to the binding sites, unlike the synthetic solution that was prepared with LiCl just like the IIP templet, which was prepared using LiCl.

Looking at the adsorption capacity of the IIP (Fig. 25), it can be observed that Qe is higher when the brine is more concentrated and decreased as it is diluted. This IIP behavior is compatible with the previous results of the synthetic solution (Fig. 17) and with the results of Luo et al. (2015) IIP used for Li^+ recovery from wastewater, where the Qe was rising as the Li^+ concentration increased until it reaches a concentration around 700 mg/L and it gets saturated. Likewise, the correlation between the IIP adsorption capacity and equilibrium concentration of Li^+ (Fig. 26A) was a positive linear correlation, while the correlation for Sr^{2+} (Fig. 26B) was a random correlation without any consistency. This insures that the IIP Qe is highly affected by the ions concentration of the ion that the IIP was prepared to selectively adsorb it.

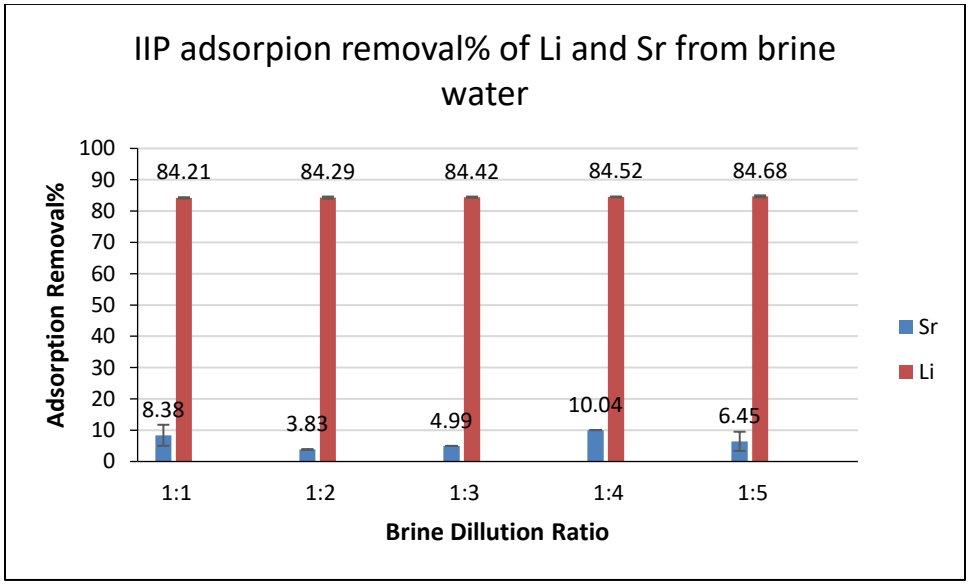

Figure 24: IIP adsorption removal% of lithium and strontium from SWRO brine using different brine : distilled water dilution ratios.

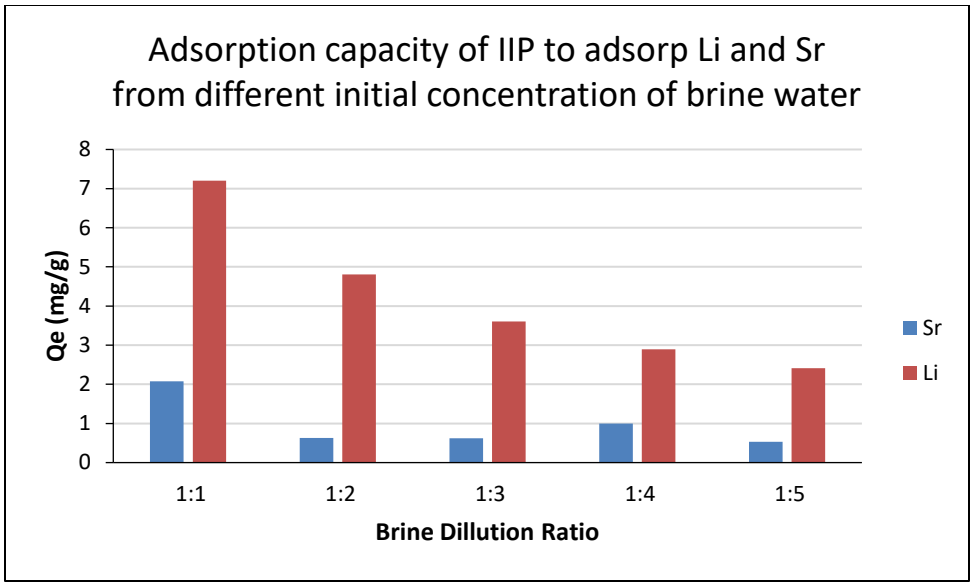

Figure 25: Adsorption capacity of the IIP toward lithium and strontium from SWRO brine using different brine : distilled water dilution ratios.

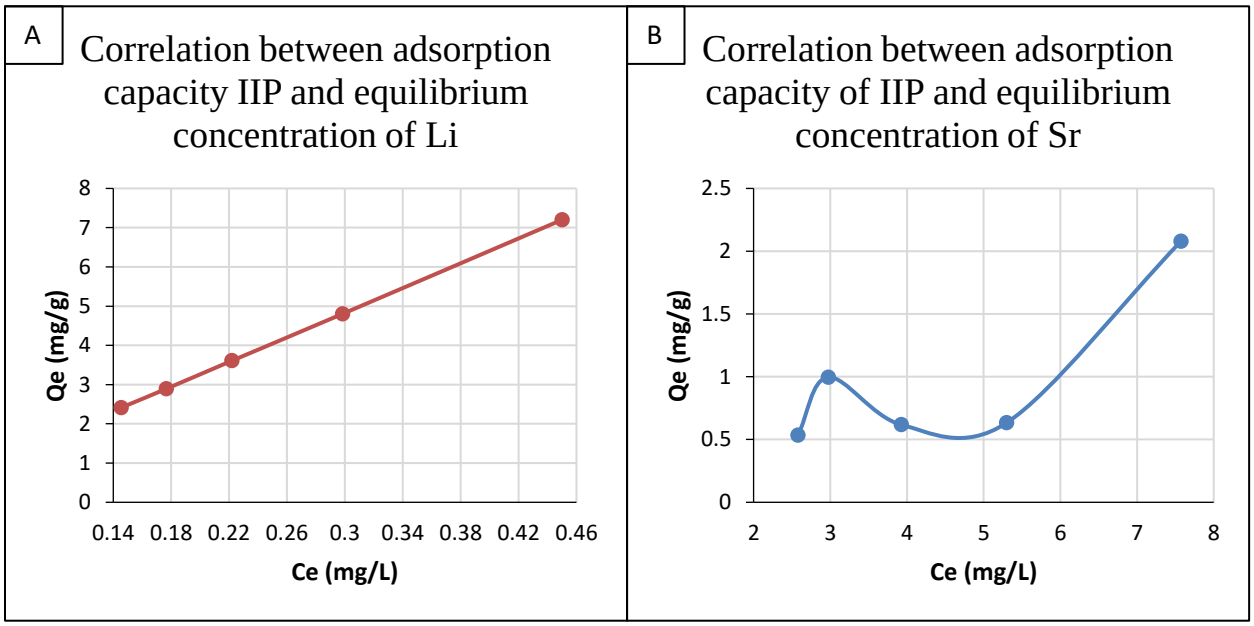

Figure 26: The correlation between the IIP adsorption capacity and equilibrium concentration of (A) Lithium and (B) Strontium from SWRO brine.

4.8. Statistical Analysis

The statistical analysis was employed to investigate the significance of the different factors and the correlation between them. Minitab statistic program was used to generate all of the results in this section. Table 10 shows the factors information that was used to calculate the analysis of variance (ANOVA) of Qe versus Temperature and Concentration for both Li^+ and Sr^{2+} adsorption isotherm experiments (Table 11). The ANOVA test is used to check the significance of the factor effect by checking the P (probability) value. P-value <0.01, <0.05, or >0.05 indicate that the factor is highly significant, significant, or not significant, respectively. The ANOVA of the Li^+ adsorption experiment shows that the temperature p-value = 0.092, which indicates that it is not a significant factor, while concentration was a highly significant factor with a P-value = 0, additionally, the two factors combined had a P-value = 0.024; indicating a significant effect. This was expected from the experimental results, as it was shown that as the temperature changes, there was no difference in the adsorption capacity, while in the case of initial concentration changes, the adsorption capacity was in a direct correlation with the changes. On the other hand, the Sr^{2+} adsorption experiment shows that all the factors have a P-value = 0, which statistically indicates that the factors are significant. However, this result is not realistic, as it was shown that the Sr^{2+} adsorption experiment was showing random results with a huge difference and no regular trend with changes of the factors, which means that this outcome was not due to the factors' significant effect.

Furthermore, Tukey pairwise comparisons were used to compare the Qe means versus temperature and concentration in the grouping method depending on the significant difference in the means. Table 12 shows the Li^+ adsorption experiment means grouping information, it can be noticed clearly that each initial concentration from the different temperatures shares the same group (same letter). Which again insure that the concentration is a significant factor while

temperature did not affect the means. On the other side, the Sr^{2+} adsorption experiment means grouping information (Table 13) did not show any specific trend behind the grouping distribution. For example, means sharing group B are from 5 different initial concentrations of Sr^{2+} (30, 45, 60, 90, and 100 mg/L) and the different three temperatures used (25°C, 35°C, and 45°C). This indicates clearly that the significance was totally due to randomness in the adsorption not due to factors effect.

Moreover, factorial plots for Qe were generated as the main factors plot and interaction plot for both Li^{+} and Sr^{2+} adsorption isotherm experiment. The main factor plot shows the effect of each factor on the Qe separately, while the interaction plot shows the effect of the interaction of the different factors together on the Qe. The results of this factorial plot are just additional evidence to assure the previous outcomes. Figure 27 shows the factorial plots of the Li^{+} adsorption experiment for Qe, where the main factors plot (Fig. 27A) shows that temperature alone has no significant effect on the mean of Qe, while concentration alone has a significant effect on the mean of Qe as it shows a direct proportion. The interaction plot (Fig. 27B) shows the effect on the mean of Qe when the two factors combine. It is clearly observed that the mean of Qe is increasing as the concentration increases despite the temperature changes. On the other hand, Figure 28 shows the factorial plots of Sr^{2+} adsorption experiment for Qe, where the main factors plot (Fig. 28A) shows a fluctuation in the effect of concentration on the mean of Qe, while the temperature effect shows that at 35°C the mean of Qe highly improved. Comparing it with the interaction plot (Fig. 28B) it is obviously observed that 35°C was not a really favorable temperature to improve the Qe, as there are higher, lower, and equal values with the other used temperatures. It is again indicating that the factors are not affecting the adsorption of strontium, but the only effect is the ion itself, as the IIP was prepared to selectively adsorb lithium only.

Table 10: Factors information.

Factor	Type	Levels	Values
Temperature	Fixed	3	25, 35, 45
Concentration	Fixed	8	5, 15, 30, 45, 60, 75, 90, 100

Table 11: Analysis of Variance (ANOVA).

Source	DF	Adj SS	Adj MS	F-Value	P-Value
Li^+ adsorption experiment					
Temperature	2	1	0.5	2.64	0.092
Concentration	7	427896	61128.1	353062.25	0.000**
Temp. x Conc.	14	6	0.4	2.48	0.024*
Error	24	4	0.2		
Total	47	427908			
Sr^{2+} adsorption experiment					
Temperature	2	4049	2024.52	39.97	0.000**
Concentration	7	12253	1750.42	34.56	0.000**
Temp. x Conc.	14	9218	658.42	13.00	0.000**
Error	24	1216	50.65		
Total	47	26735			

** Significant, ** Highly significant.*

Table 12: Grouping information using the Tukey method and 95% confidence for Li^+ adsorption experiment.

Temp.*Conc.	N	Mean	Grouping		
45 100	2	291.000	A		
25 100	2	290.400	A		
35 100	2	288.990	A		
35 90	2	261.792		B	
25 90	2	261.670		B	
45 90	2	261.643		B	
35 75	2	218.554			C
45 75	2	218.430			C
25 75	2	217.800			C
35 60	2	175.131			D
45 60	2	174.807			D

Temp.*Conc.	N	Mean	Grouping							
25 60	2	174.222			D					
35 45	2	131.328				E				
45 45	2	131.112				E				
25 45	2	130.396				E				
35 30	2	87.448					F			
45 30	2	87.345					F			
25 30	2	87.269					F			
45 15	2	43.646						G		
25 15	2	43.612						G		
35 15	2	43.295						G		
45 5	2	14.534								H
35 5	2	14.509								H
25 5	2	14.446								H

Means that do not share a letter are significantly different.

Table 13: Grouping information using the Tukey method and 95% confidence for Sr^{2+} adsorption experiment.

Temp.*Conc.	N	Mean	Grouping						
35 90	2	92.8800	A						
35 60	2	67.0500	A	B					
35 30	2	49.0050		B	C				
45 90	2	44.8200		B	C	D			
25 100	2	43.9500		B	C	D	E		
35 45	2	43.7400		B	C	D	E		
25 90	2	33.2100			C	D	E	F	
25 60	2	19.3500				D	E	F	G
45 30	2	16.4700				D	E	F	G
45 75	2	15.9750				D	E	F	G
45 60	2	15.1200					E	F	G
25 75	2	14.6250						F	G
35 100	2	11.1000						F	G
25 30	2	10.6200						F	G
35 15	2	10.4625						F	G
45 15	2	8.3250						F	G
25 15	2	7.5600						F	G
45 100	2	6.4500						F	G
25 5	2	4.6725						F	G
35 5	2	4.1475							G
45 5	2	3.0900							G

Temp.*Conc.	N	Mean	Grouping
25 45	2	2.6325	G
45 45	2	2.4975	G
35 75	2	0.7875	G

Means that do not share a letter are significantly different.

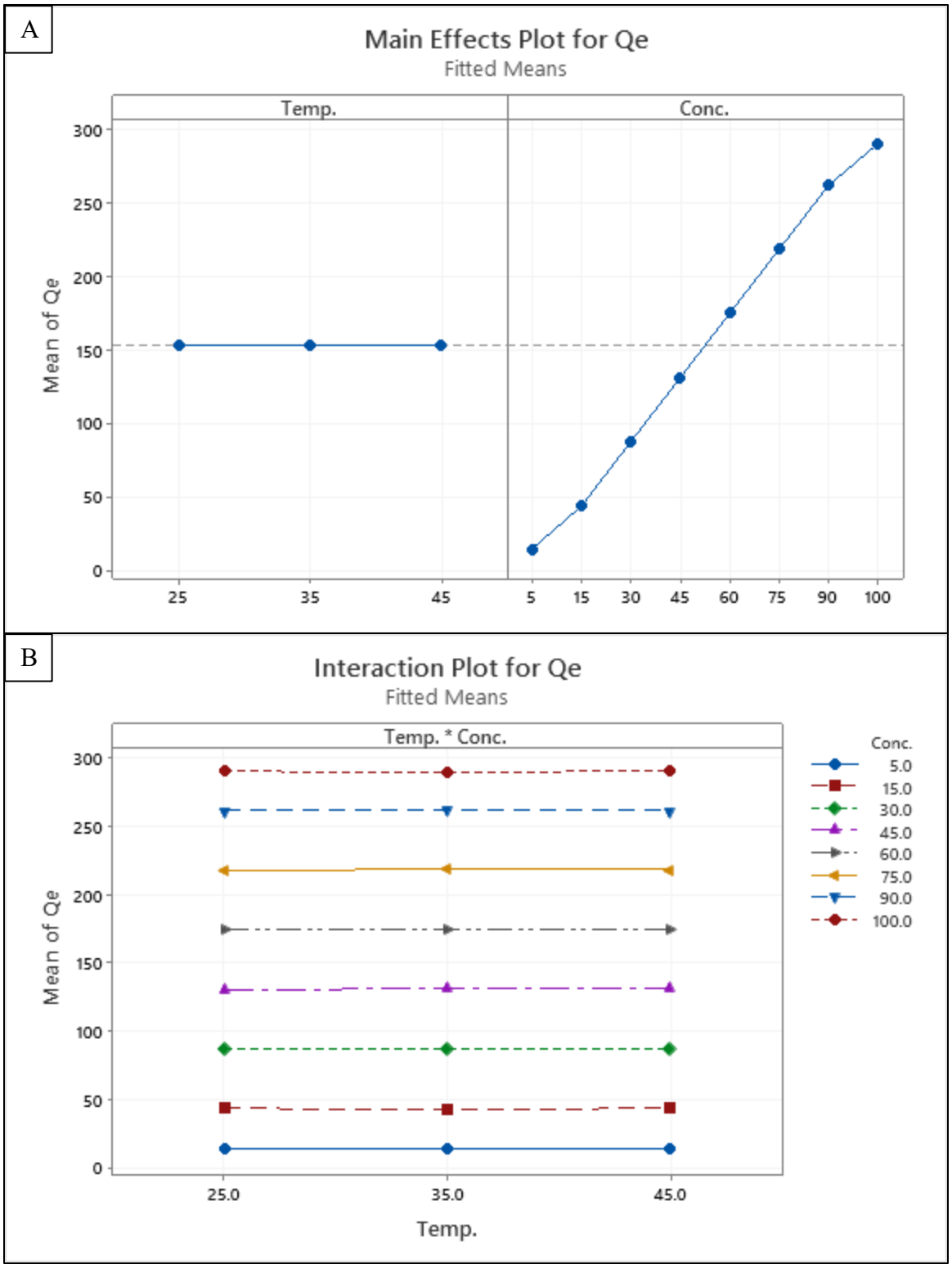

Figure 27: Factorial plots of Li^+ adsorption experiment for Qe (A) main factors plot and (B) interaction plots.

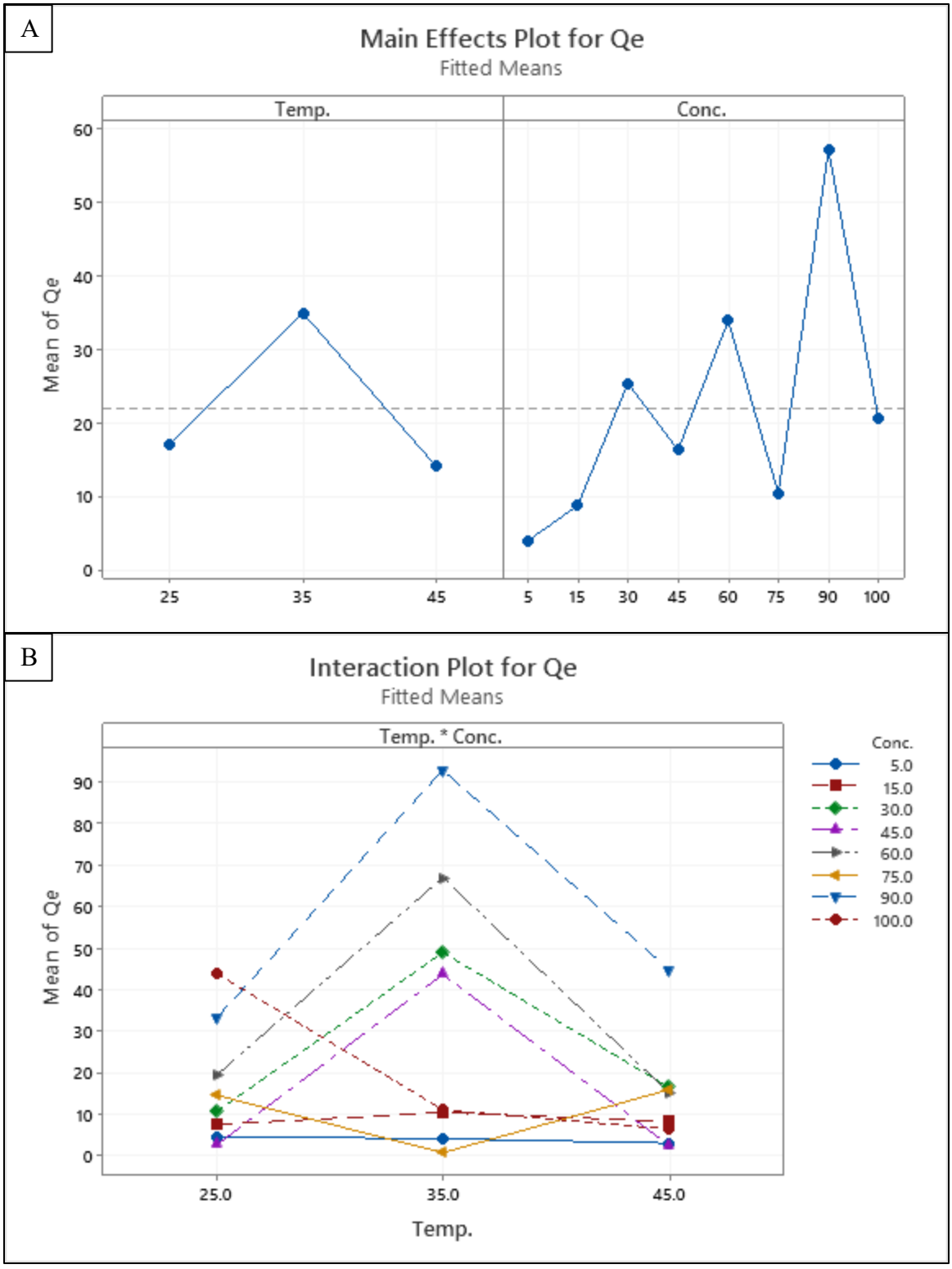

Figure 28: Factorial plots of Sr^{2+} adsorption experiment for Qe (A) main factors plot and (B) interaction plots.

5. CONCLUSION:

In conclusion, this study was undertaken to design a strategy for a major environmental concern, which is brine water and evaluate its efficiency. A novel tailored ion-imprinted polymer was successfully synthesized by polymerization technique for selective adsorption of lithium ions from reverse osmosis brine, as a cost-efficient and ecologically beneficial adsorbent to extract metals from brine. The prepared polymer was tested to adsorb lithium ions as well as strontium ions to try the selectivity of the IIP. The IIP was prepared using a Li^+ template and used under different pH values, initial concentrations, and temperatures, to optimize the experimental conditions. It was indicated that Li^+ adsorption is not affected by changing the pH or the temperature, and only the initial concentration matters. The Sr^{2+} adsorption was random with no obvious trend toward the different factors, so the experiments were optimized to room temperature and pH 10 as it was the best for Sr^{2+} adsorption. The IIP was then characterized before adsorption compared to after adsorption of Li^+ and Sr^{2+} using SEM, TEM, FTIR, XRD, BET, EDX, and XPS, to study morphology, functional groups, specific surface area, pore radius, elemental composition, and to quantify the surface composition of the polymer. It was shown that the IIP was successfully synthesized with excellent efficiency to adsorb Li^+ but not Sr^{2+}, and it was following Freundlich isotherm model behavior. The used IIP was subjected to a desorption experiment and showed efficient ions recovery% for both adsorbed ions, and a cycle of the adsorption-desorption process was done that evaluated an efficient regeneration performance of the IIP. Seawater reverse osmosis brine was physically and chemically characterized and used as the real sample for ion adsorption. The results also showed a good indicator for Li^+ adsorption removal%, unlike Sr^{2+} adsorption removal%. Li^+ adsorption capacity and the correlation between adsorption capacity and equilibrium concentration were directly proportional for both the synthesized Li^+ solution

experiment and the real brine. Statistical analysis was done using Minitab to generate ANOVA, Tukey pairwise comparison, and factorial plot, which complied with the previous outcomes, ensuring the reliability of the results of the experiment.

6. REFERENCES:

Al Bazedi, G., Ettouney, R. S., Tewfik, S. R., Sorour, M. H., & El-Rifai, M. A. (2013). Salt recovery from brine generated by large-scale seawater desalination plants. *Desalination and Water Treatment*, *52*(25-27), 4689–4697. https://doi.org/10.1080/19443994.2013.810381

Al-Ajji, M. A., & Al-Ghouti, M. A. (2021). Novel insights into the nanoadsorption mechanisms of crystal violet using nano-hazelnut shell from aqueous solution. Journal of Water Process Engineering, 44, 102354. https://doi.org/10.1016/j.jwpe.2021.102354

Alexander, C., Andersson, H. S., Andersson, L. I., Ansell, R. J., Kirsch, N., Nicholls, I. A., O'Mahony, J., & Whitcombe, M. J. (2006). Molecular imprinting science and technology: A survey of the literature for the years up to and including 2003. *Journal of Molecular Recognition*, *19*(2), 106–180. https://doi.org/10.1002/jmr.760

Al-Ghouti, M. A., & Al-Absi, R. S. (2020). Mechanistic understanding of the adsorption and thermodynamic aspects of cationic methylene blue dye onto cellulosic olive stones biomass from wastewater. *Scientific Reports*, *10*(1). https://doi.org/10.1038/s41598-020-72996-3

Alimohammadi, V., Sedighi, M., & Jabbari, E. (2017). Optimization of sulfate removal from wastewater using magnetic multi-walled carbon nanotubes by response surface methodology. *Water Science and Technology*, *76*(10), 2593–2602. https://doi.org/10.2166/wst.2017.424

Alizadeh, N., Moemeni, A., & Shamsipur, M. (2002). Poly(vinyl chloride)-membrane ion-selective bulk optode based on 1,10-dibenzyl-1,10-diaza-18-crown-6 and 1-(2-pyridylazo)-2-naphthol for Cu2+ and Pb2+ ions. *Analytica Chimica Acta*, *464*(2), 187–196.

https://doi.org/10.1016/s0003-2670(02)00477-4

Alizadeh, T., & Atayi, K. (2018). Synthesis of hydrogen phosphate anion-imprinted polymer via emulsion polymerization and its use as the recognition element of graphene/graphite paste potentiometric electrode. *Materials Chemistry and Physics*, *209*, 180–187. https://doi.org/10.1016/j.matchemphys.2018.01.068

Alkathy, M. S., Raju, K. J., & Eiras, J. A. (2021). Colossal dielectric permittivity and high energy storage efficiency in barium strontium titanate ceramics co-doped with bismuth and Lithium. Journal of Physics D: Applied Physics, 54(12), 125501.

An, J. W., Kang, D. J., Tran, K. T., Kim, M. J., Lim, T., & Tran, T. (2012). Recovery of lithium FROM Uyuni salar brine. *Hydrometallurgy*, *117-118*, 64–70. https://doi.org/10.1016/j.hydromet.2012.02.008

Araki, K., Maruyama, T., Kamiya, N., & Goto, M. (2005). Metal ion-selective membrane prepared by surface molecular imprinting. *Journal of Chromatography B*, *818*(2), 141–145. https://doi.org/10.1016/j.jchromb.2004.12.030

Babu, P. K., Waghmare, A. S., Mulla, S. M., Karle, U. S., & Saraf, M. R. (2017). Material characterization of lithium-ion battery cells by scanning electron microscopy & X-ray diffraction techniques. *2017 IEEE Transportation Electrification Conference (ITEC-India)*. https://doi.org/10.1109/itec-india.2017.8333896

Bahraini, N., Lai, E. P., Li, C., Sadi, B. B., & Kramer, G. H. (2011). MOLECULARLY imprinted polymers for 90SR URINE BIOASSAY. *Health Physics*, *101*(2), 128–135.

https://doi.org/10.1097/hp.0b013e318213a5ef

Bahrami, A., Besharati-Seidani, A., Abbaspour, A., & Shamsipur, M. (2014). A highly selective voltammetric sensor for sub-nanomolar detection of lead ions using a carbon paste electrode impregnated with novel ion imprinted polymeric nanobeads. *Electrochimica Acta*, *118*, 92–99. https://doi.org/10.1016/j.electacta.2013.11.180

Basuki, K. T., Fatuzzahroh, M., Ariyanti, D., & Saputra, A. (2021). Adsorption of Strontium from an Aqueous Solution by TiO2-Pillared Zeolite. Adsorption, 12(3).

Behbahani, M., Taghizadeh, M., Bagheri, A., Hosseini, H., Salarian, M., & Tootoonchi, A. (2012). A nanostructured ion-imprinted polymer for the selective extraction and preconcentration of ultra-trace quantities of nickel ions. *Microchimica Acta*, *178*(3-4), 429–437. https://doi.org/10.1007/s00604-012-0846-x

Bindels, M., Carvalho, J., Gonzalez, C. B., Brand, N., & Nelemans, B. (2020). Techno-economic assessment of Seawater Reverse Osmosis (SWRO) brine treatment with air gap membrane distillation (AGMD). *Desalination*, *489*, 114532. https://doi.org/10.1016/j.desal.2020.114532

Boanini, E., Gazzano, M., Nervi, C., Chierotti, M. R., Rubini, K., Gobetto, R., & Bigi, A. (2019). Strontium and zinc substitution in β-tricalcium phosphate: An X-ray diffraction, solid state NMR and ATR-FTIR Study. *Journal of Functional Biomaterials*, *10*(2), 20. https://doi.org/10.3390/jfb10020020

Branger, C., Meouche, W., & Margaillan, A. (2013). Recent advances on ion-imprinted polymers.

Reactive and Functional Polymers, *73*(6), 859–875. https://doi.org/10.1016/j.reactfunctpolym.2013.03.021

Brittain, G. (2020). Profiles of drug substances, excipients, and related methodology. *Academic Press*, i. https://doi.org/10.1016/s1871-5125(20)30003-0

Bukowsky, H., & Uhlemann, E. (1993). Selective extraction of lithium chloride FROM BRINES. *Separation Science and Technology*, *28*(6), 1357–1360. https://doi.org/10.1080/01496399308018042

Bukowsky, H., Uhlemann, E., & Steinborn, D. (1991). The recovery of pure lithium chloride from "brines" containing higher contents of calcium chloride and magnesium chloride. *Hydrometallurgy*, *27*(3), 317–325. https://doi.org/10.1016/0304-386x(91)90056-r

Bukowsky, H., Uhlemann, E., & Steinborn, D. (1991). The recovery of pure lithium chloride from "brines" containing higher contents of calcium chloride and magnesium chloride. *Hydrometallurgy*, *27*(3), 317–325. https://doi.org/10.1016/0304-386x(91)90056-r

Büning, D., Ennen-Roth, F., Walter, S. V., Hennecke, T., & Ulbricht, M. (2018). Potassium-sensitive poly(N-isopropylacrylamide)-based hydrogels for sensor applications. *Polymer Chemistry*, *9*(26), 3600–3614. https://doi.org/10.1039/c8py00490k

Cabbiness, D. K., & Margerum, D. W. (1969). Macrocyclic effect on the stability of copper(II) tetramine complexes. *Journal of the American Chemical Society*, *91*(23), 6540–6541. https://doi.org/10.1021/ja01051a091

Cai, Y.-H., Yang, X. J., & Schäfer, A. I. (2020). Removal of naturally Occurring strontium by

NANOFILTRATION/REVERSE osmosis from groundwater. *Membranes*, *10*(11), 321. https://doi.org/10.3390/membranes10110321

Carrasquel-Ursulaez, W., Reeves, R. D., Dehghany, M., Jones, C., Schomaker, J. M., & Chanda, B. (2020). Re-evaluation of the mechanism of cytotoxicity of dialkylated lariat ether compounds. *RSC Advances*, *10*(66), 40391–40394. https://doi.org/10.1039/d0ra08494h

Cejner, M., & Dobrowolski, R. (2015). Ion-imprinted polymers: synthesis, characterization and applications. *Ann. Univ. Mariae Curie-Sklodowska, Sect. AA: Chem*, *70*. https://doi.org/http://dx.doi.org/10.17951/aa.2015.70.2.67

Chen, C.-Y., Yang, C.-Y., & Chen, A.-H. (2011). Biosorption of cu(ii), zn(ii), ni(ii) and pb(ii) ions by cross-linked metal-imprinted chitosans with epichlorohydrin. *Journal of Environmental Management*, *92*(3), 796–802. https://doi.org/10.1016/j.jenvman.2010.10.029

Chen, L., Wang, X., Lu, W., Wu, X., & Li, J. (2016). Molecular imprinting: perspectives and applications. *Chemical Society Reviews*, *45*(8), 2137–2211. https://doi.org/10.1039/c6cs00061d

Cher, A. H. (2020, December 4). *Ions & Ionic bonding: O level chemistry notes*. Chem Not Cheem. Retrieved November 18, 2021, from https://chemnotcheem.com/ionic-bonding-notes/

Chung, H.-K., Kim, W.-H., Park, J., Cho, J., Jeong, T.-Y., & Park, P.-K. (2015). Application of langmuir and freundlich isotherms to predict adsorbate removal efficiency or required amount of adsorbent. *Journal of Industrial and Engineering Chemistry*, *28*, 241–246. https://doi.org/10.1016/j.jiec.2015.02.021

Ciliberto, E., Condorelli, G. G., La Delfa, S., & Viscuso, E. (2008). Nanoparticles of $Sr(OH)_2$: Synthesis in homogeneous phase at low temperature and application for cultural heritage artefacts. *Applied Physics A*, *92*(1), 137–141. https://doi.org/10.1007/s00339-008-4464-8

Dada, A., Olalekan, A., Olatunya, A., & DADA, O. (2012). Langmuir, freundlich, temkin and Dubinin–Radushkevich isotherms studies of equilibrium sorption of Zn 2+ unto phosphoric acid modified rice husk. *IOSR Journal of Applied Chemistry*, *3*(1), 38–45. https://doi.org/10.9790/5736-0313845

Dahaghin, Z., Kilmartin, P. A., & Mousavi, H. Z. (2018). Determination of cadmium(ii) using a glassy carbon electrode modified with a CD-ion imprinted polymer. *Journal of Electroanalytical Chemistry*, *810*, 185–190. https://doi.org/10.1016/j.jelechem.2018.01.014

Dakova, I., Yordanova, T., & Karadjova, I. (2012). Non-chromatographic mercury speciation and determination in wine by new core–shell ion-imprinted sorbents. *Journal of Hazardous Materials*, *231-232*, 49–56. https://doi.org/10.1016/j.jhazmat.2012.06.034

Dam, H. A., & Kim, D. (2009). Selective copper(ii) sorption behavior of surface-imprinted core−shell-type polymethacrylate microspheres. *Industrial & Engineering Chemistry Research*, *48*(12), 5679–5685. https://doi.org/10.1021/ie801321d

Damania, R., Desbureaux, S., Hyland, M., Islam, A., Moore, S., Rodella, A.-S., Russ, J., & Zaveri, E. (2017). Uncharted waters: The New economics of water scarcity and variability. https://doi.org/10.1596/978-1-4648-1179-1

Daniel, S., Babu, P., & Rao, T. (2005). Preconcentrative separation of palladium(II) using palladium(II) ion-imprinted polymer particles formed with different quinoline derivatives and evaluation of binding parameters based on adsorption isotherm models. *Talanta*, *65*(2), 441–452. https://doi.org/10.1016/j.talanta.2004.06.024

Daniel, S., Prabhakara Rao, P., & Prasada Rao, T. (2005). Investigation of different polymerization methods on the analytical performance of palladium(ii) ion imprinted Polymer Materials. *Analytica Chimica Acta*, *536*(1-2), 197–206. https://doi.org/10.1016/j.aca.2004.12.052

Darre, N. C., & Toor, G. S. (2018). Desalination of water: A review. *Current Pollution Reports*, *4*(2), 104–111. https://doi.org/10.1007/s40726-018-0085-9

Dorsey, A., Fransen, M., Diamond, G., & Amata, R. (2004). Toxicological profile for strontium. *Agency for Toxic and Substances and Disease Registry Toxicological Profiles* . https://doi.org/10.1201/9781420061888_ch141

El Ouardi, Y., Giove, A., Laatikainen, M., Branger, C., & Laatikainen, K. (2021). Benefit of ion imprinting technique in solid-phase extraction of heavy metals, special focus on the last decade. *Journal of Environmental Chemical Engineering*, *9*(6), 106548. https://doi.org/10.1016/j.jece.2021.106548

Elimelech, M., & Phillip, W. A. (2011). The future of seawater desalination: Energy, technology, and the environment. *Science*, *333*(6043), 712–717. https://doi.org/10.1126/science.1200488

El-Sonbati, A. Z., Diab, M. A., & El-Bindary, A. A. (2012). Stoichiometry of polymer complexes. *Stoichiometry and Research - The Importance of Quantity in Biomedicine*. https://doi.org/10.5772/34021

EPA. (2021). *EPA Facts about Strontium-90*. EPA. https://www.epa.gov/radiation/radionuclide-basics-strontium-90.

Esen, C., Andac, M., Bereli, N., Say, R., Henden, E., & Denizli, A. (2009). Highly selective ion-imprinted particles for solid-phase extraction of Pb2+ ions. *Materials Science and Engineering: C*, *29*(8), 2464–2470. https://doi.org/10.1016/j.msec.2009.07.012

Fasihi, J., Ammari Alahyari, S., Shamsipur, M., Sharghi, H., & Charkhi, A. (2011). Adsorption of uranyl ion onto an anthraquinone based ion-imprinted copolymer. *Reactive and Functional Polymers*, *71*(8), 803–808. https://doi.org/10.1016/j.reactfunctpolym.2011.03.014

Frank, H., Rahav, E., & Bar-Zeev, E. (2017). Short-term effects of SWRO desalination brine on benthic heterotrophic microbial communities. *Desalination*, *417*, 52–59. https://doi.org/10.1016/j.desal.2017.04.031

Frensdorff, H. K. (1971). Stability constants of cyclic polyether complexes with univalent cations. *Journal of the American Chemical Society*, *93*(3), 600–606. https://doi.org/10.1021/ja00732a007

Fu, J., Chen, L., Li, J., & Zhang, Z. (2015). Current status and challenges of ion imprinting. *Journal of Materials Chemistry A*, *3*(26), 13598–13627. https://doi.org/10.1039/c5ta02421h

Fu, X.-C., Wu, J., Nie, L., Xie, C.-G., Liu, J.-H., & Huang, X.-J. (2012). Electropolymerized

surface ion imprinting films on a gold nanoparticles/single-wall carbon nanotube nanohybrids modified glassy carbon electrode for electrochemical detection of Trace Mercury(ii) in water. *Analytica Chimica Acta*, *720*, 29–37. https://doi.org/10.1016/j.aca.2011.12.071

Gao, D., Guo, Y., Yu, X., Wang, S., & Deng, T. (2016). Extracting lithium from the high concentration ratio of magnesium and lithium brine using imidazolium-based ionic liquids with varying alkyl chain lengths. *Journal of Chemical Engineering of Japan*, *49*(2), 104–110. https://doi.org/10.1252/jcej.15we046

Gao, D., Yu, X., Guo, Y., Wang, S., Liu, M., Deng, T., Chen, Y., & Belzile, N. (2015). Extraction of lithium from salt lake brine with triisobutyl phosphate in ionic liquid and kerosene. *Chemical Research in Chinese Universities*, *31*(4), 621–626. https://doi.org/10.1007/s40242-015-4376-z

Ghodke, S. A., Maheshwari, U., Gupta, S., Sonawane, S. H., & Bhanvase, B. A. (2021). Nanomaterials for adsorption of pollutants and heavy metals: Introduction, mechanism, and challenges. *Handbook of Nanomaterials for Wastewater Treatment*, 343–366. https://doi.org/10.1016/b978-0-12-821496-1.00032-5

Ghorbani, M., Aghamohammadhassan, M., Ghorbani, H., & Zabihi, A. (2020). Trends in sorbent development for dispersive micro-solid phase extraction. *Microchemical Journal*, *158*, 105250. https://doi.org/10.1016/j.microc.2020.105250

Girão, A. V., Caputo, G., & Ferro, M. C. (2017). Application of scanning electron microscopy–energy dispersive X-ray spectroscopy (SEM-eds). *Characterization and Analysis of*

Microplastics, 153–168. https://doi.org/10.1016/bs.coac.2016.10.002

Gladis, J. M., & Prasada Rao, T. (2002). Solid phase extractive preconcentration of uranium on to 5,7-dichloroquinoline- 8-OL modified naphthalene. *Analytical Letters*, *35*(3), 501–515. https://doi.org/10.1081/al-120002683

Gu, D., Sun, W., Han, G., Cui, Q., & Wang, H. (2018). Lithium ion sieve synthesized via an improved solid state method and adsorption performance for West Taijinar Salt Lake brine. *Chemical Engineering Journal*, *350*, 474–483. https://doi.org/10.1016/j.cej.2018.05.191

Gude, V. G. (2017). Desalination and water reuse to address global water scarcity. *Reviews in Environmental Science and Bio/Technology*, *16*(4), 591–609. https://doi.org/10.1007/s11157-017-9449-7

Háková, M., Havlíková, L. C., Švec, F., Solich, P., & Šatínský, D. (2020). Nanofibers as advanced sorbents for on-line solid phase extraction in liquid chromatography: A tutorial. *Analytica Chimica Acta*, *1121*, 83–96. https://doi.org/10.1016/j.aca.2020.04.045

Hancock, R. D., & Martell, A. E. (1989). Ligand design for selective complexation of metal ions in aqueous solution. *Chemical Reviews*, *89*(8), 1875–1914. https://doi.org/10.1021/cr00098a011

Hande, P. E., Kamble, S., Samui, A. B., & Kulkarni, P. S. (2016). Chitosan-based lead ion-imprinted interpenetrating polymer network by simultaneous polymerization for selective extraction of lead(ii). *Industrial & Engineering Chemistry Research*, *55*(12), 3668–3678. https://doi.org/10.1021/acs.iecr.5b04889

Hasani, M., & Shamsipur, M. (2005). Spectrophotometric study of interaction of 2,3-dichloro-5,6-dicyano-1,4-benzoquinone with diaza-18-crown-6 and diaza-15-crown-5 in acetonitrile and chloroform solutions. *Spectrochimica Acta Part A: Molecular and Biomolecular Spectroscopy*, *61*(5), 815–821. https://doi.org/10.1016/j.saa.2004.06.004

Hashemi, B., & Shamsipur, M. (2015). Synthesis of novel ion-imprinted polymeric nanoparticles based on dibenzo-21-crown-7 for the selective pre-concentration and recognition of rubidium ions. *Journal of Separation Science*, *38*(24), 4248–4254. https://doi.org/10.1002/jssc.201500851

Hashemi, B., Shamsipur, M., & Seyedzadeh, Z. (2016). Synthesis of ion imprinted polymeric nanoparticles for selective pre-concentration and recognition of lithium ions. *New Journal of Chemistry*, *40*(5), 4803–4809. https://doi.org/10.1039/c5nj03366g

Hashemi, B., Shamsipur, M., Javadi, A., Rofouei, M. K., Shockravi, A., Tajarrod, N., & Mandumy, N. (2015). Synthesis and characterization of ion imprinted polymeric nanoparticles for selective extraction and determination of mercury ions. *Analytical Methods*, *7*(22), 9641–9648. https://doi.org/10.1039/c5ay02545a

Hassanzadeh, M., Ghaemy, M., Amininasab, S. M., & Shami, Z. (2018). An effective approach for fast selective separation of cr(vi) from water by ion-imprinted polymer grafted on the electro-spun nanofibrous mat of functionalized polyacrylonitrile. *Reactive and Functional Polymers*, *130*, 70–80. https://doi.org/10.1016/j.reactfunctpolym.2018.05.013

Hoai, N. T., Yoo, D.-K., & Kim, D. (2010). Batch and column separation characteristics of copper-imprinted porous polymer micro-beads synthesized by a direct imprinting method. *Journal*

of Hazardous Materials, *173*(1-3), 462–467. https://doi.org/10.1016/j.jhazmat.2009.08.107

Huang, Y., & Wang, R. (2019). Highly effective and low-cost ion-imprinted polymers loaded on pretreated vermiculite for lithium recovery. *Industrial & Engineering Chemistry Research*, *58*(27), 12216–12225. https://doi.org/10.1021/acs.iecr.9b01244

Işıkver, Y., & Baylav, S. (2018). Synthesis and characterization of metal ion-imprinted polymers. *Bulletin of Materials Science*, *41*(2). https://doi.org/10.1007/s12034-018-1578-2

Ivkovic, A., & Stern, T. A. (2014). Lithium-Induced Neurotoxicity: Clinical Presentations, Pathophysiology, and Treatment. *Psychosomatics*, *55*(3), 296–302. https://doi.org/10.1016/j.psym.2013.11.007

Izatt, R. M., Bradshaw, J. S., Pawlak, K., Bruening, R. L., & Tarbet, B. J. (1992). Thermodynamic and kinetic data for macrocycle interaction with neutral molecules. *Chemical Reviews*, *92*(6), 1261–1354. https://doi.org/10.1021/cr00014a005

Izatt, R. M., Pawlak, K., Bradshaw, J. S., & Bruening, R. L. (1991). Thermodynamic and kinetic data for macrocycle interactions with cations and anions. *Chemical Reviews*, *91*(8), 1721–2085. https://doi.org/10.1021/cr00008a003

Izatt, R. M., Pawlak, K., Bradshaw, J. S., & Bruening, R. L. (1995). Thermodynamic and Kinetic Data for Macrocycle Interaction with Cations, Anions, and Neutral Molecules. *Chemical Reviews*, *95*(7), 2529–2586. https://doi.org/10.1021/cr00039a010

Jagur-Grodzinski, J., & Schori, E. (1985). Solvent-Polymeric membranes for separation of Li+From other alkali metal and alkaline EARTH IONS. *Israel Journal of Chemistry*, *26*(1), 65–70. https://doi.org/10.1002/ijch.198500070

James, M. J. (1966). *recovery of lithium from brines*. Google Patents. https://patents.google.com/patent/US3268289A/en.

Jiang, C., Wang, Y., Wang, Q., Feng, H., & Xu, T. (2014). Production of lithium Hydroxide from Lake BRINES THROUGH Electro–Electrodialysis with Bipolar MEMBRANES (EEDBM). *Industrial & Engineering Chemistry Research*, *53*(14), 6103–6112. https://doi.org/10.1021/ie404334s

Jones, E., & van Vliet, M. T. H. (2018). Drought impacts on river salinity in the SOUTHERN US: Implications for water scarcity. *Science of The Total Environment*, *644*, 844–853. https://doi.org/10.1016/j.scitotenv.2018.06.373

Jones, E., Qadir, M., van Vliet, M. T. H., Smakhtin, V., & Kang, S.-mu. (2019). The state of desalination and brine production: A global outlook. *Science of The Total Environment*, *657*, 1343–1356. https://doi.org/10.1016/j.scitotenv.2018.12.076

Kalmykov, D., Makaev, S., Golubev, G., Eremeev, I., Vasilevsky, V., Song, J., He, T., & Volkov, A. (2021). Operation of Three-Stage Process of Lithium Recovery from Geothermal Brine: Simulation. *Membranes*, *11*(3), 175. https://doi.org/10.3390/membranes11030175

Kempe, H., & Kempe, M. (2008). Molecularly imprinted polymers. *The Power of Functional Resins in Organic Synthesis*, 15–44. https://doi.org/10.1002/9783527626175.ch2

Khan, M., Al-Absi, R. S., Khraisheh, M., & Al-Ghouti, M. A. (2021). A better understanding of seawater reverse osmosis brine: Characterizations, uses, and energy requirements. *Case Studies in Chemical and Environmental Engineering*, *4*, 100165. https://doi.org/10.1016/j.cscee.2021.100165

Kimaro, A., Kelly, L. A., & Murray, G. M. (2001). Molecularly imprinted ionically permeable membrane for uranyl ion. *Chemical Communications*, (14), 1282–1283. https://doi.org/10.1039/b103077a

Kunugita, E., Kim, J. H., & Komasawa, I. (1989). Extraction and separation of lithium and sodium by solvent extraction with .beta.-diketone and neutral ligand. *KAGAKU KOGAKU RONBUNSHU*, *15*(3), 504–510. https://doi.org/10.1252/kakoronbunshu.15.504

Kusumkar, V. V., Galamboš, M., Viglašová, E., Daňo, M., & Šmelková, J. (2021). Ion-imprinted polymers: Synthesis, characterization, and adsorption of radionuclides. *Materials*, *14*(5), 1083. https://doi.org/10.3390/ma14051083

Lemaire, J., Svecova, L., Lagallarde, F., Laucournet, R., & Thivel, P.-X. (2014). Lithium recovery from aqueous solution by Sorption/Desorption. *Hydrometallurgy*, *143*, 1–11. https://doi.org/10.1016/j.hydromet.2013.11.006

Li, Q., Liu, H., Liu, T., Guo, M., Qing, B., Ye, X., & Wu, Z. (2010). Strontium and calcium ion adsorption by molecularly imprinted hybrid gel. *Chemical Engineering Journal*, *157*(2-3), 401–407. https://doi.org/10.1016/j.cej.2009.11.029

Li, T., Chen, S., Li, H., Li, Q., & Wu, L. (2011). Preparation of an ion-imprinted fiber for the

selective removal of cu2+. *Langmuir*, *27*(11), 6753–6758. https://doi.org/10.1021/la200986v

Li, T., Wu, L., Chen, S., Li, H., & Xu, X. (2011). A simple scheme for grafting an ion-imprinted layer onto the surface of poly(propylene) fibers. *Macromolecular Chemistry and Physics*, *212*(19), 2166–2172. https://doi.org/10.1002/macp.201100195

Liang, Q., Geng, J., Luo, H., Fang, W., & Yin, Y. (2017). Fast and selective removal of cr(vi) from aqueous solutions by a novel magnetic cr(vi) ion-imprinted polymer. *Journal of Molecular Liquids*, *248*, 767–774. https://doi.org/10.1016/j.molliq.2017.10.114

Limjuco, L. A., Nisola, G. M., Torrejos, R. E., Han, J. W., Song, H. S., Parohinog, K. J., Koo, S., Lee, S.-P., & Chung, W.-J. (2017). Aerosol Cross-Linked Crown Ether Diols Melded with Poly(vinyl alcohol) as Specialized Microfibrous Li+Adsorbents. *ACS Applied Materials & Interfaces*, *9*(49), 42862–42874. https://doi.org/10.1021/acsami.7b14858

Limousin, G., Gaudet, J.-P., Charlet, L., Szenknect, S., Barthes, V., & Krimissa, M. (2007). Sorption isotherms: Physical Bases, modeling and measurement. *ChemInform*, *38*(44). https://doi.org/10.1002/chin.200744267

Liu, X., Chen, X., He, L., & Zhao, Z. (2015). Study on extraction of lithium from salt lake brine by membrane electrolysis. *Desalination*, *376*, 35–40. https://doi.org/10.1016/j.desal.2015.08.013

Liu, Y., Meng, X., Liu, Z., Meng, M., Jiang, F., Luo, M., Ni, L., Qiu, J., Liu, F., & Zhong, G. (2015). Preparation of a two-dimensional ion-imprinted polymer based on a graphene

oxide/SIO2 composite for the selective adsorption of nickel ions. *Langmuir*, *31*(32), 8841–8851. https://doi.org/10.1021/acs.langmuir.5b01201

Liu, Z., Nalluri, S. K., & Stoddart, J. F. (2017). Surveying macrocyclic chemistry: from flexible crown ethers to rigid cyclophanes. *Chemical Society Reviews*, *46*(9), 2459–2478. https://doi.org/10.1039/c7cs00185a

Loganathan, P., Naidu, G., & Vigneswaran, S. (2017). Mining valuable minerals from seawater: A critical review. *Environmental Science: Water Research & Technology*, *3*(1), 37–53. https://doi.org/10.1039/c6ew00268d

Long, J., Luo, X., Yin, X., & Wu, X. (2016). An ion-imprinted polymer based on the novel functional monomer for selective removal of ni(ii) from Aqueous Solution. *Journal of Environmental Chemical Engineering*, *4*(4), 4776–4785. https://doi.org/10.1016/j.jece.2016.11.004

Lu, J., Qin, Y., Zhang, Q., Wu, Y., Cui, J., Li, C., Wang, L., & Yan, Y. (2018). Multilayered ion-imprinted membranes with high selectivity towards Li+ based on the synergistic effect of 12-crown-4 and polyether sulfone. *Applied Surface Science*, *427*, 931–941. https://doi.org/10.1016/j.apsusc.2017.08.016

Lu, Y.-K., & Yan, X.-P. (2004). An Imprinted Organic−Inorganic Hybrid Sorbent for Selective Separation of Cadmium from Aqueous Solution. *Analytical Chemistry*, *76*(2), 453–457. https://doi.org/10.1021/ac0347718

Luo, X., Guo, B., Luo, J., Deng, F., Zhang, S., Luo, S., & Crittenden, J. (2015). Recovery of

Lithium from Wastewater Using Development of Li Ion-Imprinted Polymers. *ACS Sustainable Chemistry & Engineering*, *3*(3), 460–467. https://doi.org/10.1021/sc500659h

Mahamuni, N. N., & Adewuyi, Y. G. (2009). Fourier transform infrared spectroscopy (FTIR) method to monitor soy biodiesel and soybean oil in transesterification reactions, petrodiesel−biodiesel blends, and blend adulteration with soy oil. *Energy & Fuels*, *23*(7), 3773–3782. https://doi.org/10.1021/ef900130m

Marinsky, A., & Marcus, Y. (1995). Ion exchange and solvent extraction: a series of advances. *Analytica Chimica Acta*, *313*(3), 261. https://doi.org/10.1016/0003-2670(95)90099-3

McKnight, R. F., Adida, M., Budge, K., Stockton, S., Goodwin, G. M., & Geddes, J. R. (2012). Lithium toxicity profile: a systematic review and meta-analysis. *The Lancet*, *379*(9817), 721–728. https://doi.org/10.1016/s0140-6736(11)61516-x

Mekonnen, M. M., & Hoekstra, A. Y. (2016). Four billion people facing severe water scarcity. *Science Advances*, *2*(2). https://doi.org/10.1126/sciadv.1500323

Meouche, W., Branger, C., Beurroies, I., Denoyel, R., & Margaillan, A. (2012). Inverse suspension polymerization as a new tool for the synthesis of ion-imprinted polymers. *Macromolecular Rapid Communications*, *33*(10), 928–932. https://doi.org/10.1002/marc.201200039

Mero, L. (1965). The mineral resources of the sea. *Elsevier Oceanography Series*. https://doi.org/10.1016/s0422-9894(08)x7034-5

Miyoshi, N., Kimura, S., Kubo, S., Ohmura, S. D., & Ueno, M. (2020). Chemoselective Ketone Synthesis by the Strontium-mediated Alkylation or Arylation of N, N-Dimethylamides or

Urea. Asian Journal of Organic Chemistry, 9(10), 1660-1664.

Mourdikoudis, S., Pallares, R. M., & Thanh, N. T. (2018). Characterization techniques for nanoparticles: Comparison and complementarity upon studying nanoparticle properties. *Nanoscale*, *10*(27), 12871–12934. https://doi.org/10.1039/c8nr02278j

Murodjon, S., Yu, X., Li, M., Duo, J., & Deng, T. (2020). Lithium recovery from brines including seawater, salt lake brine, underground water and geothermal water. *Thermodynamics and Energy Engineering*. https://doi.org/10.5772/intechopen.90371

Murray, G. M., & Manuel Uy, M. (2001). Ionic sensors based on molecularly imprinted polymers. *Techniques and Instrumentation in Analytical Chemistry*, 441–465. https://doi.org/10.1016/s0167-9244(01)80022-6

Murray, G., Jenkins, A., Bzhelyansky, A., & Manuel Uy, O. (1997). Molecularly Imprinted Polymers for the Selective Sequestering and Sensing of Ions. *JOHNS HOPKINS APL TECHNICAL DIGEST*, *18*.

Naidu, G., Jeong, S., Choi, Y., Song, M. H., Oyunchuluun, U., & Vigneswaran, S. (2018). Valuable rubidium extraction from potassium reduced seawater brine. *Journal of Cleaner Production*, *174*, 1079–1088. https://doi.org/10.1016/j.jclepro.2017.11.042

Nguyen, C., & Do, D. D. (2001). The Dubinin–Radushkevich equation and the underlying microscopic adsorption description. *Carbon*, *39*(9), 1327–1336. https://doi.org/10.1016/s0008-6223(00)00265-7

Nguyen, Q.-M., Jeong, S., & Lee, S. (2017). Characteristics of membrane foulants at different

degrees of SWRO brine concentration by membrane distillation. *Desalination*, *409*, 7–20. https://doi.org/10.1016/j.desal.2017.01.007

Nishide, H., Deguchi, J., & Tsuchida, E. (1976). Selective adsorption of metal ions on crosslinked poly(vinylpyridine) resin prepared with a metal ion as a template. *Chemistry Letters*, *5*(2), 169–174. https://doi.org/10.1246/cl.1976.169

Onwuka, O. S., Umar, N. D., Omonona, O. V., & Idris, I. G. (2019). Heavy metals and rare earth elements distribution in the brine fields of awe, Keana and Giza, Central Benue Trough, Nigeria. *Journal of African Earth Sciences*, *157*, 103514. https://doi.org/10.1016/j.jafrearsci.2019.103514

Otero-Romaní, J., Moreda-Piñeiro, A., Bermejo-Barrera, P., & Martin-Esteban, A. (2008). Synthesis, characterization and evaluation of ionic-imprinted polymers for solid-phase extraction of nickel from seawater. *Analytica Chimica Acta*, *630*(1), 1–9. https://doi.org/10.1016/j.aca.2008.09.049

Otero-Romaní, J., Moreda-Piñeiro, A., Bermejo-Barrera, P., & Martin-Esteban, A. (2009). Inductively coupled plasma–optical emission spectrometry/mass spectrometry for the determination of Cu, Ni, Pb and Zn in seawater after ionic imprinted polymer based solid phase extraction. *Talanta*, *79*(3), 723–729. https://doi.org/10.1016/j.talanta.2009.04.066

Özkara, S., Andaç, M., Karakoç, V., Say, R., & Denizli, A. (2010). Ion-imprinted Phema based monolith for the removal of fe3+ ions from aqueous solutions. *Journal of Applied Polymer Science*, *120*(3), 1829–1836. https://doi.org/10.1002/app.33400

Panagopoulos, A., Haralambous, K.-J., & Loizidou, M. (2019). Desalination brine disposal methods and treatment technologies - a review. *Science of The Total Environment*, *693*, 133545. https://doi.org/10.1016/j.scitotenv.2019.07.351

Paranthaman, M. P., Li, L., Luo, J., Hoke, T., Ucar, H., Moyer, B. A., & Harrison, S. (2017). Recovery of Lithium from Geothermal Brine with Lithium–Aluminum Layered Double Hydroxide Chloride Sorbents. *Environmental Science & Technology*, *51*(22), 13481–13486. https://doi.org/10.1021/acs.est.7b03464

Pataer, P., Muhammad, T., Turahun, Y., Yang, W., Aihebaier, S., Wubulikasimu, M., & Chen, L. (2019). Preparation of a stoichiometric molecularly imprinted polymer for auramine O and application in solid-phase extraction. *Journal of Separation Science*, *42*(8), 1634–1643. https://doi.org/10.1002/jssc.201801234

Pedersen, C. J. (1967). Cyclic polyethers and their complexes with metal salts. *Journal of the American Chemical Society*, *89*(26), 7017–7036. https://doi.org/10.1021/ja01002a035

Pelly, I. (1978). Recovery of lithium from Dead Sea brines. *Journal of Applied Chemistry and Biotechnology*, 28(7), 469-474.

Płotka-Wasylka, J., Szczepańska, N., de la Guardia, M., & Namieśnik, J. (2016). Modern trends in solid phase extraction: New Sorbent Media. *TrAC Trends in Analytical Chemistry*, *77*, 23–43. https://doi.org/10.1016/j.trac.2015.10.010

Prasad, K., Kala, R., Prasada Rao, T., & Naidu, G. R. K. (2006). Ion imprinted polymer based ion-selective electrode for the trace determination of dysprosium(iii) ions. *Analytica Chimica Acta*, *566*(1), 69–74. https://doi.org/10.1016/j.aca.2006.02.064

Rao, T. P., Kala, R., & Daniel, S. (2006). Metal ion-imprinted polymers—novel materials for selective recognition of Inorganics. *Analytica Chimica Acta*, *578*(2), 105–116. https://doi.org/10.1016/j.aca.2006.06.065

Roberts, D. A., Johnston, E. L., & Knott, N. A. (2010). Impacts of desalination plant discharges on the Marine Environment: A Critical Review of published studies. *Water Research*, *44*(18), 5117–5128. https://doi.org/10.1016/j.watres.2010.04.036

Sarabadani, P., Sadeghi, M., Payehghadr, M., & Es'haghi, Z. (2014). Synthesis and characterization of a novel nanostructured ion-imprinted polymer for pre-concentration of y(iii) ions. *Anal. Methods*, *6*(3), 741–749. https://doi.org/10.1039/c3ay41611a

Saraji, M., & Yousefi, H. (2009). Selective solid-phase extraction of Ni(II) by an ion-imprinted polymer from water samples. *Journal of Hazardous Materials*, *167*(1-3), 1152–1157. https://doi.org/10.1016/j.jhazmat.2009.01.111

Sathiyapriya, G., Naseer, K. A., Marimuthu, K., Kavaz, E., Alalawi, A., & Al-Buriahi, M. S. (2021). Structural, optical and nuclear radiation shielding properties of strontium barium borate glasses doped with dysprosium and niobium. Journal of Materials Science: Materials in Electronics, 32(7), 8570-8592.

Schewe, J., Heinke, J., Gerten, D., Haddeland, I., Arnell, N. W., Clark, D. B., Dankers, R., Eisner,

S., Fekete, B. M., Colón-González, F. J., Gosling, S. N., Kim, H., Liu, X., Masaki, Y., Portmann, F. T., Satoh, Y., Stacke, T., Tang, Q., Wada, Y., … Kabat, P. (2013). Multimodel assessment of water scarcity UNDER climate change. *Proceedings of the National Academy of Sciences*, *111*(9), 3245–3250. https://doi.org/10.1073/pnas.1222460110

Segatelli, M. G., Santos, V. S., Presotto, A. B., Yoshida, I. V., & Tarley, C. R. (2010). Cadmium ion-selective sorbent preconcentration method using ion imprinted poly(ethylene glycol dimethacrylate-co-vinylimidazole). *Reactive and Functional Polymers*, *70*(6), 325–333. https://doi.org/10.1016/j.reactfunctpolym.2010.02.006

Shaaban, K. S., Wahab, E. A., El-Maaref, A. A., Abdelawwad, M., Wilke, H., Hillmer, H., & Börcsök, J. (2020). Judd–Ofelt analysis and physical properties of erbium modified cadmium lithium gadolinium silicate glasses. Journal of Materials Science: Materials in Electronics, 31(6), 4986-4996.

Shamsipur, M., & Besharati-Seidani, A. (2011). Synthesis of a novel nanostructured ion-imprinted polymer for very fast and highly selective recognition of copper(ii) ions in aqueous media. *Reactive and Functional Polymers*, *71*(2), 131–139. https://doi.org/10.1016/j.reactfunctpolym.2010.11.002

Shamsipur, M., & Mashhadizadeh, M. (2001). Cadmium ion-selective electrode based on tetrathia-12-crown-4. *Talanta*, *53*(5), 1065–1071. https://doi.org/10.1016/s0039-9140(00)00602-0

Shamsipur, M., Davarkhah, R., & Khanchi, A. R. (2010). Facilitated transport of uranium(VI) across a bulk liquid membrane containing thenoyltrifluoroacetone in the presence of crown ethers as synergistic agents. *Separation and Purification Technology*, *71*(1), 63–69.

https://doi.org/10.1016/j.seppur.2009.11.003

Shamsipur, M., Ghiasvand, A. R., & Yamini, Y. (2001). Extraction of uranium from solid matrices using modified supercritical fluid CO2. *The Journal of Supercritical Fluids*, *20*(2), 163–169. https://doi.org/10.1016/s0896-8446(01)00052-3

Shamsipur, M., Hashemi, B., Dehdashtian, S., Mohammadi, M., Gholivand, M. B., Garau, A., & Lippolis, V. (2014). Silver ion imprinted polymer nanobeads based on a aza-thioether crown containing a 1,10-phenanthroline subunit for solid phase extraction and for voltammetric and potentiometric silver sensors. *Analytica Chimica Acta*, *852*, 223–235. https://doi.org/10.1016/j.aca.2014.09.028

Shariatinia, Z. (2021). Cell penetration peptide-based nanomaterials in drug delivery and biomedical applications. *Biopolymer-Based Nanomaterials in Drug Delivery and Biomedical Applications*, 535–588. https://doi.org/10.1016/b978-0-12-820874-8.00005-1

Shi, C., Jia, Y., Zhang, C., Liu, H., & Jing, Y. (2015). Extraction of lithium from salt lake brine using room temperature ionic liquid in tributyl phosphate. *Fusion Engineering and Design*, *90*, 1–6. https://doi.org/10.1016/j.fusengdes.2014.09.021

Singh, D. K., & Mishra, S. (2009). Synthesis, characterization and removal of Cd(II) using Cd(II)-ion imprinted polymer. *Journal of Hazardous Materials*, *164*(2-3), 1547–1551. https://doi.org/10.1016/j.jhazmat.2008.09.112

Skoryna, S. C. (1981). *Handbook of stable strontium*. Plenum Press.

Son, H. S., Soukane, S., Lee, J., Kim, Y., Kim, Y.-D., & Ghaffour, N. (2021). Towards sustainable

circular brine reclamation using seawater reverse osmosis, membrane distillation and forward osmosis hybrids: An experimental investigation. *Journal of Environmental Management*, *293*, 112836. https://doi.org/10.1016/j.jenvman.2021.112836

Stringfellow, W. T., & Dobson, P. F. (2021). Technology for the recovery of lithium from geothermal brines. *Energies*, *14*(20), 6805. https://doi.org/10.3390/en14206805

Sun, D., Meng, M., Qiao, Y., Zhao, Y., Yan, Y., & Li, C. (2018). Synthesis of ion imprinted nanocomposite membranes for selective adsorption of lithium. *Separation and Purification Technology*, *194*, 64–72. https://doi.org/10.1016/j.seppur.2017.10.052

Sun, D., Zhu, Y., Meng, M., Qiao, Y., Yan, Y., & Li, C. (2017). Fabrication of highly selective ion imprinted macroporous membranes with crown ether for targeted separation of lithium ion. *Separation and Purification Technology*, *175*, 19–26. https://doi.org/10.1016/j.seppur.2016.11.029

Sun, S.-Y., Cai, L.-J., Nie, X.-Y., Song, X., & Yu, J.-G. (2015). Separation of magnesium and lithium from Brine using a Desal Nanofiltration membrane. *Journal of Water Process Engineering*, *7*, 210–217. https://doi.org/10.1016/j.jwpe.2015.06.012

Swain, B. (2016). Separation and purification of lithium by solvent extraction and supported liquid membrane, analysis of their mechanism: A review. *Journal of Chemical Technology & Biotechnology*, *91*(10), 2549–2562. https://doi.org/10.1002/jctb.4976

Titus, D., James Jebaseelan Samuel, E., & Roopan, S. M. (2019). Nanoparticle Characterization Techniques. *Green Synthesis, Characterization and Applications of Nanoparticles*, 303–

319. https://doi.org/10.1016/b978-0-08-102579-6.00012-5

Toba, A.-L., Nguyen, R. T., Cole, C., Neupane, G., & Paranthaman, M. P. (2021). U.S. lithium resources from geothermal and extraction feasibility. *Resources, Conservation and Recycling*, *169*, 105514. https://doi.org/10.1016/j.resconrec.2021.105514

Trivedi MK, Tallapragada RM, Branton A, Trivedi D, Nayak G, et al. (2015) Physical, Atomic and Thermal Properties of Biofield Treated Lithium Powder. *Journal of Advanced Chemical Engineering*. https://doi.org/10.4172/2090-4568.1000136

Tsoi, Y.-K., Ho, Y.-M., & Leung, K. S.-Y. (2012). Selective recognition of arsenic by tailoring ion-imprinted polymer for ICP-MS quantification. *Talanta*, *89*, 162–168. https://doi.org/10.1016/j.talanta.2011.12.007

Tsuruta, T. (2005). Removal and recovery of lithium using various microorganisms. *Journal of Bioscience and Bioengineering*, *100*(5), 562–566. https://doi.org/10.1263/jbb.100.562

Ueda, T., Nanasawa, A., & Tsukagoshi, M. (2015). Influence of electrochemical lithium penetration from various kinds of lithium solution on ASR expansion of concrete. *Concrete Repair, Rehabilitation and Retrofitting IV*, 31–31. https://doi.org/10.1201/b18972-21

van Vliet, M. T. H., Flörke, M., & Wada, Y. (2017). Quality matters for water scarcity. *Nature Geoscience*, *10*(11), 800–802. https://doi.org/10.1038/ngeo3047

Ventura, S., Bhamidi, S., Hornbostel, M., Nagar, A., & Perea, E. (2016). Selective recovery of metals from geothermal brines. https://doi.org/10.2172/1336270

Wang, X., Zhao, K., Guo, Y., Meng, L., Li, D., & Deng, T. (2019). Experimental determination and thermodynamic model of solid-liquid equilibria in the ternary system (LiCl+ SrCl 2+ H 2 O) at 273.15 K and its application in industry. Journal of Solution Chemistry, 48(4), 528-545.

Westphal, A., Lerm, S., Miethling-Graff, R., Seibt, A., Wolfgramm, M., & Würdemann, H. (2015). Effects of plant downtime on the microbial community composition in the highly saline brine of a geothermal plant in the North German Basin. *Applied Microbiology and Biotechnology*, *100*(7), 3277–3290. https://doi.org/10.1007/s00253-015-7181-1

Westphal, G., Kristen, G., Wegener, W., Ambatiello, P., Geyer, H., Epron, B., Bonal, C., Steinhauser, G., & Götzfried, F. (2010). Sodium chloride. *Ullmann's Encyclopedia of Industrial Chemistry*. https://doi.org/10.1002/14356007.a24_317.pub4

Wiśniewska, M., Franus, W., Fijałkowska, G., Ostolska, I., Wójcik, G., Nosal-Wiercińska, A., & Goscianska, J. (2020). Adsorption and electrokinetic studies of sodalite/lithium/poly(acrylic acid) aqueous system. *Physicochemical Problems of Mineral Processing*, 158–166. https://doi.org/10.37190/ppmp/127929

Xiao, J.-L., Sun, S.-Y., Song, X., Li, P., & Yu, J.-G. (2015). Lithium ion recovery from brine using granulated polyacrylamide–MnO 2 ion-sieve. *Chemical Engineering Journal*, *279*, 659–666. https://doi.org/10.1016/j.cej.2015.05.075

Xu, H., & Guo, D. (2012). Synthesis and characterization of an ion-imprinted polymer for selective adsorption of copper ions in aqueous solution. *Adsorption Science & Technology*, *30*(4), 293–306. https://doi.org/10.1260/0263-6174.30.4.293

Xu, X., Li, Y., Yang, D., Zheng, X., Wang, Y., Pan, J., Zhang, T., Xu, J., Qiu, F., Yan, Y., & Li, C. (2018). A facile strategy toward ion-imprinted hierarchical mesoporous material via dual-template method for simultaneous selective extraction of lithium and rubidium. *Journal of Cleaner Production*, *171*, 264–274. https://doi.org/10.1016/j.jclepro.2017.10.023

Yamaguchi, H., Inoshita, M., Shirakami, A., Hashimoto, S., Ichimiya, C., & Shigekiyo, T. (2013). A case of severe hypothyroidism causing cardiac tamponade associated with lithium intoxication. *Journal of Cardiology Cases*, *8*(1). https://doi.org/10.1016/j.jccase.2013.03.011

Yang, L., Li, S., & Sun, C. (2017). Selective adsorption and separation OF Cs(I) from salt LAKE BRINE by a novel surface magnetic ion-imprinted polymer. *Journal of Dispersion Science and Technology*, *38*(11), 1547–1555. https://doi.org/10.1080/01932691.2016.1261361

Yang, Y., Liu, Q., Wang, H., Ding, F., Jin, G., Li, C., & Meng, H. (2017). Superhydrophobic modification of ceramic membranes for vacuum membrane distillation. *Chinese Journal of Chemical Engineering*, *25*(10), 1395–1401. https://doi.org/10.1016/j.cjche.2017.05.003

Yang, Y., Meng, X., & Xiao, Z. (2018). Synthesis of a surface molecular imprinting polymer based on silica and its application in the identification of nitrocellulose. *RSC Advances*, *8*(18), 9802–9811. https://doi.org/10.1039/c7ra13264f

Zambrzycka-Szelewa, E., Leśniewska, B., & Godlewska-Żyłkiewicz, B. (2019). Preparation and application of ion-imprinted polymer sorbents in separation process of trace metals. *Comprehensive Analytical Chemistry*, 261–293. https://doi.org/10.1016/bs.coac.2019.05.008

Zhang, M., Zhao, H. T., Yang, X., Zhang, W. T., Wang, J., Liu, G. Y., Zhang, H., & Dong, A. J. (2016). Preparation and characterization of surface molecularly imprinted film coated on a magnetic nanocore for the fast and selective recognition of the new neonicotinoid insecticide Paichongding (IPP). *RSC Advances*, *6*(5), 3714–3722. https://doi.org/10.1039/c5ra22138b

Zhao, L., Hu, X., Zi, F., Liu, Y., Hu, D., Li, P., & Cheng, H. (2021). Preparation and adsorption properties of ni(ii) ion-imprinted polymers based on synthesized novel functional monomer. *e-Polymers*, *21*(1), 590–605. https://doi.org/10.1515/epoly-2021-0055

Zhao, Z., Jiang, H., Wu, L., Yu, N., Luo, Z., & Geng, W. (2022). Preparation of magnetic surface ion-imprinted polymer based on functionalized fe3o4 for fast and selective adsorption of cobalt ions from water. *Water*, *14*(2), 261. https://doi.org/10.3390/w14020261

Zhong, Z., Rezaee, R., Josh, M., Esteban, L., & Sarmadivaleh, M. (2022). The salinity dependence of electrical conductivity and Archie's cementation exponent in Shale Formations. *Journal of Petroleum Science and Engineering*, *208*, 109324. https://doi.org/10.1016/j.petrol.2021.109324

Zhu, G., Wang, P., Qi, P., & Gao, C. (2014). Adsorption and desorption properties of Li+ on PVC-H1.6Mn1.6O4 lithium ion-sieve membrane. *Chemical Engineering Journal*, 235, 340–348. https://doi.org/10.1016/j.cej.2013.09.068